THE UNIVERSITY OF OKLAHOMA

GRADUATE COLLEGE

DIRECT ACYLATION OF 2-METHYLFURAN WITH CARBOXYLIC ACIDS OVER ZEOLITE CATALYSTS

A DISSERTATION

SUBMITTED TO THE GRADUATE FACULTY

in partial fulfillment of the requirements for the

Degree of

DOCTOR OF PHILOSOPHY

By

ISMAEEL ALALQ
Norman, Oklahoma
2024

Downloaded from SHAREOK. Persistent Handle URL: https://hdl.handle.net/11244/340448

DIRECT ACYLATION OF 2-METHYLFURAN WITH CARBOXYLIC ACIDS OVER ZEOLITE CATALYSTS

A DISSERTATION APPROVED FOR THE SCHOOL OF SUSTAINABLE CHEMICAL BIOLOGICAL AND MATERIALS ENGINEERING

BY

Dr. Steven P. Crossley, Chair

Dr. Daniel E. Resasco

Dr. Lance L. Lobban

Dr. Bin Wang

Dr. Andrew S. Elwood Madden

© Copyright by Ismaeel Alalq 2024
All Rights Reserved.

Dedication

To my cherished parents, Ibrahim and Naerah Alalq, whose unwavering love and guidance have shaped me into the person I am today,

Acknowledgements

"In the name of God, the Most Gracious, the Most Merciful"

First and foremost, I express profound gratitude to God for His boundless blessings. His unwavering support and inspiration sustained me through every challenge and obstacle encountered on my PhD journey. I am profoundly appreciative of His unconditional love, mercy, and grace, which illuminated my path and granted me strength and guidance in every endeavor.

In 2016, I made a life-changing decision to leave a stable industrial job as a process engineer to embark on a journey towards pursuing my PhD studies. This decision was not made lightly, but with the support and assistance of numerous individuals, I was able to take this monumental step forward in my academic and personal growth.

I am indebted to my dear parents, Ibrahim and Naerah Alalq, whose constant support, motivation, and unwavering belief in me have been the foundation of my journey. Their teachings instilled in me the values of persistence, moral integrity, and a love for knowledge, shaping me into the best version of myself. I owe them a debt of gratitude that can never be repaid.

To my beloved wife, Maria Abuzaid, and our four wonderful children, your boundless support and sacrifices have been the cornerstone of my pursuit. Your patience, encouragement, and unwavering cheerfulness during moments of stress and adversity have been my source of strength. I am profoundly grateful for your presence in my life.

I extend my heartfelt appreciation to my siblings, particularly my elder brother, Ishaq Alalq, whose guidance and encouragement bolstered me during the early stages of my journey. His support lifted me up when I faltered and nearly abandoned my pursuit of a PhD.

I am deeply grateful to Dr. Steven Crossley, not only for his exceptional mentorship but also for his genuine care and belief in my potential. His willingness to provide me with the opportunity to join his research team and his unwavering support during challenging times have been instrumental in my growth as a researcher. Dr. Crossley's passion for knowledge and dedication to science have inspired me to pursue excellence in academia.

I am indebted to Dr. Daniel Resasco for his invaluable feedback and insightful guidance, which have significantly contributed to my research endeavors. His emphasis on the importance of understanding the rationale behind the research process has been pivotal in my academic development.

Dr. Bin Wang's meticulous instruction, inspirational guidance, and constructive advice have been invaluable in my academic journey.

Dr. Lance Lobban has offered invaluable insights and provided valuable recommendations throughout my academic journey. His kindness and sense of humor create a welcoming atmosphere that fosters growth.

Dr. Andrew Madden's kindness in granting me access to his laboratory and instruments has been instrumental in furthering my research endeavors.

Dr. Huy Nguyen, a friend and mentor, played a pivotal role in facilitating the publication of my first paper and has consistently guided me on the path to becoming a more adept researcher.

I extend my gratitude to our collaborators at OSU, Dr. Jeffery White and his student Anya Zornes, for their unwavering support and exceptional teamwork in our research endeavors.

I am profoundly grateful for the support of my colleagues and friends within the OU Catalysis Group. Special thanks to Nabihan Abdulrahman, Andrew D'Amico, Dr. Hien Mai, Dr. Vy Nguyen, Dr. Alejandra Gomez, Caleb Bavlnka, Dr. Nilson de Paula, Dr. Ana Jerdy, Dr. Tram Pham, Dr. Han Chau, Dai Phat Bui, Dr. Gengnan Li, and all other current and former group members for their invaluable assistance and unwavering support in both laboratory work and research endeavors.

Special thanks to the administrators of the SCBME department, Madena McGinnis, Terri Colliver, and Jennifer Jones, for their kindness, support, and guidance in navigating administrative processes.

Lastly, I express my gratitude to the University of Oklahoma, the Saudi Arabian Cultural Mission, and all research funding sources for providing the opportunity and resources to pursue my academic aspirations.

To all mentioned and unmentioned individuals who have contributed to my journey, your support and encouragement have been invaluable, and I am deeply grateful for your unwavering belief in me.

Table of Contents

Dedication ..... *iv*

Acknowledgements ..... *v*

List of Tables ..... *xii*

List of Figures ..... *xiii*

Abstract ..... *xix*

Chapter 1: Introduction *1*

Chapter 2: Shifts in catalyst deactivation mechanisms as a function of surface coverage during Friedel-Crafts acylation in zeolites *7*

2.1 Introduction **7**

2.2 Experimental section **9**

2.2.1 Chemicals and materials 9

2.2.2 Catalyst Characterization 10

2.2.2.1 IPA-TPRx measurements 10

2.2.2.2 Pore volume measurements 11

2.2.2.3 IR Spectroscopy 11

2.2.2.4 Pyroprobe System 12

2.2.2.5 Thermogravimetric analysis 12

2.2.3 Catalytic reaction 13

2.3 Results and Discussion **15**

2.3.1 Assessment of kinetic rates 15

2.3.2 Role of surface coverage of AA 17
2.3.3 Deactivation due to contact with individual species 18
2.3.4 Modification of available surface sites to investigate deactivation pathways 21
2.3.5 Analysis of the sequential reaction products 29
2.3.5.1 Soft coke 29
2.3.5.2 Hard coke (heavy carbonaceous deposits) 30
2.3.5.3 Specific contributions of reactants and products to coke formation 33
2.4 Conclusion 38
Chapter 3: Consequence of altering acid strength in MFI zeolites via Phosphorus modification and their effects on acylation reaction 40
3.1 Introduction 41
3.2 EXPERIMENTAL SECTION 44
3.2.1 Catalyst preparation 44
3.2.1.1 Phosphorous incorporation. 44
3.2.1.2 Na titration 45
3.2.1.3 Silicalite-1 synthesis 45
3.2.2 Catalyst characterization. 46
3.2.2.1 BET surface area and pore volume 46
3.2.2.2 X-ray diffraction 46
3.2.2.3 FTIR-spectroscopy 46
3.2.2.4 Solid-state NMR spectroscopy 47
3.2.2.5 IPA-TPR$_x$ measurements 47
3.2.2.6 Thermogravimetric analysis 48

3.2.3 Catalytic reaction 48

3.3 RESULT AND DISCUSSION. 50

3.3.1 Catalyst characterization 50

3.3.2 The influence of phosphorous addition to zeolites on acylation reaction. 57

3.3.3 Role of phosphorous modification on catalyst stability and selectivity 65

3.4 Conclusions 69

Chapter 4: Effect of Brønsted Acid Site's Local Environment on Zeolites' Catalytic Activities during Acylation of 2-Methylfuran with Acetic Acid 71

4.1 Introduction 72

4.2 Experimental section 76

4.2.1 Chemicals and materials. 76

4.2.2 Catalyst preparation 76

4.2.3 Catalyst Characterization 77

4.2.3.1 IPA-TPRx measurements 77

4.2.3.2 X-Ray diffraction 78

4.2.3.3 Solid-State NMR Spectroscopy 78

4.2.3.4 Scanning Electron Microscopy (SEM) 78

4.2.4 Kinetic Measurements 79

4.2.5 DFT Calculations. 80

4.3 Results and discussion 81

4.3.1 Characterization 81

4.3.2 Role of Extra-framework Aluminum and synergistic sites on acylation reaction kinetics. 84

4.3.3 Evaluating acylation energies from DFT 92

4.4 Conclusions 96

Chapter 5: Role of carbon chain length in carboxylic acids on acylation of 2-methyl furan over HZSM-5 zeolite 98

5.1 Introduction 98

5.2 Experimental section 101

5.2.1 Chemicals and materials 101

5.2.2 Catalytic reaction 101

5.3 Results and Discussion 103

5.3.1 Carbon chain length and acylation activity 103

5.3.2 Product selectivity during acylation with acid mixtures 105

5.3.3 Kinetic model and fitting parameters 107

5.3.4 Effect of carbon chain on the transition state 111

5.3.5 Effects acetic acid cofeeding on catalyst stability. 112

5.4 Conclusions 116

Bibliography 118

Appendices 129

Appendix-A: supporting information for Chapter 2 130

Appendix-B: supporting information for Chapter 3 143

Appendix-C: supporting information for Chapter 4 156

Appendix-D: supporting information for Chapter 5 161

List of Tables

Table 3-1 physical properties of the zeolite catalyst samples used in the study. 50

Table 3-2 retention of Brønsted acid sites (BAS) upon P incorporation..... 62

Table 4-1 Properties of investigated zeolite catalyst samples..... 77

Table 4-2 Values for the activation energies, Enthalpies, and Entropies of transition state during acylation under different catalyst samples. 91

Table 5-1 Optimized kinetic parameter values for acylation with different carboxylic caids composition obtained in Figure 5 from fitting measured data and calculated data. 111

Table 5-2 Enthalpies and entropies for 2-methylfuran acylation with acetic, propionic, butyric, valeric acids over HZSM5 (Si/Al =140) at temperatures between 190-210°C 112

Table 5-3 Estimated deactivation constant (k_d) during acylation of propionic, butyric, and valeric acids cofed with various acetic acid composition. Reaction carried out at 200°C and P_{acids} ~20 Torr, $P_{2\text{-}MF}$ ~ 4 Torr.....116

List of Figures

Figure 2-1: a) Testing diffusion and reaction on HZSM-5 catalyst samples with different Si/Al ratios. CBV2314 Si/Al = 11.5, CBV 5524G Si/Al = 25, CBV8014 Si/Al = 40, and CBV28014 Si/Al= 140) at 160oC after catalyst pretreatment at 300oC for 1 hour to remove the physiosorbed water. PPAA=40 Torr, PP2-MF= 2.6 Torr. Lines are to guide the eye. b) Loss of BAS activity for Na titrated Na-ZSM-5 (25% of BAS exchanged) and parent HZSM-5 both with (Si/Al = 140) at T=240°C with PAA= 40 torr, P2-MF= 2.6 torr. 15

Figure 2-2 Influence of surface coverage of AA on decay rate(a) Turnover frequency vs time on stream of low and high AA coverages. (b) Reaction order wrt AA at low and high coverages of AA. (c) Catalyst activity vs turnover number at low and high coverage AA. Results in (a), (b), and (c) obtained from reaction on HZSM-5 (Si/Al=40) at 160oC. Data in (d), (e), and (f) was collected from reaction on HZSM-5 (Si/Al=140) at 240°C 18

Figure 2-3: (▲) Comparing initial active site loss resulting from the introduction of 2-MF for 1,2,5, and 10 minutes prior to adding the other reactant (AA) to the feed to start the reaction. (■) Comparing initial active site loss resulting from the introduction of the product (Ac-MF) for 1,2,5, and 10 minutes prior to adding the reactants to the feed to start the reaction. (●) Comparing initial active site loss resulting from the introduction of AA for 15, 60 ,120, and 180 minutes prior to adding the other reactant (2-MF) to the feed to start the reaction. All reactions run on HZSM-5 (Si/Al=40) at 160°C after catalyst pretreatment at 300°C for 1 hour to remove the physiosorbed water. PP_{AA}=40 Torr, $PP_{2\text{-}MF}$= 2.6 Torr. Molar flow rates during prefeed for both 2-MF and Ac-MF are equal. 20

Figure 2-4 Reaction of (1) 2-MF on BAS forming (2) dimers through dehydration then self-coupling or hydration then ring opening to (3) 4-oxopentanal followed by dehydration and self-coupling to form (4) trimers.[30] 21

Figure 2-5: Proposed cause of deactivation. (A) 2-MF compete with adsorbed acetic acid. (B) Product re-adsorption along the diffusion path. (C) sequential reaction of product prior to desorption..... 22

Figure 2-6: a) Rate of AA-MF formation at constant partial pressure of AA and 2-MF while varying inert (toluene) partial pressure. b) Rate of product formation at constant 2-MF partial pressure as a function AA and toluene partial pressure. c) contrasting deactivation profiles for two different AA-toluene ratios with constant 2-MF pressure. d) comparing modified partial pressures as a function of 2-MF with two different AA-toluene ratios e) Decay rate and deactivation constants as a functions of reaction temperature. Reactionsconducted over HZSM-5 (Si/Al = 40) at T=160°C with P_{AA}= 40 torr, $P_{2\text{-}MF}$= 2.6 torr, $P_{Toluene}$ = 0-40 torr. 28

Figure 2-7: a) Comparison between rate of acylation PAA= 40 torr, P2-MF= 2.6 torr at 160°C on fresh and spent HZSM-5 (Si/Al=40) catalyst with TPS-N2 at different treatment temperatures 300°C and 500°C under flowing N2 (125 SCCM). b) Comparison between rate of acylation PAA= 40 torr, P2-MF= 2.6 torr at 240°C on fresh and spent HZSM-5 (Si/Al=140) catalyst with TPS-N2 at 300°C under flowing N2 (125 SCCM). 30

Figure 2-8: Hard coke analysis (a) Evolution of IR spectra of spent HZSM-5 Si/Al= 40 as a function of temperature (BT= before treatment at 300°C, AT= after treatment at 300°C). Spectra are offset for clarity. (b) Propylene signals resulted from IPA-TPRx of fresh and spent HZSM-5 (Si/Al=40) catalyst samples used for BAS density quantification (c)

Estimating the mass of hard coke using TPO-TGA of spent HZSM-5 (Si/Al=40) catalyst after TPS-N2. 33

Figure 2-9: FTIR spectroscopy of HZSM-5 (Si/Al =40) at 160°C before treatment (BT) and after treatment at 300°C under flowing helium (AT) of spent catalyst after exposure of (a) 2-MF only for 60 min, (b) AA only for 60 min, (c) Ac-MF only for 60 min, (d) Ac-MF for 30 min followed by 2-MF for 30 min, (e) Ac-MF for 30 min followed by AA for 30 min, (f) Ac-MF for 30 min followed by water for 30 min, (g) Normal reaction conditions (rxn) for 3 hours. 36

Figure 2-10: FTIR spectroscopy of spent HZSM-5 (Si/Al=40) at 160°C after temperature treatment at 300°C under flowing helium (AT) of spent catalyst after exposure of, 2-MF only for 60 min (spent-2-MF-AT), AA only for 60 min (spent-AA-AT), Ac-MF only for 60 min(spent-Ac-MF-AT), Ac-MF for 30 min followed by 2-MF for 30 min, (spent-Ac-MF+2-MF-AT), Ac-MF for 30 min followed by AA for 30 min (spent-Ac-MF+AA-AT), Ac-MF for 30 min followed by water for (spent-Ac-MF+H2O-AT), (g) Normal reaction conditions (rxn) for 3 hours (spent-rxn-AT). A line to highlight the feature in the C=O bond stretching region is added to all spectra. 38

Figure 3-1 (a) XRD result suggests minimum effect on zeolite crystallinity upon relatively low phosphorous addition. (b) Propylene desorption signal obtained from IPA-TPRx for strong BAS quantification for the phosphorous modified ZSM-5 (Si/Al =140). (c) FTIR spectra for -OH stretching various phosphorous modified P-ZSM5 compared with parent HZSM-5 51

Figure 3-2 Solid-state ^{31}P -NMR of (a) 4P: Al (1.3wt%P) ZSM-5(140) (b) 1.3wt%P Silicalite-1 56

Figure 3-3 Comparisons of acylation rate of 2-MF with AA parent zeolite (0P) and various phosphorous modified zeolite with different loadings. Reactions were carried out at (a) 180C and b) 240C. 59

Figure 3-4: Measured activation energies for acylation of 2-MF with AA over 0P (parent zeolite), 2P, and 4P under reaction temperatures between 220-240°C 60

Figure 3-5 Initial Turnover frequencies (TOFs) of acylation over parent ZSM-5 zeolite (0P) and phosphorous modified ZSM-5 60

Figure 3-6 The decoupled rates for of strong BAS and P-induced sites as a function of phosphorous loading (b) Deconvoluted Activation barriers of acylation of 2-MF with AA over phosphorus induced BAS in 2P and 4P catalysts compared with parent zeolite (0P) at temperature range between 220-240°C. (c) The activation energy measured over 0.66wt% phosphorous silicalite-1 at temperature range between 240- 280°C 64

Figure 3-7 Measured deactivation constants for acylation of 2-MF with AA over parent zeolite (0P) and phosphorous modified zeolite (2P and 4P) at 240°C 66

Figure 3-8 the conversion of acetic acid to acetone over parent zeolite HZSM-5(40) (0P); compared with different phosphorous modified (P/Al= 0.5, 1, 2, 5) at 250°C. 69

Figure 4-1 Al^{27}-NMR for (a) H-MFI(40), AHFS-MFI(40) and H-MFI(140) (b) H-BEA(150) and AHFS-BEA(150) elucidating the tetrahedral coordinated Al (framework Al) in the chemical shift at 60 ppm, while the partially coordinated Al (non-framework Al) represented in the chemical shift at 0 ppm. 82

Figure 4-2 XRD result suggests removal of EFAL species via AHFS washing does not have any detectable damage to both (a) MFI and (b) BEA zeolites crystal structures 83

Figure 4-3 SEM images for (a) H-BEA(150) (b) AHFS-BEA(150) (c)H-MFI(40) (d) AHFS-MFI(40) (e) H-MFI(140) illustrating non-observable change in zeolite crystal morphology after AHFS treatment. 84

Figure 4-4 Initial turnover frequencies (TOFs) of H-MFI(40), AHFS-washed MFI(40), H-MFI(140), H-BEA(150), and AHFS-washed BEA(150) were determined under a reaction temperature of 160°C with a nitrogen flow rate of 125 ml/min. The catalyst loadings ranged from 5 to 20 mg, corresponding to a narrow range of Brønsted acid site density measured by IPA-TPRx. 86

Figure 4-5 Arrhenius plot presenting the median activation energies of (a) H-MFI(40) and H-BEA(15) zeolites that contains EFAL species contrasted with (b) H-MFI(140), AHFS-washed MFI(40), and AHFS-washed BEA(150) zeolites samples which does not have EFAL. Experiments were conducted under reaction temperatures 160,170 and 180°C and flowing N_2 at 125 ml/min. 89

Figure 4-6 Eyring plot of acylation over (a) H-MFI(40) and H-BEA(15) zeolites that contains EFAL species contrasted with (b) H-MFI(140), AHFS-washed MFI(40), and AHFS-washed BEA(150) zeolites samples which does not have EFAL. Experiments were conducted under reaction temperatures 160,170 and 180°C and flowing N2 at 125 ml/min. 90

Figure 4-7 Energy profile of acylation of 2-MF with acetic acid on BAS with the presence of EFAL $Al(OH)_2^+$ in two different proximities 94

Figure 4-8 Energy profile of acylation of 2-MF with acetic acid on BAS with the presence of EFAL $Al(OH)_2^+$ in proximity. The solid line represents reaction pathway 1 and dash line represents reaction pathway 2. 95

Figure 5-1 Reaction rate as a function of carbon chain length at 200°C 5-1 mol (Acid-2MF).. 104

Figure 5-2 Measured Activation of 2-MF acylation with different acyl donor at T =190-210°C and 5:1 mol (Acid-2MF). 105

Figure 5-3 Product selectivity of reaction of (a) Propionic-Acetic, (b) Butryic-Acetic, (c) Valeric-Acetic acids mixtures with ranging molar ratios at 200°C and fixed 5:1 mol (Acids: 2-MF) 106

Figure 5-4 Selectivity of acyl donor in acid mixture (Acetic: C_{3-6} 8:1 mole) toward Acylation of 2-MF at fixed 5:1 mol (Acids: 2-MF) at 200°C over HZSM-5 (Si/Al=140)..... 107

Figure 5-5 Parity plot of the calculated from Eley-Rideal model in Equation 5-5 reflected in the dashed line compared with measured rates for the different carboxylic acids acylation (acetic ■ , propionic ✳ , butyric ◆ ,valeric ▲) at 200°C and P_{acids} ~20 Torr $P_{2\text{-}MF}$ ~ 4 Torr. 110

Figure 5-6 Linear fitting plots of the natural logarithm fitting of activity a(t) for acylation with various acetic acid composition in (a) propionic, (b) butyric, and (c) valeric acid mixture. Reaction carried out at 200°C and P_{acids} ~20 Torr $P_{2\text{-}MF}$ ~ 4 Torr.....115

Abstract

Zeolites have garnered considerable attention in recent years as highly promising catalysts for direct Friedel-Crafts acylation reactions, employing renewable carboxylic acids, leading to the production of a versatile range of high-value fuels and essential commodity chemicals. In particular, the acylation of furanic compounds using carboxylic acids offers an enticing avenue for the sustainable synthesis of surfactants. Despite significant progress in recent years in enhancing our understanding of acylation reactions involving sustainable biomass-derived compounds via heterogeneous zeolite catalysis, there remains a notable knowledge gap concerning certain aspects of catalyst behavior, including activity, stability, and the factors influencing product selectivity.

In chapter 2, the catalyst deactivation mechanisms during acylation are investigated using commercial ZSM-5 zeolites with different Si/Al ratios. The role of 2-MF self-coupling, side reactions with ketenes, and sequential reactions with formed products are decoupled by feeding each species independently and comparing activity loss rates with those of varying surface coverage. The specific reactants employed in this study are 2-methylfuran (2-MF) and acetic acid (AA) to yield the product was 2-acetyl-5-methylfuran (Ac-MF). We reveal that the deactivation constant associated with direct 2-MF adsorption on a clean catalyst surface is approximately twice that of product self-coupling under identical conditions. Co-feeding carboxylic acids improves catalyst stability by diminishing the deactivation rate by several orders of magnitude via inhibiting adsorption of 2-MF and the formed products. Furthermore, evaluating the prominent route toward catalyst deactivation at high acid coverage was determined by systematic modification of surface coverage and the diffusion path of produced products. These results uncover the critical role of acetic acid to limit direct interaction between highly reactive acyl

acceptors with surface Bronsted sites. Moreover, the addition of varying partial pressures of non-reactive adsorbent molecules with significant adsorption constants allows manipulation of surface coverage while maintaining the gas phase chemical potential. These experiments show that the product (Ac-MF) reacting with gas phase 2-MF is the primary mechanism of deactivation at high acid coverage, not sequential reactions along the diffusion path or direct interaction of 2MF with the zeolite surface.

Based on the aforementioned results, we proposed that attenuating the acid strength could accelerate the product (Ac-MF) desorption which in return decreases the probability of a sequential reaction between the product and the gas phase 2-MF. A method was developed in chapter 3 involving incorporation of phosphorus in MFI zeolites which leads to decrease the acidity of Brønsted acid site in the catalyst. Here we report the acylation of 2-methylfuran with acetic acid over phosphorus-modified MFI zeolites with various phosphorus loadings. We show that at lower reaction temperatures (160°C), only the sites that are not titrated by phosphorus exhibit activity for acylation. However, when increasing the reaction temperature to 240°C the weaker phosphorus-modified sites begin to exhibit activity for acylation. Interestingly, the phosphorus-modified samples exhibited slower coke formation, and therefore deactivation, due to diminished side reactions.

The active sites in aluminosilicate zeolite have distinct activity that is subjective to several factors associated with the local environment. For example, the proximity of extra-framework aluminum (EFAL) to Brønsted acid sites (BAS) gives rise to distinct active sites exhibiting notably enhanced activity. In chapter 4, we undertake a comprehensive investigation into the acylation of 2-methylfuran (2-MF) using acetic acid (AA) over EFAL-incorporating MFI (Si/Al=40) and BEA (Si/Al=150) zeolites, then contrasting their behaviors after EFAL removal

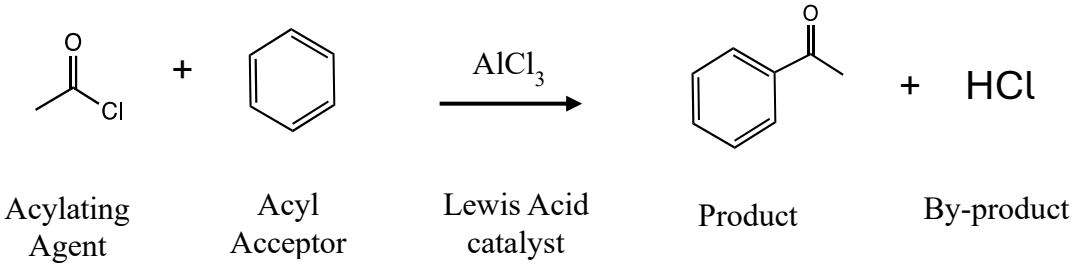
via ammonium hexafluorosilicate (AHFS) washing. EFAL concentrations were measured via solid-state Al^{27}-NMR analysis. Acylation under mild conditions, specifically within the 160-180°C range, remarkably uncovers higher activity over zeolites possessing EFAL, whereas reaction rates experience a pronounced decline post-AHFS treatment. Interestingly, the removal of EFAL leads to a twofold increase in measured activation barriers, aligning them with those observed for all-framework aluminum MFI (Si/Al=140) zeolites. DFT calculations are presented that agree with the experimental activation energies, highlight modifications to adsorbed intermediates and kinetically relevant transition states. Understanding this complex interplay between extra-lattice alumina and Brønsted acid sites is significant for comprehending the underlying factors that govern the kinetics of the reaction and holds key implications for optimizing catalytic performance. This study substantially contributes to understanding of zeolite-catalyzed acylation, offering a pivotal framework to enhance catalytic efficiency within the territory of renewable chemical synthesis.

The properties of acyl donor in acylation reactions play a significant role in determining the behavior of resulting products and their industrial applications in the commodity chemicals. In Chapter 5, we investigate the role of carbon chain length in direct acylation of 2-MF over HZSM-5 zeolite under varied conditions. Our research reveals that reaction rates increase with larger acids, despite the accompanying rise in activation barriers, due to the formation of more stable surface acyl intermediates. This increased stability can be attributed to a stronger adsorption, which was obtained from fitting Eley-Rideal kinetic model. Additionally, our experiments show varying deactivation rates of the catalyst during acylation with different carboxylic acid mixtures, underscoring the importance of co-feeding acetic acid alongside larger

carboxylic acids. The addition of acetic acid not only mitigates catalyst deactivation but also maintains product selectivity towards acylation with larger carboxylic acids.

Chapter 1: Introduction

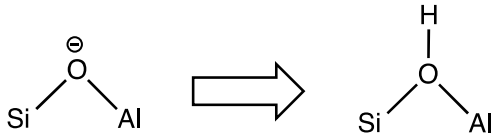
Organic chemistry represents a vast and highly complex area of research, offering boundless opportunities for the synthesis of essential compounds. In the world of organic synthesis, the Friedel-Crafts acylation reaction stands as a crucial foundation, offering a versatile platform for the manufacturing of numerous structurally diverse organic compounds[1]. First introduced by Charles Friedel and James Crafts in 1877[2], this important reaction has since evolved into a fundamental tool in chemical synthesis, enabling the rapid and efficient synthesis of valuable aromatic ketones from simple aromatic acyl acceptor compounds and acylating agents[3]. Indeed, these compounds serve as fundamental intermediates in the manufacturing of a wide array of essential products, including pharmaceuticals, cosmetics, and detergents, underlining the significance of the Friedel-Crafts acylation reaction in modern chemical synthesis[4].



Current industrial practices in acylation predominantly rely on non-sustainable methodologies utilizing acyl halides or acid anhydrides as acylating agents and petroleum-derived aromatic acyl acceptors. These processes necessitate the use of stoichiometric quantities and some cases more of homogeneous Lewis acid catalysts such as aluminum chloride ($AlCl_3$). Consequently, this conventional approach leads to significant waste generation and corrosion issues, posing notable hurdles to both economic feasibility and environmental sustainability of this chemical process[5].

Over the past decades, numerous research efforts have focused on exploring the application of solid acid catalysis in acylation reactions[4]. The advantages of utilizing heterogeneous catalysis extend beyond cost-effective separation of reaction mixtures to include non-sacrificial and reusable characteristics. Additionally, heterogeneous catalysts typically exhibit noncorrosive properties and produce minimal problematic side products. Among the array of solid materials investigated, aluminosilicate zeolite catalysts have emerged as particularly promising and extensively utilized catalysts in various industrial processes. Zeolite catalysts have gained attention for several decades owing to their high activity, selectivity, and stability in industrial processes[6].

Zeolites are microporous crystalline materials composed of tetrahedrally coordinated silicon and aluminum atoms, with oxygen atoms bridging between them, resulting in a framework structure consisting of interconnecting channels and cavities. The presence of Al^{3+} in the lattice results in negatively charged bridging oxygen between Si and Al, which is counterbalanced by a positively charged cation, typically hydrogen ions, formally by Brønsted protons, thus becoming the active site in zeolite catalysts[7].



Direct acylation over zeolite catalysts began to attract attention in the 1980s as a means to transition away from homogeneous Lewis acid catalysts[8-10]. B. Chiche et al. investigated the catalytic reaction of toluene and p-xylene with various carboxylic acids over Y zeolites, reporting yields exceeding 50% and impressive selectivity towards toluene with all tested carboxylic acids. Notably, the para/ortho isomer ratio was found to be 0.94, higher than the 0.79 observed with acylation over Lewis acidic catalyst $AlCl_3$. This improvement was attributed to the

shape selectivity of zeolites, arising from their confined channels within the microporous structure. In another study, the acylation of anisole with acyl chlorides and carboxylic acids was investigated over HY, HZSM-5, and H-BEA zeolites[9]. It was observed that zeolite mediated acylation resulted in a significantly higher ratio of intermolecular to intramolecular acylation compared to the use of the Lewis acidic catalyst $AlCl_3$. While the transition to a reusable heterogeneous catalyst offers economic and environmental benefits, the reliance on finite petroleum-derived reactants such as benzene or toluene raises sustainability concerns.

Biomass stands as a promising renewable reservoir for the production of fuels and chemicals, offering notable advantages in terms of life-cycle sustainability and scalability[11-13]. In recent years, there has been a surge in research attention towards upgrading biomass-derived chemicals using zeolite catalysts to yield biofuels and fine chemicals[14]. These biofuels and chemicals derived from biomass hold considerable potential as alternative energy sources, offering a promising pathway for addressing environmental challenges. Not only do they contribute to the reduction of net CO_2 emissions, but they also facilitate progress towards sustainability.

The fast pyrolysis of lignocellulosic biomass generates a complex array of chemically diverse oxygenated compounds, including phenolics, furanics, and carboxylic acids[15, 16]. These compounds serve as promising precursors for various carbon-carbon coupling reactions aimed at producing renewable fuels and commodity chemicals[17]. Direct acylation of biomass streams holds significant potential for selectively yielding renewable intermediates and additives capable of replacing conventionally produced acylated products. Dehydration of carboxylic acids over zeolites generates surface acyl species with characteristics akin to acylating agents, facilitating coupling with heteroaromatic acyl acceptors such as furanics. Despite the promise of

this direct acylation approach for bio-based chemicals over zeolites, challenges persist in optimizing catalyst activity, stability, and product selectivity, underlining the need for continued research and development in pursuit of green chemistry and sustainability goals.

Extensive studies have been conducted to investigate the utilization of biomass-derived compounds, such as 2-methylfuran (2-MF) and acetic acid (AA), as probe molecules for direct acylation over zeolites[18-20]. These investigations have encompassed a range of experimental methodologies, including kinetic measurements, catalyst assessments, and computational calculations aimed at elucidating kinetically relevant transition states. The findings from these studies have unveiled the remarkable selectivity of zeolite catalysts towards acylated products over self-ketonization of acetic acids, attributed to significant disparities in apparent activation energies[18]. It is important to note that maintaining a high molar ratio of AA to 2-MF has been identified as crucial for enhancing catalyst stability[18, 19]. It has been proposed that operating at a high surface coverage of AA can impede the direct interaction of 2-MF with active Brønsted acid sites (BAS), thereby inhibiting self-oligomerization and the formation of heavy carbonaceous deposits that contribute to catalyst deactivation. However, under certain conditions, an excess surface acyl species can lead to the generation of ketenes capable of oligomerization, further exacerbating catalyst deactivation. Despite ongoing research efforts focused on the direct acylation of 2-MF with AA over zeolite catalysts, many aspects, including alternative deactivation mechanisms, the nature of active sites, and the role of zeolite catalyst additives, remain relatively unexplored. Consequently, significant gaps in our understanding persist, presenting research opportunities to advance sustainable acylation pathways.

The primary objective of this dissertation is to conduct a comprehensive investigation into the direct acylation of 2-methylfuran with carboxylic acids over zeolite catalysts, building

upon our current understanding of the process. This research effort involves a systematic exploration of alternative deactivation mechanisms that may arise under conditions of fully saturated acyl surfaces. Furthermore, we aim to elucidate the role of common zeolite catalyst additives in mitigating deactivation phenomena and extending catalyst lifespan. Additionally, this study will investigate the local environment of Brønsted acid sites within zeolite structures and its implications for acylation activity.

In Chapter 2, evidence is presented that demonstrates a shift in catalyst deactivation mechanisms as a function of acetic acid surface coverage. The investigation focused on the acylation of 2-methylfuran with acetic acid over MFI catalysts, revealing a significant alteration in deactivation trends linked to the surface coverage of acetic acid. The results illustrate that a fully saturated surface with acetic acid effectively diminishes the deactivation rate by obstructing the direct interaction between furanic species and surface sites. Conversely, when the surface is saturated with acetic acids, deactivation occurs through reactions between adsorbed products and gas-phase methylfuran reactants.

The identification of deactivation mechanisms in Chapter 2 served as a motivation for investigating the role of phosphorus additives in modulating the acidity of active sites in Chapter 3, aimed at expediting product desorption and consequently mitigating catalyst deactivation. This section studies the acylation of 2-methylfuran with acetic acid over phosphorus-modified MFI zeolites with varying phosphorus loadings. At lower temperatures, the addition of phosphorus appears to impede catalyst activity; however, as the reaction temperature rises, phosphorus addition enhances activity. Notably, the incorporation of phosphorus into zeolites appears to suppress side reactions that lead to coke formation, thereby reducing catalyst deactivation.

Chapter 4 systematically investigates the influence of the local environment of Brønsted acid sites (BAS) in zeolites on acylation, with a specific focus on the presence of extra framework aluminum species (EFAL) in close proximity to BAS, which creates sites with distinct activities. The study explores the acylation of 2-methylfuran using acetic acid over EFAL-incorporating MFI and BEA zeolites, subsequently contrasting their behaviors and activities after the extraction of EFAL species. Notably, the catalyst's activity experiences a significant decline in acylation rates and approximately a twofold increase in activation energy following the extraction of EFAL species. Computational calculations support these experimental findings, suggesting that the presence of EFAL species enthalpically stabilizes the kinetically relevant transition states, thereby contributing to the observed enhancement in activity.

Chapter 5 sheds light on the influence of carbon chain length in acyl donors on reaction activity, product selectivity, and catalyst stability in sustainable acylation reactions. The study investigates the acylation of 2-methylfuran with various carboxylic acids (acetic, propionic, butyric, valeric, and hexanoic acids) over a zeolite catalyst. The results underscore the significance of surface reaction intermediate stability in enhancing both rates and selectivities, despite the higher measured activation energies associated with larger acids. This observation is corroborated by the prediction of adsorption constants obtained from fitting the Eley-Rideal kinetic model. Additionally, estimated deactivation constants for acylation with each acyl donor indicate that larger acids tend to contribute to catalyst deactivation. Addressing catalyst stability necessitates the co-feeding of acetic acid to dilute larger acids in the stream, which does not compromise product selectivity due to the stronger adsorption of carboxylic acids with longer alkyl groups.

Chapter 2: Shifts in catalyst deactivation mechanisms as a function of surface coverage during Friedel-Crafts acylation in zeolites

This chapter is a published work in "Journal of Catalysis 426, 222-233". The authors are Ismaeel Alalq, Huy Nguyen-Phu, and Steven Crossley

Abstract

The production of commodity chemicals from renewable resources is often accompanied by rapid catalyst deactivation rates. An important example is direct Friedel Crafts acylation, which can yield a range of valuable products from surfactants to renewable transportation fuels. Furanic acyl acceptors are among the most intriguing and promising possible acceptors; however, they undergo self-coupling reactions in the presence of Brønsted acid surface sites leading to rapid catalyst deactivation. In this contribution, we study acylation of 2-methylfuran with acetic acid over HZSM-5 catalysts at temperatures ranging from 160-240°C, revealing the remarkable shift in deactivation behavior as a function of surface coverage of acetic acid. We reveal that a surface saturated with acetic acid lowers the deactivation rate by blocking the direct access of furanic species to surface sites. However, on surfaces fully saturated with carboxylic acids, deactivation is revealed to proceed via reactions between adsorbed products with gas phase methylfuran reactants.

2.1 Introduction

Friedel-Crafts acylation is an important and attractive process for the formation of C-C bonds with renewable feedstocks. Products of this reaction are typically commodity chemicals such as fragrances, surfactants, and renewable fuels.[4] This reaction involves an acylating agent such as acyl chloride and an acyl acceptor, which usually consists of aromatic or heteroaromatics rings. The traditionally common catalyst for this reaction is aluminum trichloride ($AlCl_3$).[21] This

catalyst, however, produces large amounts of waste, which detrimentally influence the economic and environmental impact of this chemistry[5].

In contrast, upgrading biomass-derived chemicals via the direct acylation of heteroaromatics with carboxylic acids over zeolite catalysts can enable more renewable and sustainable routes toward producing valuable chemicals while minimizing waste and improving efficiency. The acylation of furans directly over zeolites has been reported both with acetic acid (AA) [18] and with larger organic acids/anhydrides[22] to produce fuels and high value chemicals. The prospective use of acylation chemistry to yield fuels is potentially more carbon efficient resulting in higher overall efficiency and resulting lifecycle energy return on investment when compared with other more common catalytic upgrading approaches that lose some C to light gas phase biproducts such as ketonization.[23-25]

Further advancement in acylation chemistry requires advancement in our understanding of not only the chemistry occurring on the zeolite surface that influence reaction rates, but also the aspects that lead to catalyst deactivation. A variety of carboxylic acids found in biomass-derived streams could serve as promising acylating agents, while promising acyl acceptor candidates include cellulose and hemicellulose derived furanics[18] and lignin-derived phenolics[22, 26, 27], both of which represent common platform molecules from biomass [17-20, 22, 28-30] and are typically better acyl acceptors than unfunctionalized aromatics. While many advancements have been made in recent years regarding improved understanding of acylation mechanisms on the catalyst surface with these renewable precursors, much less is understood regarding the side reactions that occur in parallel and ultimately lead to catalyst deactivation.

Furanic species, while appealing as acyl acceptors, have a tendency to cause catalyst deactivation when in contact with Brønsted zeolites. Recent reports have shown that this deactivation can be significantly influenced by the concentration of furanics in the feed, and the surface coverage of carboxylic acids which limit direct interactions of furanics with the Brønsted sites on the zeolite surface.[18, 19] The well-known propensity to form coke when furanic species are in direct contact with the catalyst suggests that this is the primary factor of consideration when improving catalyst stability. However, at high coverage of carboxylic acids, deactivation still persists via an unknown mechanism. This work aims to clarify the pathways responsible for deactivation under these regimes, allowing for further improvements in yields and stability.

In this manuscript, the reason behind the catalyst deactivation during the acylation reaction of 2-methylfuran (2-MF) with acetic acid (AA) over HZSM-5 zeolites is evaluated over clean and acid saturated surfaces. We show how each reactant and product species influences deactivation rates via controlled independent introduction of each compound under a wide range of conditions. Rates of active site loss are quantified, clarifying the underlying cause of catalyst deactivation. Further insight is attained by introducing toluene, which due to its diminished rates as an acyl acceptor serves as a strongly binding site inhibitor under these conditions. Modifying toluene partial pressure, as well as manipulation of acid site density via selective exchange of active sites, allows us to evaluate the role of sequential reactions along the diffusion path within the zeolite crystallites under reaction conditions.

2.2 Experimental section

2.2.1 Chemicals and materials

The HZSM-5 catalysts sample used in this study are commercial grade obtained from Zeolyst international (CBV2314 Si/Al = 11.5, CBV 5524G Si/Al = 25, CBV8014 Si/Al = 40, and

CBV28014 Si/Al= 140). These samples were received in the ammonium-ion form and calcined to obtain the proton form. The calcination was carried out in 1 inch quartz tube under air flow of 100 standard cubic centimeters per minute (SCCM) and heated inside an oven at ramp rate of 2°C/min to 600°C then kept for 5 hours. CBV8014 Si/Al = 40 catalyst was employed in most reactions while other catalyst samples will be noted in when are used. The sodium exchanged sample (Na-ZSM-5) was obtained by partially titrating Brønsted acid sites (BAS) in CBV28014 Si/Al= 140. This was prepared by adding 2 grams of CBV28014 in a 40 mL 0.004M $NaNO_3$ solution under stirring at 700 rpm for 30 min at room temperature then washed and filtered five times. The collected sample was dried and calcined using the same procedure mentioned earlier. The acylating agent is acetic acid (glacial, ACS reagent, ≥99.7%, Sigma-Aldrich). The acyl acceptor is 2-Methylfuran (98+%, stab., Alfa Aesar). Toluene (ACS reagent, ≥99.5%, Sigma-Aldrich) was added as non-reactive adsorbant in some cases to manipulate the surface coverage of the catalyst. The carrier gas used for the experiments was nitrogen (ultra high purity GD 5.0). The trace levels of the stabilizer butylated hydroxytoluene present in purchased 2-Methylfuran was removed via distillation prior to use as a reactant.

2.2.2 Catalyst Characterization

2.2.2.1 IPA-TPRx measurements

Isopropylamine temperature-programmed reaction (IPA-TPRx) was used to quantify Brønsted acid site density in the catalyst samples. Catalyst samples were packed in 1/4-inch quartz tube and then pretreated under helium flow of 30 ml/min heated at 10°C/min to 300°C and held for 1 hour. The temperature was then reduced to 100°C. Catalyst samples were exposed to several 2uL IPA pulses to saturate the Brønsted acid sites thoroughly, then allowed the helium to flow for 1 hour to remove the physiosorbed or weakly adsorbed IPA. The TPD started by ramping the

temperature from 10°C/min to 600°C. The evolution of desorbed species was continuously monitored by a Cirrus mass spectrometer (MKS) recording the following signals m/z = 17 and (NH_3), 44 (IPA), and 41 (propylene). The Brønsted acid site density was quantified by calibrating the MS signals using the average of several 0.5 mL-pulses of propylene.

2.2.2.2 Pore volume measurements

The micropore volume of fresh and spent catalyst samples were evaluated by the T-plot method. Nitrogen adsorption analysis was implemented on a Micromeritics ASAP 2020 at liquid nitrogen temperature (-196 °C). Catalyst samples were degassed at 350 °C with a heating rate of 5 °C/min in vacuum pressure for 10 hours to remove physiosorbed moisture and volatile impurities. The weight of the dried sample after degassing was measured and corrected. Then, the sample was cooled down to -196 °C for nitrogen adsorption analysis.

2.2.2.3 IR Spectroscopy

The retained species on the surface of the spent HZSM-5 catalyst has been analyzed using infrared spectroscopy in a PerkinElmer Spectrum 100 FT-IR Spectrometer equipped with Harrick Praying Mantis chamber. The background was measured using KBr (FT-IR grade, ≥99% trace metals basis) from Sigma Aldrich. The spent catalyst was placed on top of a layer of KBR to reduce sample thickness and increase signal during diffuse reflectance. The spent catalyst was heated at a ramp rate of 10°C to temperatures 160°C, 200°C, 240°C and 300°C under flowing helium at rate of 50 ml/min where 64 scans has been performed for each temperature to track the evolution of the spectra of the spent catalyst. Then, the temperature was cooled down to 160°C (the usual reaction temperature) to observe the spectra region of the retained species (hard coke) after removal of the soft coke by helium sweeping.

2.2.2.4 Pyroprobe System

Retained surface species (soft coke) was analyzed using a CDS Analytical Pyroprobe 5250T. Spent catalyst sample (ranging between 2 mg and 3 mg) was loaded into a fire polished quartz tube *(CDS Analytical, 10A1-3015).* A filler rod *(CDS Analytical, 10A1-3016S)* was inserted within the quartz tube to seal the bottom. Small amount of quartz wool *(CDS Analytical, 0100-9014)* is placed on top of the filler rod where the spent catalyst sample rests. The sample tubes are sent via autosampler to a platinum coil jacket which is heated rapidly to temperatures between 300-500C° and held for 5 min. Concurrently, a sweeping flow of helium gas at 14 mL/min directly carries out the vapor of the desorbed species from the spent catalyst and then sent to a GC-MS (Shimadzu QP2010S + GC/MS-FID system). The GC-MS is equipped with a 60 m semi-polar Restek RTX-1701 column with thickness and diameter of 0.25 μm and 0.25mm.

2.2.2.5 Thermogravimetric analysis

Thermogravimetric analysis (TGA) was performed on a Netzsch STA 449F1 equipped with a pin thermocouple and a Netzsch nano balance to quantify the amount of coke formed on the spent HZSM-5 catalyst sample during acylation reactions. After the reaction, N_2 sweeping at 125mL/min was employed on spent catalyst at ramp rate of 10 °C/min to 500°C for 1 hour to remove the soft coke and accurately account for the hard coke. Then, temperature program oxidation (TPO) was carried out under flowing air (50 ml/min). The spent catalyst sample was heated from room temperature up to 600 °C at the ramp rate of 10 °C/min, held at 600 °C 30 min and cooled down to the original temperature of 40 °C. The coke on the sample was determined by the weight loss of the sample after the TPO experiment.

2.2.3 Catalytic reaction

The acylation of 2-MF with AA over HZSM-5 zeolites was carried out in the gas phase in a fixed bed tubular reactor. A measured amount of catalyst between 4-100 mg mixed with glass beads packed between quartz wool in a 1/4-inch quartz reactor tube was then pretreated at 10°C/min to 300°C and held for 1 hour under flowing nitrogen to remove physiosorbed moisture then cooled down to reaction temperature (160°C in most cases). The nitrogen carrier gas flow was set at 125 SCCM and adjusted accordingly to maintain a constant partial pressure of 2-MF (introduced at 0.1 mL/hr via a liquid phase syringe). Reactions carried out with AA under 1^{st} order reaction conditions were performed at an AA flowrate between 0.05-0.15 mL/hr in a room temperature liquid syringe, while AA was fed at flow rate between 1-2 mL/hr when operating in the 0^{th} order regime with respect to AA. No detectable gas phase reaction products were observed under our reaction conditions aside from the acylation product reported. The reactor temperature was controlled via an attached thermocouple to the external surface of the reactor tube aligned with the center of the catalyst bed. After the catalyst pretreatment, the temperature was set to the desired reaction temperature and, the reactant feed rate was controlled using syringe pumps. The reactor outlet streamline was heated to 250°C to avoid condensation of leaving species. A micro electric actuator controlled the six-port valve used to send the sample to an inline connected gas chromatograph Agilent 7890B equipped with a flame ionization detector and Zebron Phase: ZB-WAX (L × ID × thickness = 30m ×0.25mm ×0.25μm) column for separation of molecules in this reaction. The samples were collected from a glass trap connected to the vent line and products identified via Shimadzu GCMS-QP2010S. The reactant's response factor was achieved by flowing the reactant at the desired rate through a glass beads bed to mimic the catalyst bed, while the product response factor was attained by injection of standards. These response factors are used for

further data analysis, such as conversion and carbon balance. The values for turnover frequency (TOF) were obtained using the following equation: -

$$\boldsymbol{TOF} = \frac{\boldsymbol{Moles\ of\ product\ formed\ per\ gram\ of\ catalyst}}{\boldsymbol{Moles\ of\ Brønsted\ acid\ sites\ per\ gram\ of\ fresh\ catalyst}} \left(\frac{\boldsymbol{1}}{\boldsymbol{s}}\right) \qquad \textbf{\textit{Equation 2-1}}$$

We emphasize here that the TOF references the number of active sites in the catalyst prior to introduction of the reactant. Thus the loss in what is referred to as TOF as a function of time is actually a reduction in the number of accessible active sites. Thus, if TOF is reported it is to facilitate an easier comparison between catalyst samples with varying site density. The dimensionless turnover number (TON) was calculated by integration of the turnover frequency with respect to time on stream using Equation 2-2: -

$$\boldsymbol{TON} = \int_0^t \boldsymbol{TOF}\ (\boldsymbol{t})\boldsymbol{dt} \qquad \textbf{\textit{Equation 2-2}}$$

All conversion levels of the limiting reactant 2-MF were maintained at under 10% unless explicitly mentioned and estimated using the following equation: -

$$\boldsymbol{methylfuran\ conversion} = \frac{\boldsymbol{Moles\ of\ acylated\ product\ formed\ per\ hour}}{\boldsymbol{Moles\ of\ 2-methylfuran\ fed\ per\ hour}}\ (\boldsymbol{mol}\%) \qquad \textbf{\textit{Equation 2-3}}$$

The initial reaction rates were obtained by extrapolation to zero time on stream and used to accurately evaluate the catalyst deactivation during acylation.

2.3 Results and Discussion

2.3.1 Assessment of kinetic rates

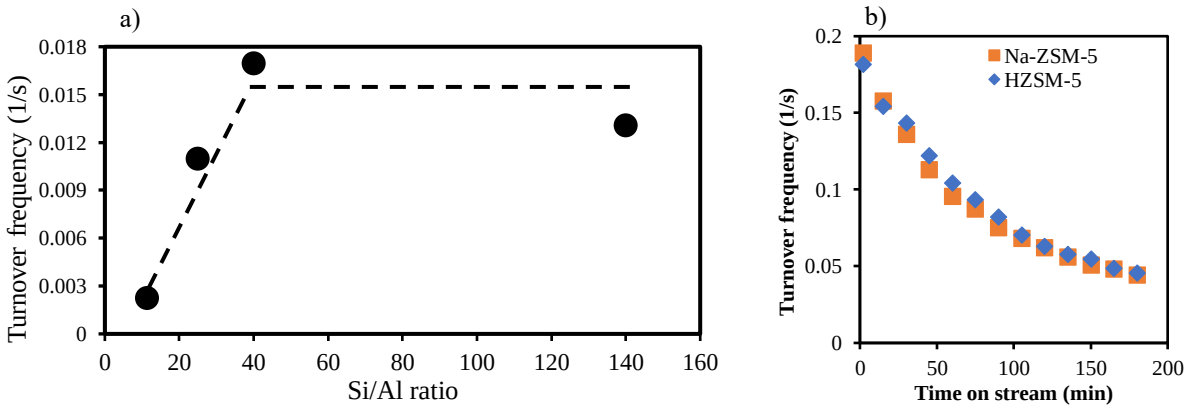


Figure 2-1: a) Testing diffusion and reaction on HZSM-5 catalyst samples with different Si/Al ratios. CBV2314 Si/Al = 11.5, CBV 5524G Si/Al = 25, CBV8014 Si/Al = 40, and CBV28014 Si/Al= 140) at 160°C after catalyst pretreatment at 300°C for 1 hour to remove the physiosorbed water. PPAA=40 Torr, PP2-MF= 2.6 Torr. Lines are to guide the eye. b) Loss of BAS activity for Na titrated Na-ZSM-5 (25% of BAS exchanged) and parent HZSM-5 both with (Si/Al = 140) at T=240°C with PAA= 40 torr, P2-MF= 2.6 torr.

The acylation of 2-MF with AA over HZSM-5 occurs at temperatures as low as 160°C to yield acetyl-methylfuran (Ac-MF) isomers and water. We note that these temperatures are considerably lower than those used in most acylation studies, which is an attempt to readily achieve acid saturated conditions at modest pressures. Operating under these conditions also facilitates avoidance of thermodynamic and diffusion limitations that would corrupt the kinetic data that is obtained.[31] All rates reported here are far from thermodynamic equilibrium values, as verified by increasing the catalyst loading as shown in Figure S2-1a. This conversion level of 37% with the limiting reactant (2MF) results in an equilibrium constant obtained at 160°C of 0.014 as defined by Equation 2-4.

$$K = \frac{(Acylation\ product)*(H_2O)}{(2-methylfuran)*(acetic\ acid)} \qquad \textit{Equation 2-4}$$

This equilibrium constant is remarkably similar to the equilibrium constant obtained based upon the overall Gibbs free energy of reaction at 250°C of 4.5 kcal/mol reported recently for the same reaction by Chen et al.[20], which translates to an equilibrium constant of 0.013 obtained via Equation 2-5.

$$K = exp\left(\frac{-\Delta G}{RT}\right) \qquad \textit{Equation 2-5}$$

Other groups [19] have recently reported even higher equilibrium constants for this reaction, implying that the conditions we are reporting here are all far from corruption due to approaching thermodynamic equilibrium values.

As mentioned in the section 2, all experiments were performed at conversion levels of the limiting reactant 2-MF of 10% or below unless otherwise noted. The only exceptions are the experiments carried out at 240°C with AA partial pressures ranging between 40-60 Torr, as lower conversion levels could not be obtained while maintaining a sufficient catalyst bed size. Under these conditions, the conversion of 2-MF was 23%. We note that under these conditions, the reaction is still far from the equilibrium conversion of 44% (Figure S2-1b), which translates to an equilibrium constant of 0.023 at this temperature.

In order to confirm that the rates reported here are not controlled by internal or external diffusion to the active sites, various HZSM-5 catalysts with different Brønsted acid site (BAS) densities (CBV2314 Si/Al = 11.5, CBV 5524G Si/Al = 25, CBV8014 Si/Al = 40, and CBV28014 Si/Al= 140) were employed. This is following the Koros-Nowak criteria, [32] later elaborated upon by Madon-Boudard,[33] which presumes that by altering active site density within a catalyst particle, without modifying the nature of the particle or active site itself, one may compare turnover frequencies to assess the importance of diffusion corruptions to the data. It is clear from these results that over the Si/Al =140 catalyst, internal diffusion does not limit reaction rates as shown

in Figure 2-1. We acknowledge that this conclusion presumes that the activity per site is identical for each of these catalysts, which carry varying Si/Al ratios. It is generally accepted that the acid strength of various Brønsted sites resulting from Al incorporation within zeolites are approximately the same. However, we acknowledge that the presence of more proximate acid sites, varying site location, or sites with extra lattice Al species may perturb reaction rates.[34-36] Therefore, by taking the lowest acid site density catalyst (Si/Al=140) and performing Na exchange and carrying out the reaction under significantly higher temperatures (240°C) where the role of diffusion is more likely to impact rates, one observes that identical turnover frequencies result. This suggests that the MFI 140 catalyst is clearly not corrupted by diffusion under these reaction conditions. The slightly elevated TOF observed with Si/Al= 40 when compared with Si/Al=140, in spite of the higher acid site density of the former, could be attributed to modest enhancements in rate due to the other factors described above (site location, proximity, or extra lattice species).

2.3.2 Role of surface coverage of AA

Catalyst deactivation can inherently be assessed under conditions that are limited by the rate of the reaction on the catalyst surface. Figures 2-2 a and c reveal that the reaction rate steadily declines with time on stream across a wide range of acetic acid partial pressures. The rate of activity loss is indeed a strong function of acetic acid coverage, which as depicted in Figure 2-2b spans from nearly first order at low AA partial pressures (2-6 Torr) to 0th order at high pressure (40-80 Torr). Figure 2-2c clearly demonstrates that the loss in activity is far less pronounced at higher acid coverage (higher AA partial pressure), as has been observed in prior studies, [18, 19, 37] but deactivation persists. While the direct interaction of 2-MF with the Brønsted sites on the zeolite[18, 19, 37] have been proposed as the main cause of activity loss at low acid coverage, there is an alternative and unexplored deactivation mechanism that becomes prevalent under high

coverage conditions. To ensure that operating at lower temperatures does not lead to any experimental artifacts such as reactant or product condensation within the pores that would otherwise corrupt this analysis, we conducted the same reaction at elevated temperature of 240°C and observed similar deactivation behavior with respect to AA surface coverage as presented in Figures 2-2 d, e, and f.

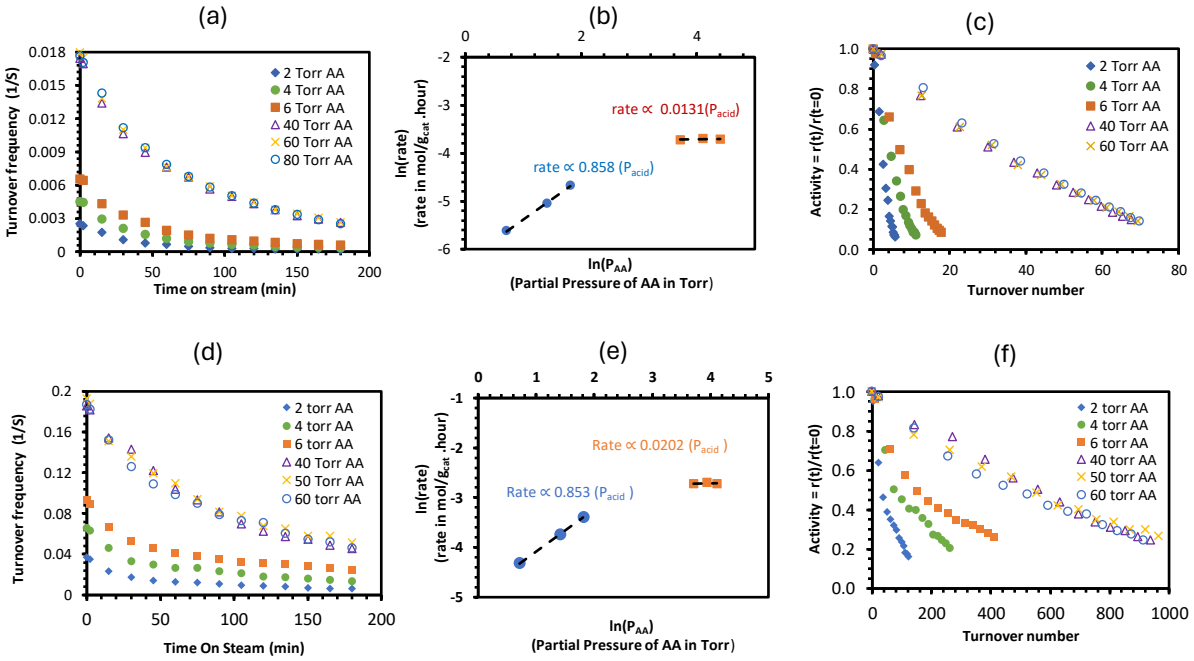


Figure 2-2 Influence of surface coverage of AA on decay rate(a) Turnover frequency vs time on stream of low and high AA coverages. (b) Reaction order wrt AA at low and high coverages of AA. (c) Catalyst activity vs turnover number at low and high coverage AA. Results in (a), (b), and (c) obtained from reaction on HZSM-5 (Si/Al=40) at 160°C. Data in (d), (e), and (f) was collected from reaction on HZSM-5 (Si/Al=140) at 240°C

2.3.3 Deactivation due to contact with individual species

To decouple the severity of each contributing species on deactivation rates, each species was fed independently for a certain period before introducing both reactants. By pre-introducing the acyl acceptor (2-MF), acylated product (Ac-MF), and acylating agent (AA) independently prior to introducing all reactants, one can discern the independent deactivation rates posed by each over a bare catalyst surface at 160°C over HZSM-5 (Si/Al=40).

Figure 2-3 shows that pre-feeding 2-MF for only 1 min led a loss of more than 67% the initial catalytic activity. This illustrates the potential of methylfuran to severely form coke over a bare catalyst surface, even at moderate temperatures. It has been previously reported that 2-MF can form dimers and trimers through hydration/dehydration and self-coupling on BAS[30] as illustrated in Figure 2-4 , eventually yielding species that are unable to desorb from the catalyst surface. While 2-MF has often been proposed as a main cause of deactivation,[38-40] these results illustrate just how rapidly it can deactivate Brønsted sites.

Introducing the product Ac-MF, followed by a purge in inert gas prior to introducing acetic acid and measuring reaction rates, also results in rapid activity losses. The Ac-MF was pre-fed at a rate equimolar to 2-MF. Interestingly, the rate of deactivation due to product self-coupling reactions appears to be less rapid than those observed upon injection of 2-MF alone, as shown in Figure 2-3. The rapid deactivation rates observed are in agreement with previous reports where the acylated product was proposed as a coke precursor. [29]

Exposure of only acetic acid is known to yield both acyl species and ketenes, but the contribution of these species to deactivation under these conditions is minimal. This is evident in Figure 2-3, where pre-feeding AA for extended periods of time results in much lower rates of activity loss when contrasted with the other pre-fed molecules. The losses reported are likely due to reactions with the formed ketenes that are produced in low concentrations.[41]

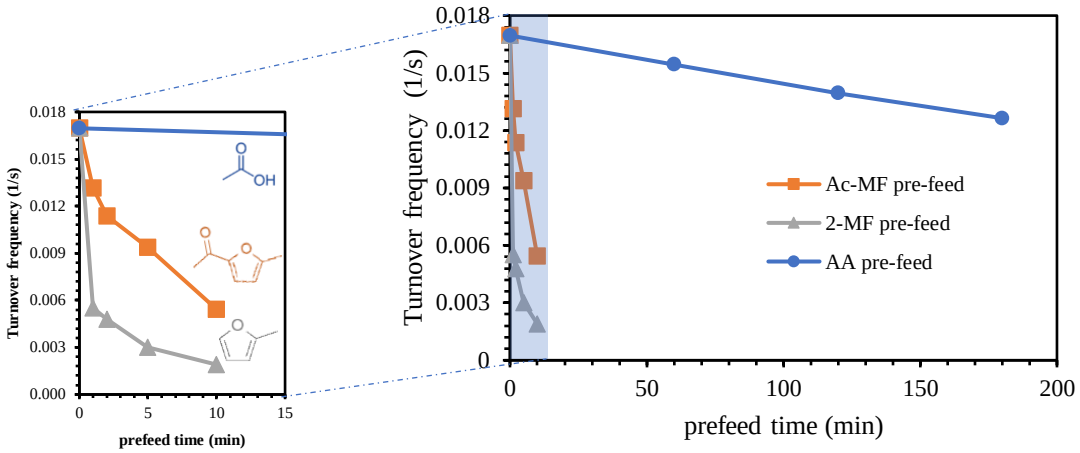


Figure 2-3: ***(▲) Comparing initial active site loss resulting from the introduction of 2-MF for 1,2,5, and 10 minutes prior to adding the other reactant (AA) to the feed to start the reaction. (■) Comparing initial active site loss resulting from the introduction of the product (Ac-MF) for 1,2,5, and 10 minutes prior to adding the reactants to the feed to start the reaction. (●) Comparing initial active site loss resulting from the introduction of AA for 15, 60 ,120, and 180 minutes prior to adding the other reactant (2-MF) to the feed to start the reaction. All reactions run on HZSM-5 (Si/Al=40) at 160°C after catalyst pretreatment at 300°C for 1 hour to remove the physiosorbed water. PP_{AA}=40 Torr, $PP_{2\text{-}MF}$= 2.6 Torr. Molar flow rates during prefeed for both 2-MF and Ac-MF are equal.***

While the very distinct contributions to catalyst deactivation shown in Figure 2-3 are obvious upon exposure to a bare catalyst surface, it is helpful to compare these results with those when both reactants are fed simultaneously in Figure 2-2. Deactivation rates in all cases when acetic acid is co-fed along with 2-MF are dramatically reduced when contrasted with 2-MF or product introduced to the catalyst alone. However, the rate of catalyst deactivation in figure 2-2 upon co-introduction of reactants is still significantly larger than those observed in Figure 2-3 upon exposure to acid alone. This implies that ketenes resulting from surface acyl species, or ketones formed from acid self-coupling are not the main sources of deactivation under these reaction conditions.

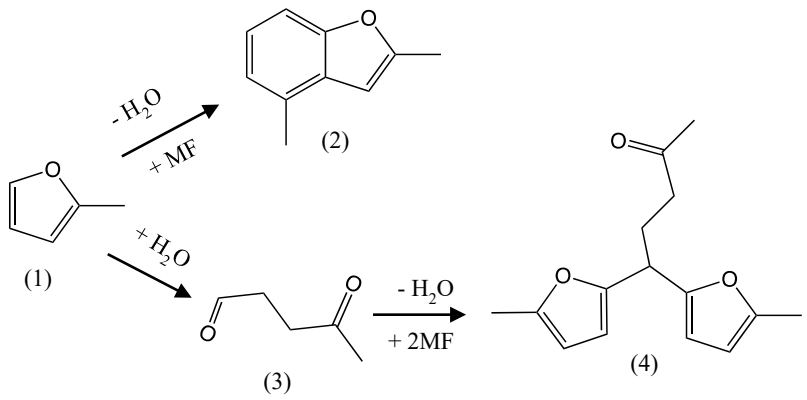


Figure 2-4 Reaction of (1) 2-MF on BAS forming (2) dimers through dehydration then self-coupling or hydration then ring opening to (3) 4-oxopentanal followed by dehydration and self-coupling to form (4) trimers.[30]

2.3.4 Modification of available surface sites to investigate deactivation pathways

Because it is known that both the product Ac-MF and the feed 2-MF rapidly deactivate the catalyst when exposed to Brønsted acid sites, the underlying cause of deactivation can result from a variety of potential pathways. The three most likely deactivation pathways are depicted in Figure 2-5. The simplest explanation (scenario A) is the competitive adsorption of the coke forming agent (2-MF) with acetic acid, where the adsorbed 2-MF is rapidly activated and further reacts with gas phase 2-MF species to yield larger species that do not leave the surface and ultimately deactivate said active sites, such as those depicted in Figure 2-4. Deactivation rates following this pathway would be dictated by the ability of 2-MF to compete for surface sites. A graphical representation of this case is shown in Figure 2-5a. Alternatively, in the scenario B, the formed product may desorb and subsequently react along the diffusion path of the zeolite to form larger species that ultimately lead to deactivation. This would imply product desorption and sequential interaction of these products with other surface species, such as other adsorbed products along the diffusion path to form species that do not desorb and deactivate sites. In this scenario, a longer diffusion path (larger crystallite size or higher site density) would promote more rapid deactivation. Scenario C

postulates that the adsorbed products sequentially interact with gas phase reactants such as 2-MF before they desorb from the active site where they were formed.

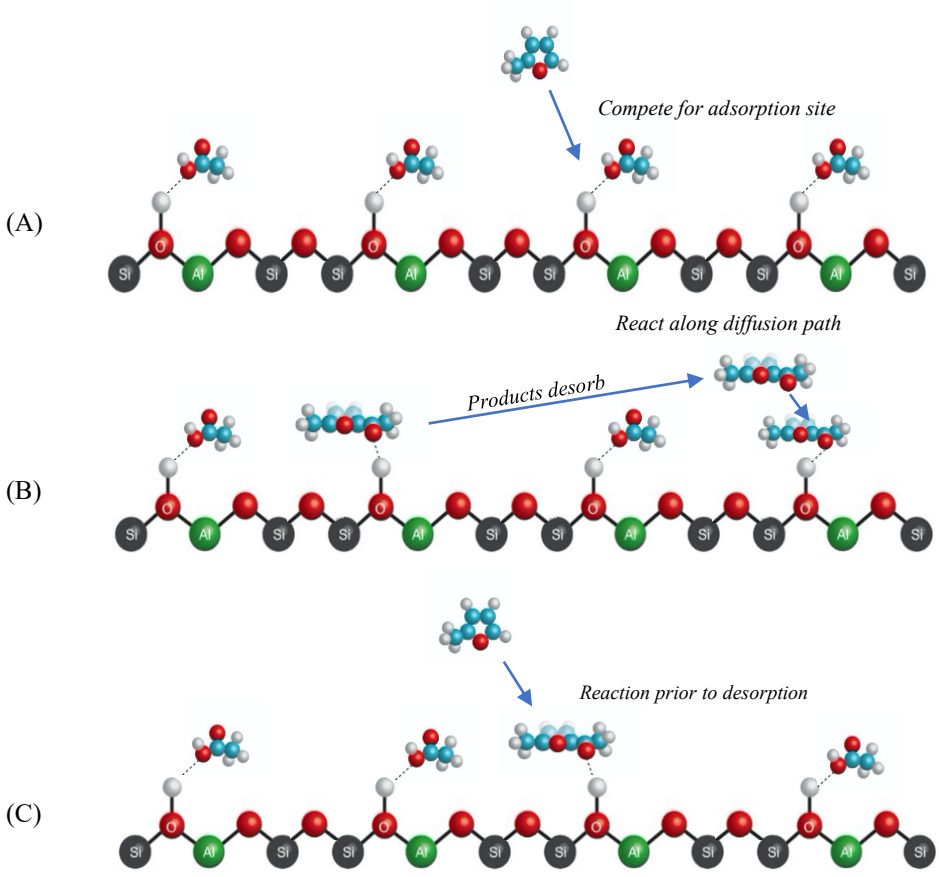


Figure 2-5: Proposed cause of deactivation. (A) 2-MF compete with adsorbed acetic acid. (B) Product re-adsorption along the diffusion path. (C) sequential reaction of product prior to desorption

Under conditions depicted here where the partial pressure of the acyl acceptor 2-MF is maintained as constant, the reaction rate is proportional to the coverage of acetic acid on the surface, as shown in Equation 2-6 and Figure 2-2b and 2-2e, which subsequently converts to form surface acyl species. For simplicity, adsorption of 2-MF and product are not incorporated within the equation, as the partial pressure of 2-MF is low and constant, and the conversion is maintained at low levels.

$$\textbf{Acylation rate } (\textbf{at constant } P_{2MF}) \propto k\theta_{AA} \propto \frac{kK_{AA}P_{AA}}{1+K_{AA}P_{AA}} \qquad \textbf{Equation 2-6}$$

We note that prior reports have used TPD studies to suggest that acetic acid is bound to the surface with at least comparable energetics as 2-MF,[19] implying that at the high excess concentration of AA, 2-MF direct competition for active sites as depicted in Scenario A will be challenging. To further study the role of site competition, we employ additional species to make this site competition even more challenging to evaluate its relevance in deactivation pathways. Under conditions where the surface is saturated with acetic acid, added non-reactive species that adsorb to surface sites will simply lower acetic acid surface coverage, and therefore lower observed rates, requiring consequential increased partial pressures of acetic acid to compensate and increase the rate to that which was observed without inclusion of these additional non-reactive species. The reaction rate in this case can be described by Equation 2-7. Adding a non-reactive species (in this case toluene) not only influences reaction rates, but also can modify deactivation (Equation 2-8). The outcome of this will depend heavily on the particular species responsible for deactivation, which could be either adsorbed 2-MF undergoing self-coupling reactions (scenario A or B) or the adsorbed product participating in secondary reactions with gas phase 2-MF (scenario C), as discussed above. P_D in Equation 2-8 is used to represent this deactivating species, either adsorbed 2-MF or the product Ac-MF. Regardless of the species responsible, it is reasonable to assume that this species is activated over the catalyst and interacts with 2-MF to yield higher molecular weight species that ultimately result in catalyst deactivation.

$$\boldsymbol{Acylation\ rate\ (at\ constant\ P_{2MF}) \propto k\theta_{AA} \propto \frac{kK_{AA}P_{AA}}{1+K_{AA}P_{AA}+K_{toluene}P_{toluene}}} \qquad \textbf{Equation 2-7}$$

Assuming the species that ultimately interacts with either a) surface or b) adsorbed species to form larger products that result in catalyst deactivation is equilibrated with the gas phase, the addition of toluene will diminish deactivation rates, as would be the case in scenario A or scenario

B in Figure 2-5. Scenario C assumes the product is not yet equilibrated with the gas phase and therefore the presence of toluene will not influence deactivation rates.

$$\textbf{\textit{Deactivation rate}} \propto k_D\theta_D \propto \frac{k_D K_D P_D P_{2MF}}{1+K_{AA}P_{AA}+K_{toluene}P_{toluene}+K_D P_D} \qquad \textit{Equation 2-8}$$

In this case, toluene is employed as a non-reactive species due to its strong binding affinity for Brønsted acid sites as well as the well-established high barrier for the acylation reaction. Toluene is a far inferior acyl acceptor when compared with 2-MF.[18, 42] When contrasting the ability of toluene to compete for adsorption sites along with 2-MF and AA, we note that the proton affinity (PA) of Toluene is (784 kJ/mol)[43], which is identical value to the PA of AA[19] (784 kJ/mol). Although PA of 2-MF is higher (866 kJ/mol) than both AA and Toluene, it is suggested that adsorption competition can be further influenced may multiple factors in addition to proton affinity, such as the size of the molecule within the confining environment, hydrogen bonding, [19] and other factors that can alter adsorption energetics, which implies that factors in addition to proton affinity influence interactions of various molecules with the active sites.[44] The potential of toluene to compete for sites coupled with the lack of reactivity under these conditions makes toluene a promising candidate to modify surface coverages. Introducing non-reactive compounds is sometimes proposed as a route to mitigate catalyst deactivation rates.[45]

The influence of toluene on reaction rates is shown in Figure 2-6a, where it is clear that toluene effectively competes with acetic acid and diminishes observed reaction rates as would be expected from Equation 2-7. It is important to note that the gas phase partial pressure of AA and 2-MF were maintained constant in all cases. Figure 2-6b then shows that by further increasing the partial pressure of AA, turnover frequencies consistent with an acid saturated surface are achieved once again. The conditions consisting of a 1:0 vs. 2:0.5 molar ratio of AA to toluene are ideal for investigating deactivation reaction pathways. In this instance, following Equation 2-8, because 2-

MF is maintained at an identical partial pressure, the coverage of 2-MF on the surface will be significantly reduced in the latter case where there is the competitive adsorption of toluene, while conversion and turnover frequency is constant. The same experiments were conducted at a higher temperature (240°C) as presented in Figures S2-8a and b, reveal similar behavior when varying toluene and AA molar ratios. However, operating at high temperature toluene begins to participate in the reaction, leading to the formation of acylated toluene products and faster deactivation as illustrated in figure S2-10 which can be expected since these products are known to lead to sequential oligomerization reactions.[37]

Figure 2-6c reveals the rate of activity loss as a function of time on stream when comparing two cases with different AA: toluene ratios, where the surface coverage of 2-MF is not the same, but the conversion and TOF in the two cases are equal. Interestingly, a similar deactivation profile exists in these two cases. This illustrates that under conditions where the catalyst surface is saturated by acetic acid, competition for active sites is not a significant contributor to the observed deactivation rates. This contrasts the observations over a non-saturated catalyst surface (Figure 2-3) where 2-MF self-coupling reactions clearly enhance deactivation rates. Because scenario A proposes that the competitive adsorption of 2-MF causes catalyst deactivation, the sum of the above observations effectively rules out scenario A in Figure 2-5 on an acid saturated surface.

Scenario B implies sequential readsorption of the product as it exits the catalyst pore, which would be a strong function of diffusion path. While sequential reactions along a diffusion path, especially in microporous environments, is a common explanation of deactivation pathways [46] this is unlikely to be a significant cause of catalyst deactivation under the acid saturated conditions reported here. This is supported by the similar observation as discussed above, that any species that desorbs into the gas phase will undergo competition for active sites as it progresses along the

diffusion path. The toluene that is introduced will inhibit readsorption of the product Ac-MF along this diffusion path as Equation 2-7 would suggest and subsequently diminish deactivation rates. Further supporting this argument, reaction rates over a partially Na titrated sample (without adding toluene) Na-ZSM-5 also reveals a lack of correlation between diffusion path and deactivation rates. The measured BAS density is reduced from 0.102 to 0.076 mmol/g upon Na exchange as shown in Figure S2-12. Figure 2-6d shows that Na exchange results in similar initial acylation rates per active site as well as identical loss of activity with time on stream. The fact that deactivation rates are identical in the cases depicted in Figure 2-6c and d suggests that Scenario B is unlikely to play a significant role under these conditions.

Scenario C, where a gas phase molecule interacts with the product prior to desorption is in agreement with the observations depicted here. Therefore, we propose this as the most likely path to deactivation on a fully saturated surface. If deactivation proceeds via the interaction of adsorbed product species and a gas phase molecule, 2-MF is the most likely gas phase deactivating agent considering its concentration. If this were the case, deactivation rates would be a strong function of 2-MF gas phase partial pressure. Figure 2-6e illustrates that this is indeed the case, modification of gas phase 2-MF partial pressure also alters reaction rates, so to compensate for this, toluene is added to decrease the AA coverage on the surface such that the initial rates at two different gas phase 2-MF concentrations are equivalent. This implies that the rate of formation of product and therefore the concentration of product is equivalent in the two cases. In this scenario, it is observed that the lower gas phase 2-MF concentration indeed results in diminished deactivation rates over the catalyst surface.

Scenario C should be influenced by the lifetime of product on the surface as well. Accordingly, a faster product desorbing will reduce the probability of the proposed sequential

reaction and hence catalyst deactivation, while the rate constant for deactivation would decrease as temperature increases. Deprotonation of the adsorbed Wheland intermediate to regenerate the surface acid site, which is the step prior to product desorption, is an energetically demanding step and has been referred by some authors as the rate controlling step.[20, 29] If the enthalpy of adsorption of the product is greater in magnitude than the activation energy of sequential reactions of the product with gas phase 2-MF leading to the formation of heavier products, deactivation rates should be less pronounced as temperature is increased. Directly altering the adsorption energy of the formed products, however, would require implementation of a different catalyst with either a different proton affinity or confining environment. Considering the observations from previous studies, the influence of the reaction temperature on catalyst deactivation was tested where obtained results are presented in Figure 2-6f. It is clear that the trajectories of the decay rate change with temperature and the deactivation constants decrease as temperature increases, which further supports the relevance of scenario C on deactivation rates as depicted in Figure 2-5c.

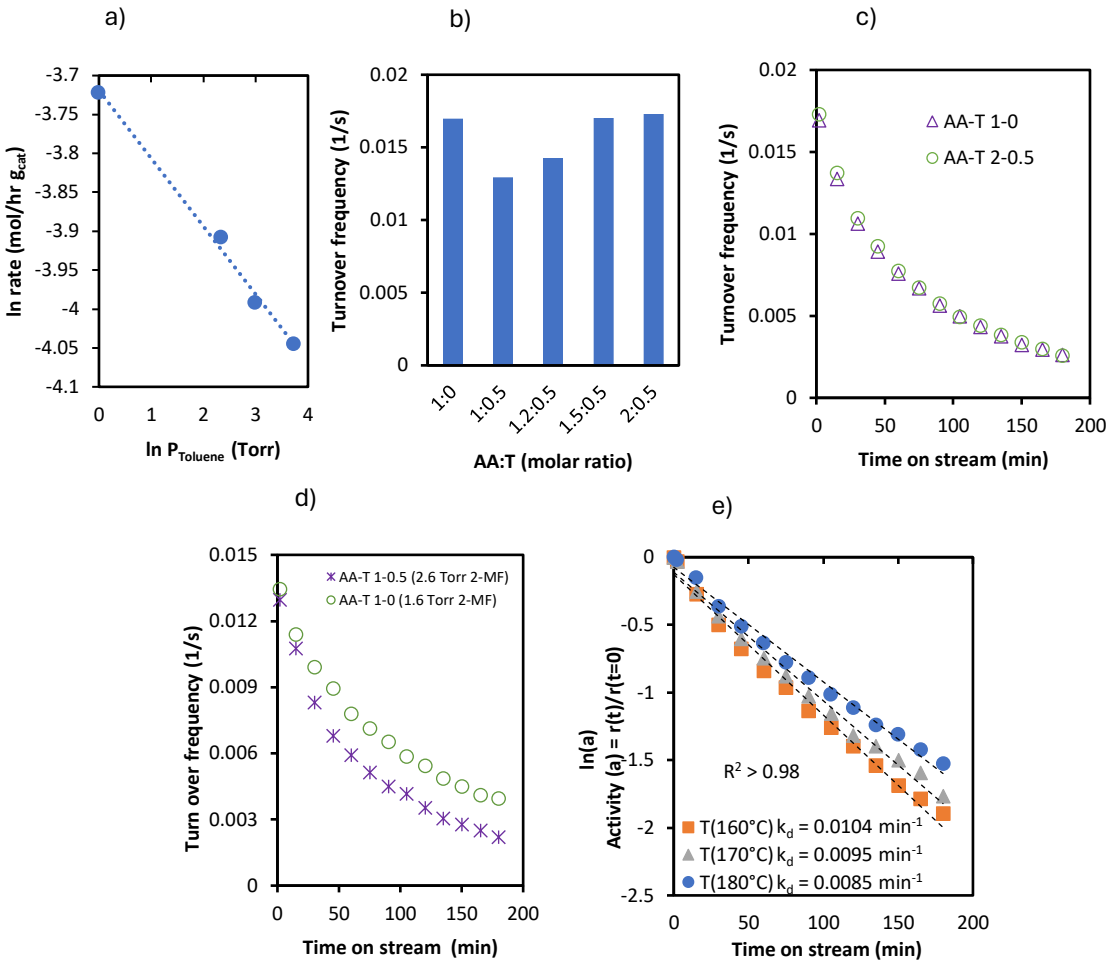


Figure 2-6: a) Rate of AA-MF formation at constant partial pressure of AA and 2-MF while varying inert (toluene) partial pressure. b) Rate of product formation at constant 2-MF partial pressure as a function AA and toluene partial pressure. c) contrasting deactivation profiles for two different AA-toluene ratios with constant 2-MF pressure. d) comparing modified partial pressures as a function of 2-MF with two different AA-toluene ratios e) Decay rate and deactivation constants as a functions of reaction temperature. Reactions conducted over HZSM-5 (Si/Al = 40) at T=160°C with P_{AA}= 40 torr, $P_{2\text{-}MF}$= 2.6 torr, $P_{Toluene}$ = 0-40 torr.

2.3.5 Analysis of the sequential reaction products

2.3.5.1 Soft coke

To decouple the responsible species for the catalyst deactivation, two types of coke were considered and distinguished as soft coke (light oligomers) and hard coke (heavy oligomers). It is intriguing that some of the more prevalent observed species appear to be products of self coupling reactions of furanics. The presence of these two types were recognized and reported by Corma et al.[47] The soft coke was extracted and analyzed using two different methods. The first method is temperature program sweeping with N_2 (TPS-N_2) in which the spent catalyst after the acylation reaction was heated from the reaction temperature (160°C) to 500°C at a ramp rate of 10°C/min and held at 500°C for 1 hour in flowing N_2. Under these conditions, soft coke is removed from the catalyst pores and was collected and dissolved in a cold n-decane trap. Then, the liquid solution was directly injected and analyzed by a GC-MS. High amounts of retained aromatics and heteroaromatics were observed as shown in Figure S2-13. As a complementary approach, the spent catalyst was also analyzed in a pyroprobe system. Three different samples were treated under different temperatures (300, 400, and 500°C). The spectra of evolved species found using this technique in Figures S2-14a-c is similar to what was found via TPS-N_2 in figure S2-13, which confirms the presence of these light oligomers that are mostly alkylated aromatics. Treatment through TPS-N_2 is expected to rejuvenate the active sites in the catalyst by removing and eliminating aromatics and light oligomers. To examine this theory, the spent catalyst (after 3 hours TOS at 160°C) was subjected to sweeping in N_2 at either 300°C or 500°C for 1 hour. At this point, the reactor was cooled down to the reaction temperature at 160°C prior to reactant reintroduction under the previously stated reactant conditions to assess activity after the sweeping treatment. Interestingly, the reaction only recovered approximately 50% of the initial rate regardless of the treatment temperature employed as presented in Figure 2-7a. This is a similar recovery of activity

post N_2 sweeping as others have observed upon reacting biomass-derived oxygenates over HZSM-5. [48] Adsorbed species that do not leave through thermal sweeping alone will continue to become more graphitic and eventually will convert to heavy carbonaceous oligomers, or hard coke.[49, 50] When repeating this experiment using a lower site density catalyst (HZSM-5-140) at higher reaction temperature of 240°C followed by sweeping in inert at 300°C reveals a nearly identical fractional recovery of activity post N_2 sweeping. Consequently, the oligomers produced under these conditions serve as precursors to heavy more graphitic species that require combustion to recover additional activity as will be discussed in the next section.

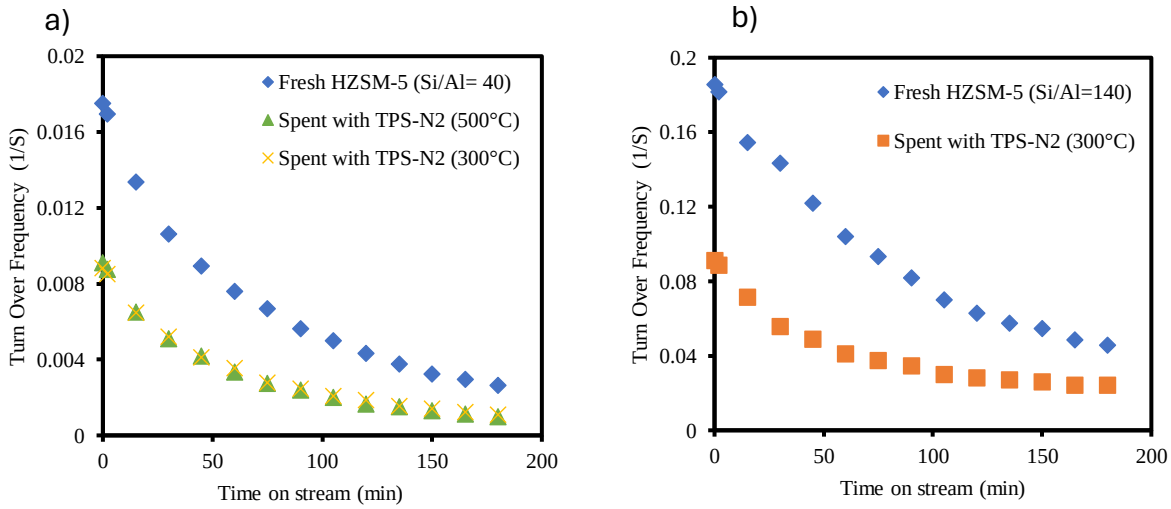


Figure 2-7: a) Comparison between rate of acylation PAA= 40 torr, P2-MF= 2.6 torr at 160°C on fresh and spent HZSM-5 (Si/Al=40) catalyst with TPS-N2 at different treatment temperatures 300°C and 500°C under flowing N2 (125 SCCM). b) Comparison between rate of acylation PAA= 40 torr, P2-MF= 2.6 torr at 240°C on fresh and spent HZSM-5 (Si/Al=140) catalyst with TPS-N2 at 300°C under flowing N2 (125 SCCM).

2.3.5.2 Hard coke (heavy carbonaceous deposits)

Unlike soft coke, characterizing heavy oligomers designated as hard coke is a challenging task. In order to precisely evaluate the hard coke, the spent catalyst was pretreated by TPS-N_2 at 500°C for 1 hour to selectively remove the soft coke while maintaining the hard coke in the spent catalyst. Characterization techniques such FT-IR spectroscopy and TGA have been implemented.

Additionally, BET measurements and IPA-TPRx on the spent catalyst samples were conducted to elucidate the influence of hard coke on the physiochemical properties.

Figure 2-8a shows the common regions of vibration in the FTIR spectra of the hard coke deposits on the spent HZSM-5 after acylation. The spectra region 3200-2700 cm^{-1} corresponds to vibrations associated with olefins and aromatics,[50, 51] which can be observed before and after temperature treatment under flowing helium. The deconvoluted IR spectra in Figure S2-15 reveals prominent CH_2 and CH_3 stretching in 3 peaks at 2960, 2930, and 2870 cm^{-1} assigned to olefins while C-H band stretching at 3155 cm^{-1} can be ascribed to aromatics and alkylated aromatics. These IR vibrations of olefins and aromatics of the coke in the spent catalyst match those in literature for biomass conversion.[52] The stretching regions found in IR spectra coincide with the species analyzed by GC-MS using TPS-N_2 and pyroprobe presented in Figures S2-13,2-14a-c.

The loss of activity found in Figures 2-7a, b even after high temperature treatment under flowing N_2 is attributed to the loss of BAS caused by heavy coke deposits. IPA-TPRx was used to quantify BAS densities both fresh and spent catalysts as illustrated in Figure 2-8b with a noticeably lower propylene peak in the spent catalyst. BAS density was quantified by calculating the area under the curves giving 0.394 and 0.327 mmol/g for the fresh and spent HZSM-5 catalyst, respectively. These losses could be ascribed to both active sites that are covered with large unsaturated hydrocarbons as well as pore blockage that limits accessibility to active sites. The total pore volume (and micropore volume) of the zeolite was measured by using the classical single-point method of converting the total measured gas quantity adsorbed into a liquid quantity, assuming that the adsorbate density is the same as bulk liquid nitrogen. The Horvath-Kawazoe method was used to estimate the micropore volume—which showed about a 30% difference between the spent and fresh catalysts (0.14 mL/g vs 0.18 mL/g, respectively), which is similar to

the trend observed for the total pore volume (0.20 mL/g vs 0.26 mL/g). The greater reduction in rate after inert sweeping in Figure 2-7a and 2-7b (~50%) when contrasted with the more modest loss in BAS density via IPA TPRx could be explained by either a) partial pore blockage that impede access of bulky acylation reactants and products or b) selective deactivation of sites with higher intrinsic activity. Acid site characterization is carried out under conditions such that sufficient time is given to ensure that isopropylamine is able to diffuse to all accessible Bronsted acid sites. Therefore, pore narrowing due to carbon deposits or other features that may slow diffusion of larger molecules may still be counted as active sites via this technique. We speculate that this is the primary cause of the discrepancy. Further in support of argument (a) above this is the similar reduction in TOF reported for the two zeolites with different concentrations in active sites. The MFI 140 zeolite, given its low Al content is generally assumed to have isolated sites at intersections, so a significant fraction of highly active sites that are preferentially titrated as presumed in (b) is unlikely. The amount of heavy coke accumulated in the spent catalyst was calculated via burning the hydrocarbons via TGA in a flowing stream containing oxygen, and evaluating the weight loss from the sample. Figure 2-8c demonstrates the weight % loss progress as temperature increases resulting a loss of 4.5 weight % of the total mass of spent catalyst.

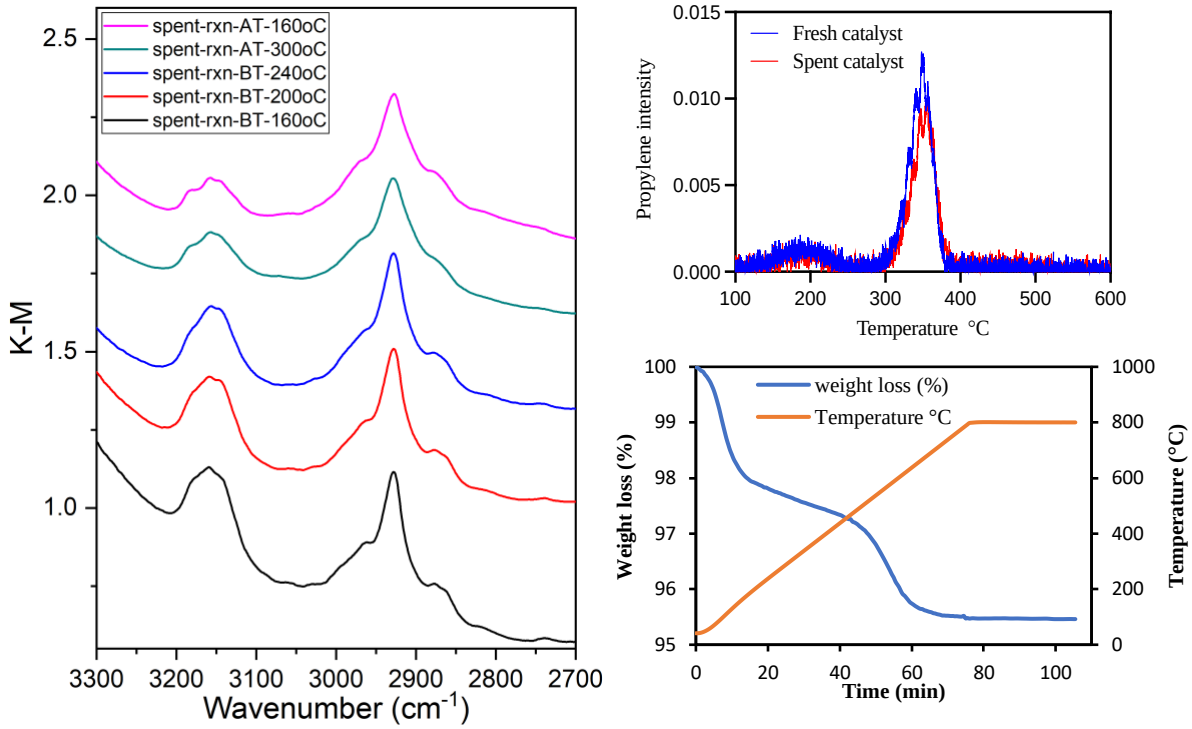


Figure 2-8: Hard coke analysis (a) Evolution of IR spectra of spent HZSM-5 Si/Al= 40 as a function of temperature (BT= before treatment at 300°C, AT= after treatment at 300°C). Spectra are offset for clarity. (b) Propylene signals resulted from IPA-TPRx of fresh and spent HZSM-5 (Si/Al=40) catalyst samples used for BAS density quantification (c) Estimating the mass of hard coke using TPO-TGA of spent HZSM-5 (Si/Al=40) catalyst after TPS-N2.

2.3.5.3 Specific contributions of reactants and products to coke formation

Although the loss of activity due to direct contact of involved chemical species has been discussed previously, it is constructive to examine the surface of the catalyst after exposure to each participating molecule to correlate surface species with the reaction behavior described above. During this acylation reaction, there are 4 relevant species, two reactants (AA and 2-MF) and two products (Ac-MF and water). Therefore, 6 scenarios were investigated that could lead to coke formation on the surface of clean catalyst particles by directly introducing the involved chemical species at the standard reaction temperature (160°C). Figures 2-9a-f reflect the FTIR spectra of spent HZSM-5 (Si/Al=40) catalysts for each scenario and is contrasted to figure 2-9g for FTIR

analysis of the spent catalyst collected after a typical acylation reaction. The peak intensities for the C-H vibrations in the regions of 3200-2700 cm^{-1} correspond to the scale of the coke generated for each scenario while the O-H vibrations in the 3600 cm^{-1} reflect the Brønsted acid sites.[35]

To this point, 2-MF alone undoubtedly forms large amounts of coke on the catalyst surface and leads to major losses in activity. Figure 2-9a, indicates that heavy oligomers are relatively preserved even after high temperature (300°C) treatment and consequently minimize active site recovery. Unlike 2-MF, oligomerization due to AA extended exposure is negligible. In fact, Figure 2-9b illustrates how heating up the catalyst under flowing helium regenerates nearly all the BAS. This aligns with previous findings in Figure 2-3 where it was shown how it takes several hours of AA feeding to observe significant losses in activity of the zeolite.

We proposed that under extremely high ratio of AA to 2-MF, AA will limit 2-MF absorption and limit its ability interact directly with BAS, and the product (Ac-MF), which arrives on the surface through 2-MF interaction with surface acyl species would become the more significant major coke precursor. This can occur through Ac-MF self-oligomerization, or Ac-MF interaction with the other involved species (2-MF, AA, or water). Self-oligomerization would require Ac-MF products to either migrate along the surface or equilibrate with the gas phase and somehow contribute significantly to deactivation rates by interacting with adsorbed species. We hypothesize that this pathway is unlikely due to the much lower partial pressure of the products when contrasted with the 2-MF feed itself, which may similarly interact with adsorbed products. Figure 2-9c suggests that the adsorption of the product itself indeed forms some features representing olefinic species in regions located at 2960, 2930, 2870 cm^{-1}, as well as aromatic species at 3155 cm^{-1}. However, after mild temperature treatment those peaks alleviate including a major reduction in the aromatic peak region resulting a significant growth in the O-H stretching peak at the 3600 cm^{-1}

and hence a major BAS regeneration. Similar effects were observed in Figures 2-9e, f when adsorbed Ac-MF was exposed to AA or water, which suggests that these chemical species do not contribute to sequential reactions to the same irreversible extent as those that are kinetically relevant contributors to the deactivation rates observed during acylation reactions. On the other hand, when mimicking the proposed deactivation mechanism in figure 2-5c via introducing 2-MF to a surface saturated with Ac-MF, this results in large carbonous species that show minimal removal from the catalyst surface even after elevated temperature treatment as illustrated in Figure 2-9d. Additionally, BAS recovery was negligible as opposed to the ability of active site regeneration in scenarios when exposing AA or water to adsorbed Ac-MF. The scenario in Figure 2-9d show similar minimal BAS recovery when compared with a typical acylation reaction in Figure 2-9g, which suggests the predominant mode of deactivation under acylation reaction conditions on an acid saturated surface does indeed result from 2-MF interacting with adsorbed products, in alignment with the conclusions inferred by modifying surface coverages of various species in prior sections.

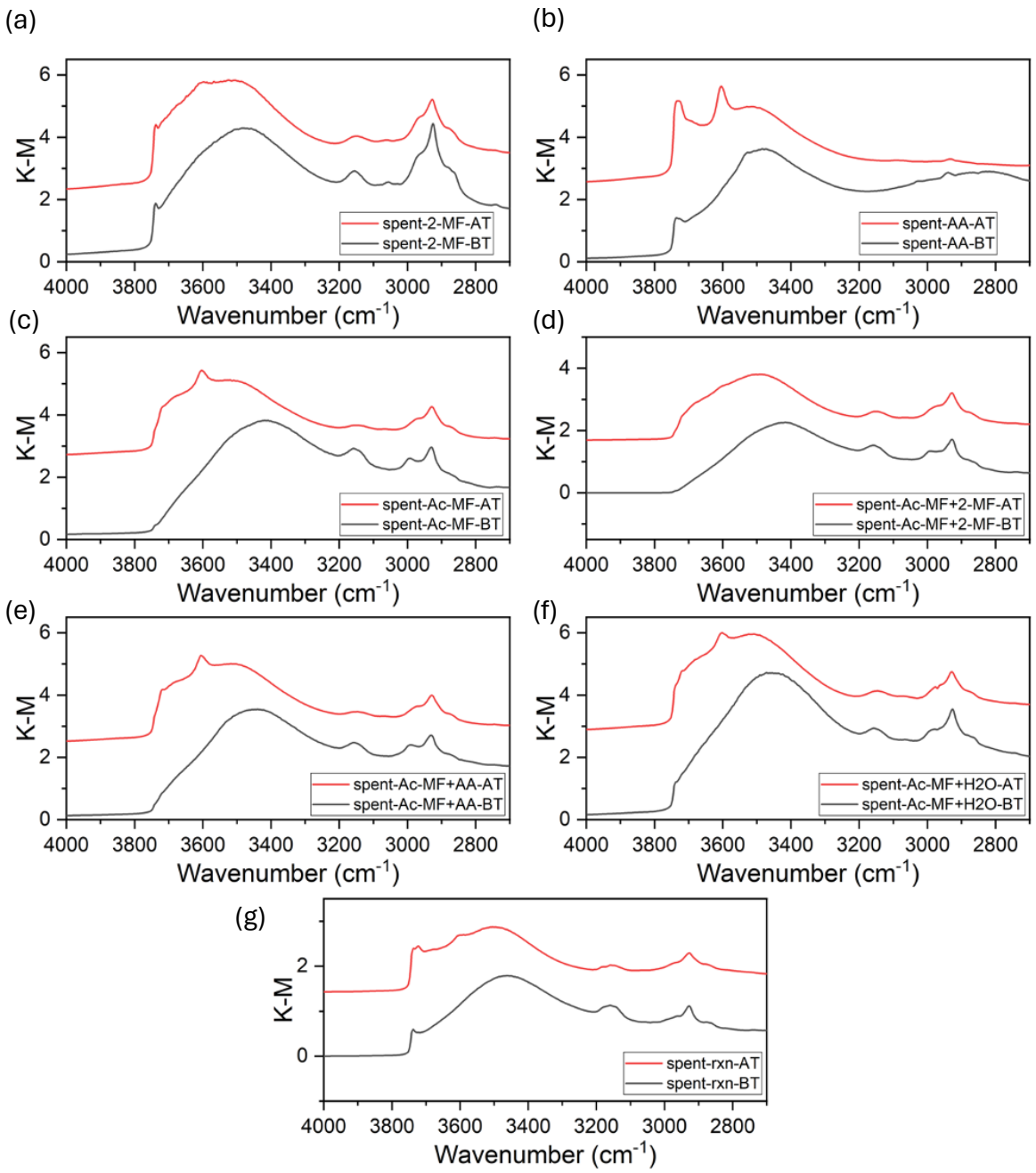


Figure 2-9: FTIR spectroscopy of HZSM-5 (Si/Al =40) at 160°C before treatment (BT) and after treatment at 300°C under flowing helium (AT) of spent catalyst after exposure of (a) 2-MF only for 60 min, (b) AA only for 60 min, (c) Ac-MF only for 60 min, (d) Ac-MF for 30 min followed by 2-MF for 30 min, (e) Ac-MF for 30 min followed by AA for 30 min, (f) Ac-MF for 30 min followed by water for 30 min, (g) Normal reaction conditions (rxn) for 3 hours.

Implementing the scenarios shown in Figure 2-9 using FTIR spectroscopy solidify the argument of shifting catalyst the deactivation mechanism from 2-MF self-coupling at low AA coverage to sequential reactions between adsorbed Ac-MF surface species prior to desorption and gas phase 2-MF at high AA coverage as discussed previously in Figure 2-2. As further contrasting the IR spectra in all scenarios in Figure 2-9, a common peak in the 1800 cm^{-1} region in Figure 2-10 corresponds to C=O stretching[53] was observed in both scenario created by flowing 2-MF on adsorbed Ac-MF, as well as the spent catalyst after normal acylation reaction on an acid saturate surface. Such a peak suggests a mutual heavy oligomer is produced when a sequential reaction occurs between gas phase 2-MF and adsorbed Ac-MF product.

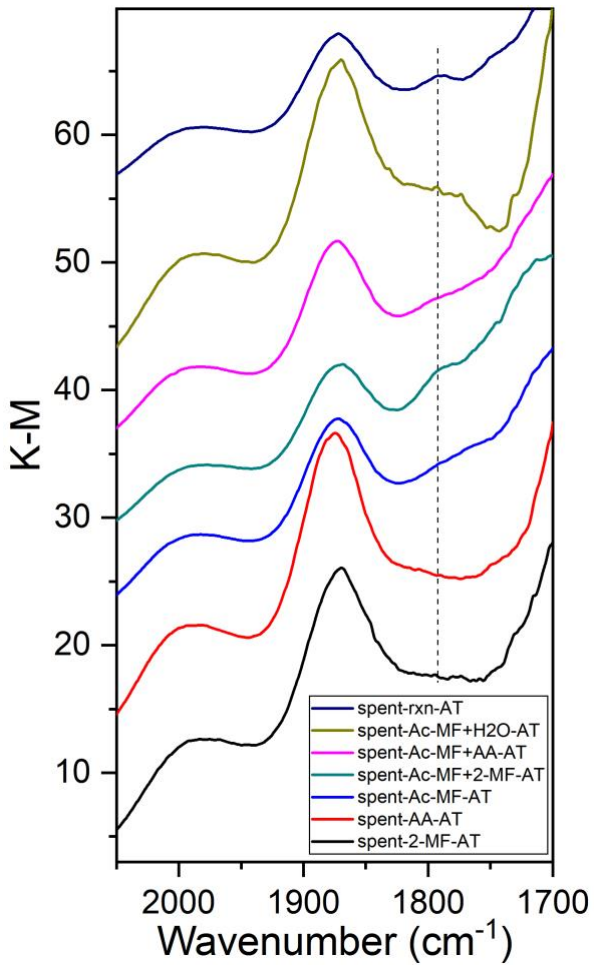


Figure 2-10: FTIR spectroscopy of spent HZSM-5 (Si/Al=40) at 160°C after temperature treatment at 300°C under flowing helium (AT) of spent catalyst after exposure of, 2-MF only for 60 min (spent-2-MF-AT), AA only for 60 min (spent-AA-AT), Ac-MF only for 60 min(spent-Ac-MF-AT), Ac-MF for 30 min followed by 2-MF for 30 min, (spent-Ac-MF+2-MF-AT), Ac-MF for 30 min followed by AA for 30 min (spent-Ac-MF+AA-AT), Ac-MF for 30 min followed by water for (spent-Ac-MF+H2O-AT), (g) Normal reaction conditions (rxn) for 3 hours (spent-rxn-AT). A line to highlight the feature in the C=O bond stretching region is added to all spectra.

2.4 Conclusion

This study reveals the pathways responsible for catalyst deactivation during Friedel Crafts acylation under conditions where the surface is saturated with the acylating agent, where deactivation mechanisms have not been previously studied. At low AA surface coverages, direct 2-MF interactions with available Brønsted acid sites lead to rapid coke forming reactions. As acid concentrations are increased and the surface becomes saturated with carboxylic acids and surface acyl species, deactivation rates are markedly reduced. Under saturated conditions, however,

deactivation still persists. By manipulating surface coverage and introducing strongly binding species that does not participate in the reaction, it is revealed that the pathway responsible for deactivation under saturated surface conditions shifts to interactions of adsorbed products with gas phase 2-MF species. Direct competition of 2-MF with the catalyst surface no longer significantly contributes to deactivation rates under these conditions. Readsorption and reaction of produced products along the diffusion path similarly do not contribute to observed rate losses under these conditions. Deactivation rates can therefore be mitigated simply by altering the gas phase partial pressure of the highly reactive acyl acceptors, or by altering the adsorption energy and therefore lifetime of products to decrease the probability of reaction prior to desorption from the active sites. These results reveal a blueprint for further extending the lifetime of Friedel Crafts catalysts upon employing highly reactive acyl acceptors.

Acknowledgements:

The authors are grateful for funding from NSF grants 1653935 and 2029394. IA acknowledges support from the Saudi Arabian Cultural Mission (SACM) for partial funding of his graduate studies. The authors are thankful for assistance with the TGA studies by Ana Jerdy, Erich Metzger for assistance with the fast pyrolysis studies, and Andrew D'Amico for his assistance with the pore volume measurements.

Chapter 3: Consequence of altering acid strength in MFI zeolites via Phosphorus modification and their effects on acylation reaction

The work in this chapter is a collaboration between the University of Oklahoma and Dr. Jeffery White's group at Oklahoma State University. Solid state ^{31}P-NMR characterizations were obtained from Dr. White's group at OSU, while the rest of the work conducted by our research group at OU. This work is planned for future publication involving the authors Ismaeel Alalq, Ana Carolina Jerdy, Huy Nguyen-Phu, Anya Zornes, Daniel Resasco, Jeffrey White, Steven Crossley.

Abstract

Friedel-Crafts acylation is an important reaction for the formation of C-C bonds to produce a variety of commodity chemicals. Recent efforts have been made to reduce the environmental footprint of these reactions by utilizing renewable carboxylic acids directly (rather than halogenated species), using renewable acyl acceptors, and using zeolites as non-sacrificial catalysts. While the direct conversion of acids to valuable products is appealing, little is known regarding the role of acid strength and the local environment on rates and stability for this reaction. Here we report the acylation of 2-methylfuran with acetic acid over phosphorus-modified MFI zeolites with various phosphorus loadings. We show that while P modification increases observed activation barriers for acylation when compared with traditional Bronsted sites, net rates of reaction can be increased. Further, selectivity is improved by diminishing rates of acid self-coupling side reactions to a greater extent. Interestingly, the phosphorus-modified samples also exhibit slower coke formation, and therefore deactivation, due to diminished side reactions.

3.1 Introduction

In recent years, there has been a noticeable surge in research dedicated to enhancing the value of lignocellulosic biomass streams, with a particular focus on harnessing renewable sources of commodity chemicals, surfactants, and fuel[54-58]. Among the intriguing chemical transformations explored in this context, Friedel-Crafts acylation stands out as a promising avenue for generating valuable biomass-derived chemicals[4, 5, 8]. Notably, recent research has highlighted the promise of replacing environmentally problematic halogenated chemicals and catalysts via direct acylation of heteroaromatic compounds using biomass-derived carboxylic acids over zeolites[18, 19, 59, 60]. However, the use of more easily regenerable aluminosilicate zeolites as catalysts for acylation reactions involving biomass-derived oxygenates introduces new challenges in terms of stability and selectivity [60-62]. Efforts to improve selectivity for these transformations without necessitating halogenated chemicals is essential toward advancing this field.

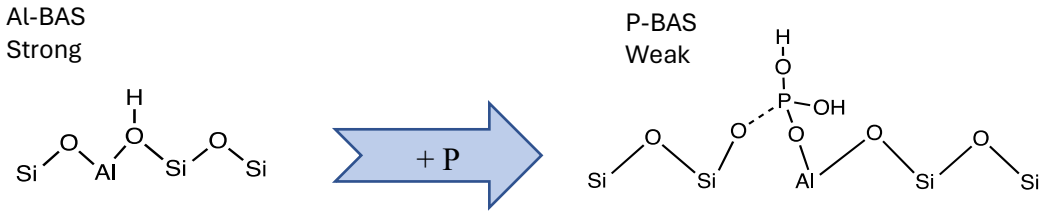
One approach often employed industrially to modulate the properties of ZSM-5 zeolites for petrochemical upgrading commonly involves the incorporation of phosphorus into the catalyst crystals. The incorporation of phosphorus to improve catalytic performance of zeolites has been a subject of continuous investigation since the 1970s, when researchers at Mobil pioneered its use to explore the promotional effects on various chemical reactions, including alkylation and methanol to hydrocarbons (MTH)[63-65]. A recent review on the topic of phosphorus incorporation into zeolitic materials has summarized the numerous physicochemical changes that occur upon the addition of phosphorus[66]. Across many of these studies, a consistent theme observed among many types of chemistries is the observation of a prolonged catalyst lifespan and improved hydrothermal stability. While alterations in the local confinement environment within the zeolite have been shown to influence catalyst rates and selectivity, the observed

promotional effects have largely been attributed to the attenuation of Brønsted acid site (BAS) strength [67, 68].

The utilization of phosphorus-incorporated zeolites in the processing of oxygenated and biomass-derived chemicals has gained significant attention and has yielded promising outcomes in previous studies[69-73]. For instance, Yao et al. reported improved product distribution toward aromatics while diminishing coke formation upon incorporating P within ZSM-5 for the catalytic co-pyrolysis of biomass and plastics[69]. Additionally, another study by Cho et al. explored the consequences of introducing phosphorus into dealuminated BEA zeolites [71] for the Diels-Alder cycloaddition of 2,5-dimethylfuran and ethylene, reporting improved stability accompanied by a substantial increase in p-xylene yields. The study concluded that the enhancement in catalyst performance could be attributed to the reduction in acid strength brought about by phosphorus addition, which subsequently weakened the binding of reactants and/or products to the phosphorous-generated active sites. It is worth noting that while phosphoric acid can serve as a homogeneous catalyst for certain reactions, incorporating it into solid materials like zeolitic structures has been proposed to substantially enhance its catalytic activity and selectivity [74] due in part to unique interactions with traditional Bronsted sites, as well as the unique environments created within the microporous zeolite pores.

Utilizing phosphorus (P) in catalysis has emerged as a strategic pathway to address some of the challenges associated with processing biomass-derived chemicals. A notable example is the direct acylation of 2-methylfuran (2-MF) with carboxylic acids, a promising reaction that suffers from side reactions that influence catalyst stability. Incorporating phosphorus into the catalytic system can offer a solution to these challenges. Our prior investigation into the acylation of 2-MF with AA over HZSM-5 zeolites highlighted the propensity for coke formation and

subsequent catalyst deactivation when exposing 2-MF alone to a clean BAS [18]. To extend the catalyst's lifespan, it was illustrated that it is necessary to increase the surface coverage of AA to minimize the direct interaction of 2-MF with the catalyst surface[18, 19, 60]. This approach aligns with reports from other studies emphasizing the role of AA partial pressure in inhibiting the oligomerization of co-reactants [19, 75]. However, in our most recent investigation into the direct acylation of 2-MF with AA over HZSM-5, we noted that even under a surface that is saturated with acid (0th order with respect to AA), non-negligible rates of deactivation persist. Upon further investigation, we proposed that the predominant mechanism of deactivation shifts as a function of available sites that may interact directly with the highly reactive 2-MF reactant. At low AA coverage, when some vacant Bronsted sites remain, deactivation is caused via direct interaction of 2-MF with the Bronsted sites on the surface, leading to ring opening and oligomerization chemistry that results in catalyst deactivation. At high AA coverage, however, 2-MF is unable to compete for surface sites, and the predominant mechanism of deactivation shifts to the direct interaction of gas phase 2-MF with acetyl-methylfuran (Ac-MF) product prior to desorption from the catalyst surface[60]. As a corresponding solution, we anticipate that accelerating the product desorption step will substantially reduce the suggested sequential reaction and consequently alleviate catalyst deactivation.



Scheme 3-1: Depiction of a proposed result of phosphorus addition to zeolites in which aluminum-based strong BAS transform to phosphorous-based weaker BAS.

In this study, we introduce the unique capability of phosphorus (P) to modulate the strength of aluminum-based BAS as depicted in Scheme 3-1. To achieve this, P is introduced

into commercially available zeolites and synthesized silicalite-1 materials across a wide range of P loadings. These P-modified MFI catalyst samples will be employed for the acylation of 2-MF with AA, and their performance is compared to that of the parent HZSM-5 zeolite. Reactions are conducted under carefully controlled reaction conditions to ensure that equilibrium conversion or diffusion limitations do not corrupt the results [60]. Importantly, we assess how the introduction of P reduces acylation rates per gram of catalyst at lower temperature by titrating strong framework BAS, but rate enhancements are observed at elevated temperatures. P incorporation also results in slower catalyst deactivation and a hindrance of undesired side and sequential reactions. Furthermore, the nature of the coke formed on the spent catalyst is explored, as well as the role of P to inhibit the formation of more graphitic coke, thus improving catalyst activity, selectivity, stability as well as regenerability.

3.2 EXPERIMENTAL SECTION

3.2.1 Catalyst preparation

3.2.1.1 Phosphorous incorporation.

The MFI catalyst samples utilized in this study were commercial grade materials sourced from Zeolyst International, primarily CBV28014 with a Si/Al ratio of 140 and CBV8014 with a Si/Al ratio of 40. These samples were initially received in the ammonium-ion form and were subsequently converted to the proton form through air calcination at 600°C for a duration of 5 hours. The phosphorus-modified MFI samples were prepared using the ammonium form CBV28014 (Si/Al = 140) and an incipient wetness impregnation technique with ammonium dihydrogen phosphate ($(NH_4)H_2PO_4$, Sigma Aldrich, 99.999% trace metals basis) as the phosphorus source. Following impregnation, the samples were allowed to naturally dry for 24 hours and were then subjected to heating in a vacuum oven at 80°C for 5 hours, followed by air

calcination at 600°C for an additional 5 hours. The resulting samples were designated based on the phosphorus-to-aluminum (P/Al) ratio, with, for example, 2P corresponding to (P/Al = 2), while the parent zeolite was labeled as 0P. It's important to note that the moles of aluminum were accounted for based on BAS quantification, determined through IPA-TPRx analysis. The preparation of P-modified silicalite-1 followed the same procedures as those used for modifying ZSM-5, with the designation indicating the weight percentage of phosphorus loaded e.g., (x)wt%P-Silicalite-1.

3.2.1.2 Na titration

The sodium-exchanged sample (Na-ZSM-5) was derived from CBV28014 with a Si/Al ratio of 140. This conversion was achieved using a 0.004M sodium nitrate solution (NaNO3, Sigma Aldrich ACS reagent, ≥99.0%). Specifically, the conversion process involved immersing 2 gram of the catalyst in a 40 mL sodium nitrate solution. The mixture was stirred at a speed of 700 rpm for a duration of 30 minutes at room temperature. Subsequently, it underwent five rounds of washing and filtration before being subjected to drying and calcination, following the established procedure[35].

3.2.1.3 Silicalite-1 synthesis

Silicalite-1 was synthesized using a well-established technique from the literature[76]. To create the gel, we used molar ratios of 1 SiO_2/0.25 TPAOH/8.3 H_2O, which were sourced from tetraethyl orthosilicate (TEOS, Sigma Aldrich, ≥99.0% (GC)) and tetrapropylammonium hydroxide (TPAOH, Sigma Aldrich, 40% solution in water). The mixture was stirred for 24 hours on a hot plate at 80°C and then transferred to an autoclave for crystallization at 160°C. Following this, the heterogeneous solution was washed and filtered five times before undergoing drying in a vacuum oven at 80°C for 5 hours, followed by air calcination, utilizing the same

procedure as previously mentioned. The crystal structure of the resulted material was characterized and confirmed using XRD as seen in Figure S3-1.

3.2.2 Catalyst characterization.

3.2.2.1 BET surface area and pore volume

Nitrogen adsorption analysis was performed using a Micromeritics ASAP 2020 instrument at a low temperature of -196 °C. Prior to analysis, catalyst samples underwent degassing at 350 °C, employing a heating rate of 5 °C/min, in a vacuum pressure environment for 10 hours. This step was crucial for eliminating physiosorbed moisture and volatile impurities. The weight of the dried sample, post-degassing, was measured and subsequently corrected. Subsequently, the sample was cooled down to -196 °C for nitrogen adsorption analysis. The obtained results allowed for the determination of BET surface area, and the pore volumes of phosphorus-modified ZSM-5 (Si/Al = 140) samples were assessed utilizing the Horvath-Kawazoe (H-K) plot method.

3.2.2.2 X-ray diffraction

X-ray diffraction (XRD) studies of catalysts were conducted on a Rigaku diffractometer, utilizing Cu Kα radiation generated at 44 mA and 40 kV; the diffraction angle range was $2\theta = 2-70°$.

3.2.2.3 FTIR-spectroscopy

The surface of the parent and phosphorus modified zeolites has been analyzed using infrared spectroscopy in a PerkinElmer Spectrum 100 FT-IR Spectrometer equipped with Harrick Praying Mantis chamber. The background was measured using KBr (FT-IR grade, ≥99% trace metals basis) from Sigma Aldrich. Both fresh and spent catalyst samples were heated at a ramp rate of 10°C to temperatures to 300°C under flowing helium at rate of 50 ml/min to remove

physiosorbed moisture and light oligomers from the spent catalyst then cooled down to 120°C where 64 scans have been performed to record the IR spectra.

3.2.2.4 Solid-state NMR spectroscopy

^{31}P NMR experiments were acquired at 9.4 T with a Bruker Avance II console using a 4-mm double-resonance MAS probe. 1024 transients per spectrum were obtained with a single 90° pulse of 4.66 µs, recycle delay of 50 s, and a spinning speed of 10 kHz. Pulse durations and chemical shifts were calibrated using chiraphos (bis(diphenylphosphino)-butane). Samples underwent stepwise vacuum dehydration, heating 0.5°C/min to 100°C, holding for 2 hours, then heating at 2°C/min to 450°C and holding for 12 hours. Following dehydration, samples were packed in ZrO_2 rotors in an inert argon gas atmosphere using a VAC Atmosphere glovebox. Initial spectra were obtained without exposing samples to atmosphere, while subsequent spectra were obtained after controlled hydration by exposure of samples to ambient air without removing from the NMR rotor.

3.2.2.5 IPA-TPR$_x$ measurements

Isopropylamine temperature-programmed reaction (IPA-TPRx) was employed to quantify the density of strong Brønsted acid sites (BAS) capable of facilitating the IPA Hoffman elimination reaction within the catalyst samples. Firstly, catalyst samples were packed into 1/4-inch quartz tubes and subjected to pretreatment under a helium flow of 30 ml/min, with the temperature ramped at 10°C/min up to 300°C, followed by a 1-hour hold at this temperature. The temperature was subsequently lowered to 100°C. To saturate the Brønsted acid sites thoroughly, the catalyst samples were exposed to several 2 uL IPA pulses, after which helium flow was allowed for 1 hour to remove any physiosorbed or weakly adsorbed IPA. The temperature-programmed desorption (TPD) commenced by ramping the temperature from 10°C/min to

600°C. Throughout this process, the evolution of desorbed species was continuously monitored using a Cirrus mass spectrometer (MKS), recording signals at m/z = 17 (NH_3), 44 (IPA), and 41 (propylene) as shown in Figure S3-1. The density of Brønsted acid sites was quantified by calibrating the mass spectrometer signals based on the average of several 0.5 mL pulses of propylene.

3.2.2.6 Thermogravimetric analysis

Thermogravimetric analysis (TGA) was carried out using a Netzsch STA 449F1 instrument equipped with a pin thermocouple and a Netzsch nano balance. The objective was to quantify the quantities of both light and heavy carbonaceous oligomers formed on the spent zeolite catalyst samples following the acylation reactions. After completion of the reactions, helium sweeping at a rate of 50 mL/min was applied to the spent catalyst samples, with a temperature ramp of 10 °C/min, up to 300 °C for 1 hour. This step effectively removed the light oligomers. Subsequently, the samples were cooled to 100 °C in preparation for temperature program oxidation (TPO), allowing for the accurate determination of the heavy carbonaceous deposits. TPO was conducted under a flowing air atmosphere (50 ml/min) on the spent catalyst samples. The temperature was ramped from 100 °C up to 600 °C at a rate of 10 °C/min, held at 600 °C for 30 minutes, and then cooled back to the initial temperature of 40 °C. The quantification of light and heavy oligomers within the spent catalyst was achieved through calibration using calcium carbonate as a reference in TGA.

3.2.3 Catalytic reaction

The acylation reaction involving 2-methylfuran (2-MF) (98+%, stabilized, Alfa Aesar) and acetic acid (AA) (glacial, ACS reagent, ≥99.7%, Sigma-Aldrich) over both phosphorous modified and non-modified catalyst samples was conducted in the gas phase, utilizing a fixed-bed tubular

reactor following standard procedures. A quantity of catalyst ranging between 4 to 25 mg was mixed with glass beads and packed between layers of quartz wools within a 1/4-inch quartz reactor tube. Subsequently, the catalyst was subjected to pretreatment, with a temperature ramp of 10°C/min, up to 300°C. This pretreatment lasted for 1 hour under flowing nitrogen to eliminate any physically adsorbed moisture. The reactor temperature was then gradually lowered to the desired reaction temperature, which typically ranged from 160 to 240°C. Nitrogen served as the carrier gas, maintained at a flow rate of mainly 125 ml/min, and adjusted as needed to maintain a constant partial pressure of 2-MF, which was fed into the system at 0.1 mL/hr. AA was introduced at a flow rate ranging from 1 to 1.5 mL/hr (1 ml/hr in most cases). To ensure precise control, syringe pumps were used to manage the reactant feed rates. To prevent the condensation of leaving species, the outlet stream from the reactor was heated to 250°C. A micro electric actuator controlled a six-port valve, facilitating the transfer of products from the 500µm sample loop to an inline-connected gas chromatograph (GC) HP 6890 GC-FID. The GC was equipped with a flame ionization detector and featured an Agilent HP-INNOWAX column (30m × 0.32mm × 0.50µm) for the separation of reaction products. Samples were collected from a glass trap connected to the vent line, and product identification was accomplished using a Shimadzu GCMS-QP2010S. Response factors for the reactants were determined by flowing the reactants at their respective rates through a glass bead bed to replicate the catalyst bed. For product response factors, injection of standards was employed. These response factors played a crucial role in subsequent data analysis, including the calculation of conversion and carbon balance. Reaction rates per gram of catalyst were determined using the following equation: -

$$\boldsymbol{Rate} = \frac{\boldsymbol{Moles\ of\ product\ formed\ per\ hour}}{\boldsymbol{Gram\ of\ catalyst}} \left(\frac{\boldsymbol{mol}}{\boldsymbol{hr\ g_{cat}}}\right) \qquad \textbf{Equation 3-1}$$

While the turnover frequency (TOF) was calculated based on the following: -

$$TOF = \frac{Moles\ of\ product\ formed\ per\ gram\ of\ catalyst}{Moles\ of\ Brønsted\ acid\ sites\ per\ gram\ of\ catalyst}\left(\frac{1}{s}\right) \qquad \textit{Equation 3-2}$$

All product formation conversion were kept under 26% to avoid the reported equilibrium conversion[19, 60] and estimated using the following equation: -

$$Conversion = \frac{Moles\ of\ product\ formed\ per\ hour}{Moles\ of\ 2-methylfuran\ fed\ per\ hour}\ (mol\%) \qquad \textit{Equation 3-3}$$

The initial reaction rates were determined by extrapolating to the zero time on stream point, offering a precise method for kinetic assessments of the catalyst's performance prior to deactivation during acylation reaction.

3.3 RESULT AND DISCUSSION.

3.3.1 Catalyst characterization

The physical changes to MFI zeolites upon phosphorus addition are presented in Table3-1. These measurements reveal varying degrees of reduction in sample crystallinity, pore volumes, and overall acidity. Each of these trends will be discussed in more detail below.

Table 3-1 physical properties of the zeolite catalyst samples used in the study.

Catalyst Sample	(P/Al) mol[a]	wt%P	R_C [b]	V_{micro}[c] (cm^3/g)	V_{total} (cm^3/g)	BAS[d] (mmol/g)
0P	0	0	100%	0.156	0.239	0.102
0.5P	0.5	0.17	96%	0.152	0.232	0.095
1P	1	0.33	93%	0.148	0.226	0.086
2P	2	0.66	97%	0.141	0.221	0.075
4P	4	1.3	98%	0.135	0.206	0.051

[a] Al content was determined based on quantified BAS. [b] Relative crystallinity calculated using Equation S3-1. [c] Micropore volume as estimated from the Horvath-Kawazoe method. [d] Determined using IPA-TPR_x measurements.

The relative crystallinity of phosphorous modified samples was calculated using Equation S3-1 based on characteristic MFI peaks following[77]. XRD patterns of all the samples used in acylation reaction are displayed in Figure 3-1a. The diffraction patterns of the phosphorus-

modified ZSM-5 samples were similar to those of the found in parent zeolite (0P) with minimal crystallinity losses and no observation of new crystalline phase upon P incorporation.

It is important to note that some prior research has indicated that zeolite XRD crystallinity can sometimes lead to more pronounced[68, 78-80] decreases following phosphorus modification due to framework defects resulting from dealumination. The minimal loss of crystallinity reported here is due to relatively low amount of phosphorus added (maximum of 1.3% by weight), as well as the relative stability of MFI zeolites in the Al concentration ranges used here.

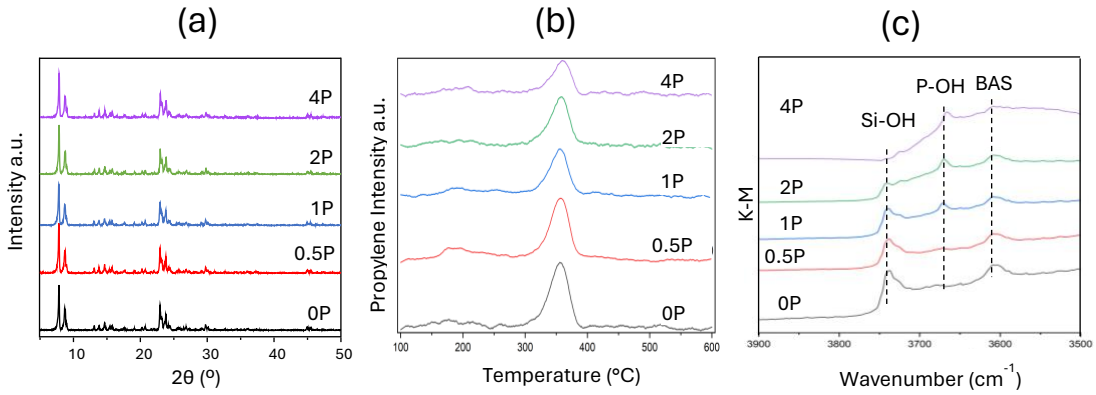


Figure 3-1 (a) XRD result suggests minimum effect on zeolite crystallinity upon relatively low phosphorous addition. (b) Propylene desorption signal obtained from IPA-TPRx for strong BAS quantification for the phosphorous modified ZSM-5 (Si/Al =140). (c) FTIR spectra for -OH stretching various phosphorous modified P-ZSM5 compared with parent HZSM-5

The nitrogen adsorption experimental results including total pore volume, and micropore volume for the modified catalyst samples presented in Table 3-1 reveal modest losses to accessible pore volume upon P incorporation. Detailed adsorption isotherms and H-K plots for the various catalyst samples as well as other reported outcomes can be found in Figure S3-3,. We acknowledge that the addition of phosphorus to the zeolite could potentially lead to micropore plugging[81-83], which may introduce internal diffusion limitations and, consequently, affect the kinetic evaluation of the catalyst[33, 84, 85]. However, the nitrogen adsorption results indicate

that the decrease in micropore volume is approximately 15% for the highest phosphorus loading (1.3 wt% P), a relatively minor effect that will be further assessed in kinetic observations.

While we observed some modest changes to catalyst structure upon incorporating various phosphorus loadings, which may play a role in the diffusion of reactants and products within zeolite pores[86, 87], the modification of active sites is expected to have a more profound impact on reaction rates [88-90]. Indeed, the introduction of phosphorus into our ZSM-5 zeolite samples resulted in a proportional reduction in strong Brønsted acid sites. This is illustrated by the decrease in sites strong enough to convert isopropylamine (IPA) to propylene via Hoffman elimination[91], as illustrated in Figure 3-1b and quantified in Table 3-1. However, it is noteworthy that utilizing the approach we employed here of incipient wetness impregnation, some phosphorous species reside in zeolite pores in locations that do not titrate strong BAS, resulting in residual increases in the total amount of weak acid sites. For example, in the relatively hydrophobic low Al containing zeolite ZSM5(140), four phosphorus atoms are included per one aluminum in order to reduce the strong acid site density as measured by IPA TPRx by 50%. Although phosphorus can exist in various forms within zeolites, including monophosphate, diphosphate, and polyphosphates species [92, 93], these species can also bind to silanol groups[71, 74].

FTIR spectroscopy serves as a valuable tool for probing phosphorus interactions with the various functional -OH groups within zeolites, shedding light on the surface behavior of these phosphorus species[94]. FTIR spectra upon adding and increasing phosphorus loading are shown in Figure 3-1c. While the (BAS) peak intensity associated with bridged hydroxyls (~3610 cm^{-1})[94] gradually decreases with phosphorus loading, the OH stretching signals in the silanol groups external (~3745 cm^{-1}) and internal (~3725 cm^{-1})[94] experience a pronounced drop,

compared to the bridging hydroxyl, and nearly vanish at the highest phosphorus loading. Simultaneously, a new peak emerges and evolves upon phosphorus addition in the ~3675 cm^{-1} region, likely resulting from phosphorus hydroxyl group[94-96]. To confirm that phosphorus is indeed responsible for the OH stretching signals in this region, we conducted FTIR analysis on Silicalite-1, the MFI framework without aluminum, with different phosphorus loadings, as illustrated in Figure S3-4. In this case, the IR spectra of Silicalite-1 shows a reduction in the SiOH band accompanied by an increase in the P-OH region ~3675 cm^{-1} upon the incorporation of phosphorus. This provides definitive evidence that this modification leads to the generation of new phosphorus-induced active sites by binding to silanol species. P interacting with aforementioned silanol nests, free phosphoric acid species, and P species interacting with bridging Al may all contribute to this emerging signal, requiring further clarification to identify each of these species.

^{31}P MAS (magic-angle spinning) NMR experiments were conducted on a phosphorus-modified ZSM-5 and a similarly treated silicalite control sample. Each host sample was loaded with 1.3 wt% H_3PO_4, corresponding to four P atoms per Al in the zeolite case. Spectra were acquired for each sample in the initial dry state, as well as a function of exposure time to ambient humidity. While the ^{31}P chemical shifts of H_3PO4 and diphosphoric acid in nanoporous hosts are well established at 0 and ca. -10 ppm, respectively, there exists significant overlap in the chemical shift ranges for P atoms in polyphosphates, P-O-Si moieties, and species with P-O-Al linkages[97-103]. Thus, ^{31}P chemical shift values can be ambiguous in terms of identifying specific groups formed following P-modification in zeolites. Recent reports indicate that ^{31}P spectra depend upon whether the zeolite is dry or exposed to moisture, and to the total phosphorus loading.[97, 104] Multinuclear NMR experiments can reveal the structure of first-

formed P-O-Al zeolite framework species when sub-stoichiometric H_3PO_4 loadings relative to framework Al are used, as was recently discussed for an HZSM-5 catalyst with Si/Al=40.[104] ^{31}P chemical shifts depend on loading due to chemical exchange effects between surface-coordinated and free phosphate species, and signals can be broadened due to dipolar coupling to quadrupolar Al nuclei and the distribution of their bonding arrangements following phosphorus treatment, drying, and calcination.

Figure 3-2a and 3-2b compare the ^{31}P MAS NMR spectra for ZSM-5 and silicalite, respectively, as a function of exposure time to ambient (ca. 50 % relative humidity) moisture. Given that H_3PO_4 is present in 4-fold excess relative to framework Al, and that framework Al is dilute in a zeolite with Si/Al = 140, the expected dominant spectral features in 3-2a would arise from phosphoric acid or phosphates interacting with SiOH groups. Indeed, a priori one would expect very similar spectra for the zeolite (3-2a) and the silicalite (3-2b) hosts. The ^{31}P spectra in 4b reflecting the distribution of species adsorbed on silicalite as a function of moisture are completely consistent with previous reports,[97] in that the predominantly Q_3 surface-bound phosphorus species that do not contain hydroxyl groups change to Q_1 and Q_2 hydroxyl-bearing species with hydration. The subscripts denote the number of surface Si-O-P bonds. Further, hydrolysis of polyphosphate species with 3 or 4 P-O-P bonds, i.e. P_3 and P_4, results in similar chemical shift changes as P_1 and P_2 are formed. In 3-2a, however, the spectra are markedly different for the Al-containing zeolite, with the most clear differences observed at the hydration limits. Conversely, the dry spectrum in 3-2a lacks any of the same resolved signals as shown in the dry 3-2b spectrum, with a ca. 40-ppm broad signal that is almost identical to previous data acquired on dry HZSM-5 catalysts with Si/Al = 40 following H_3PO_4 treatment.[104] Based on multiple types of two-dimensional correlation experiments, signals in this region could be

confidently assigned to P-O-Al moieties arising from surface-bound phosphates at framework Al sites. Even at full hydration, there exists a broad upfield shoulder extending beyond the diphosphoric acid resonance that is characteristic of previously observed signals with long T_1 relaxation time constants, indicative of surface-adsorbed species, which are not observed in the fully-hydrated silicalite spectrum in 3-2b. In total, the data in Figure 3-2 indicate that surface-associated P-O-Al species form for the P-ZSM-5 catalysts.

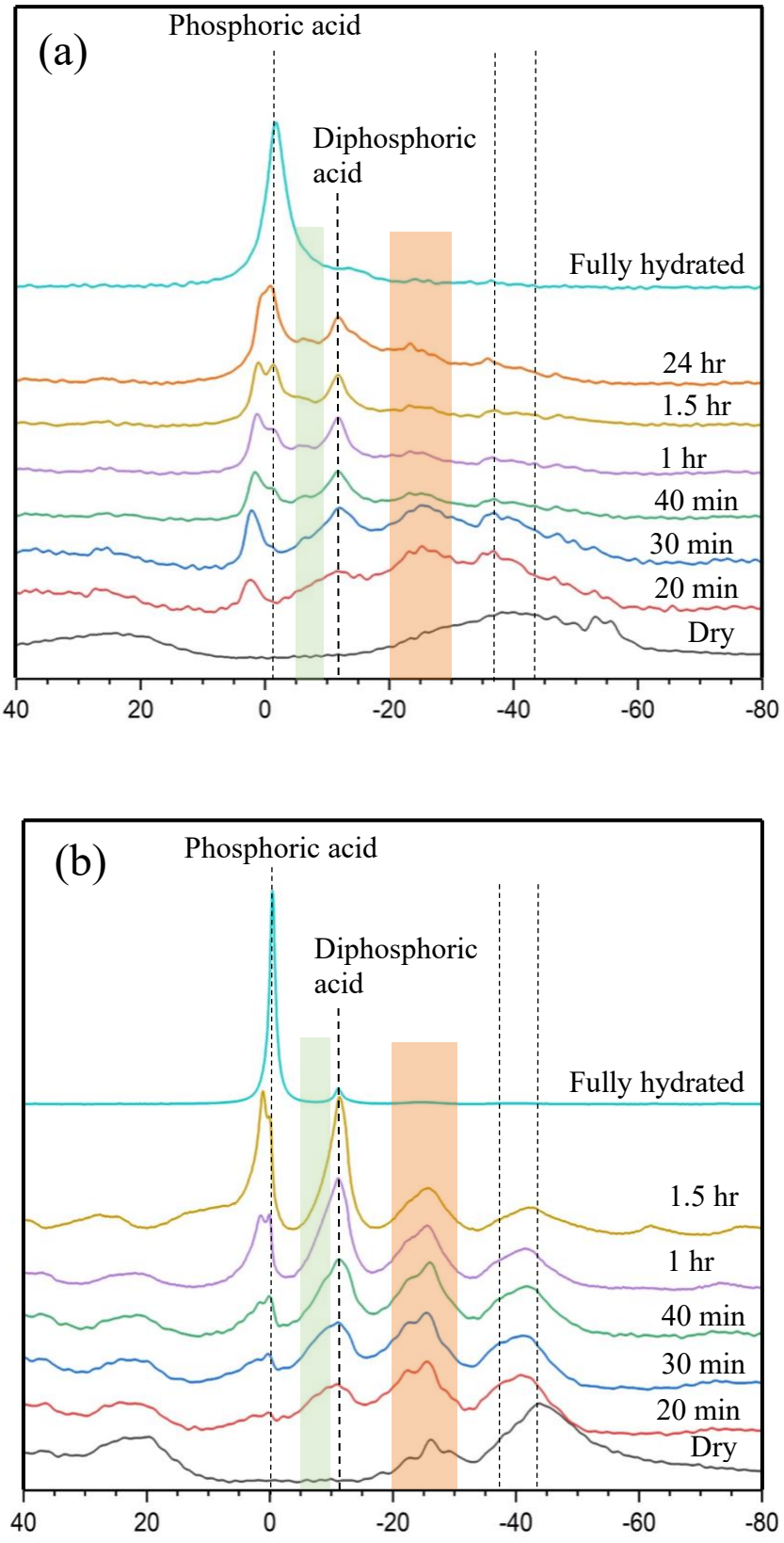


Figure 3-2 Solid-state ^{31}P -NMR of (a) 4P: Al (1.3wt%P) ZSM-5(140) (b) 1.3wt%P Silicalite-1

3.3.2 The influence of phosphorous addition to zeolites on acylation reaction.

The acylation rates of the phosphorus-modified ZSM-5 samples were assessed across a temperature range of 160-240°C, revealing intriguing temperature dependent behaviors and activities, as illustrated in Figure 3-3. At lower temperatures, a noticeable decline in reaction rates was observed with increasing phosphorus loading, indicative of a behavior akin to a catalyst poison that hinders catalytic activity, as shown in Figure 3-3a. However, at higher temperatures, the catalytic behavior exhibited a significant shift, with phosphorus in the zeolite samples acting as a catalyst promoter and leading to an increase in reaction rates with higher phosphorus loading. This observation suggests the presence of certain weak active sites with notably higher activation barriers, rendering them less effective at lower temperatures. While the decrease in catalytic activity due to phosphorus modification in zeolites is a well-established phenomenon for some reactions[90, 105-107], the enhancement in rates, as observed here, is less common in the literature.

When measuring the activation energies for the acylation of 2-MF with AA over the parent zeolite (0P) and comparing them to those found for different phosphorus loaded ZSM-5 samples, we observed an increase in activation barriers as phosphorus loading increased, as shown in Figure 3-4. This suggests that under these conditions, the reaction is unlikely to be limited by diffusion within the zeolite pores, as diffusion restrictions are well known to decrease observed reaction barriers with porous catalysts. This, in turn, indicates that the impact of addition of phosphorus within the zeolites modifies the nature of active sites. The observed increase in activation barriers also suggests that these measurements are influenced by the fraction of phosphorus induced strong Brønsted acid sites (P-BAS), as presented in Figure 3-4. A similar observation was observed in alkylation of toluene with methanol over H-ZSM5 zeolite in which phosphorous addition increases the activation energies of the reaction[108]. Indeed, the

measurement of turnover frequency (TOF) over these samples revealed intriguing performance trends, as illustrated in Figure 3-5. At lower temperatures (160-180°C), all samples exhibited identical TOFs per strong BAS, as measured by IPA-TPRx. This indicates that only the strong, unperturbed Bronsted sites are active under this temperature range. However, as the temperature increased to 200°C and beyond, the TOFs over phosphorous zeolites notably surpassed those measured over the parent zeolite. This observation implies the existence of other, weaker active sites that require higher temperatures to effectively catalyze the acylation reaction.

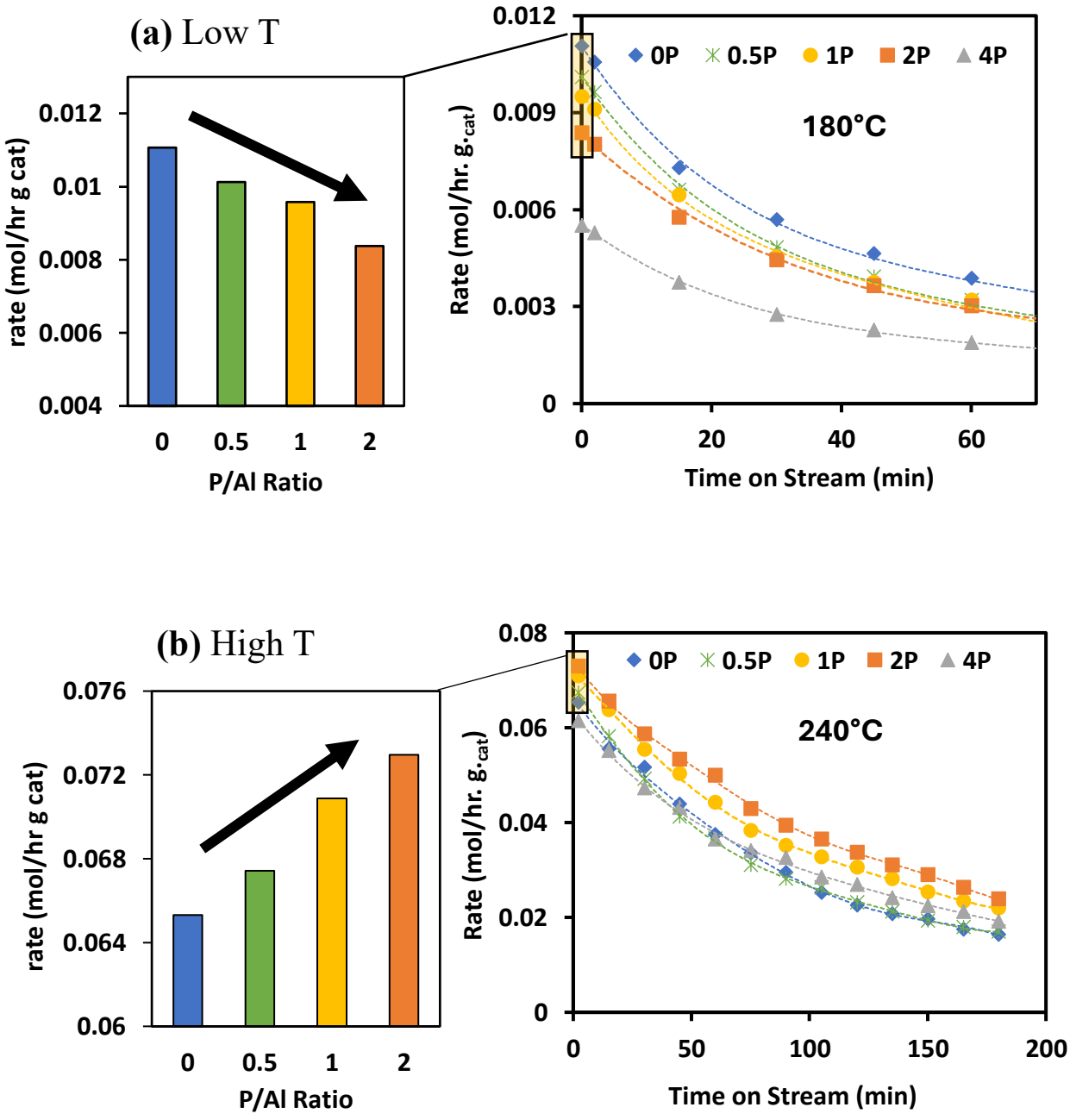


Figure 3-3 Comparisons of acylation rate of 2-MF with AA parent zeolite (0P) and various phosphorous modified zeolite with different loadings. Reactions were carried out at (a) 180C and b) 240C.

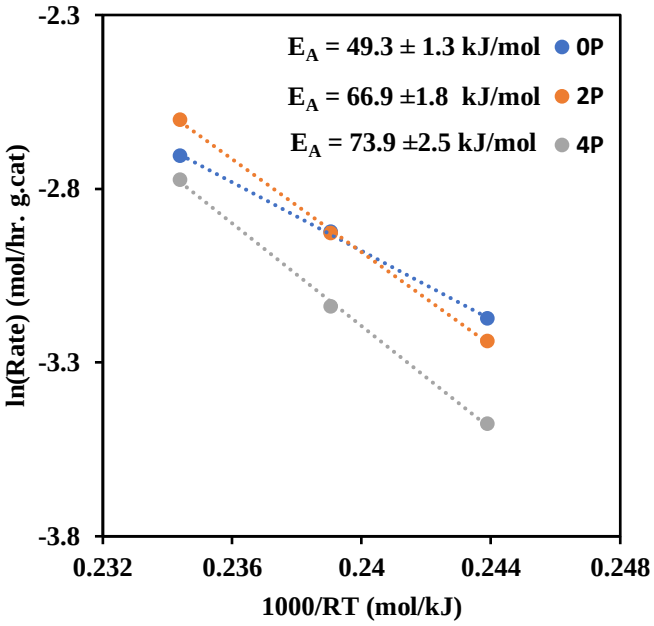


Figure 3-4: Measured activation energies for acylation of 2-MF with AA over 0P (parent zeolite), 2P, and 4P under reaction temperatures between 220-240°C

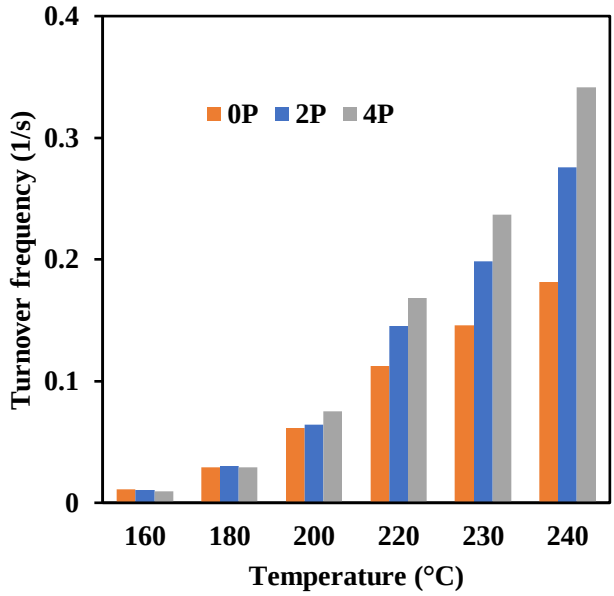


Figure 3-5 Initial Turnover frequencies (TOFs) of acylation over parent ZSM-5 zeolite (0P) and phosphorous modified ZSM-5

The deconvolution of the rate and activation energy associated with P-sites was accomplished using an approach similar to that described in the literature[34]. To isolate these values for the newly formed, weak P-induced BAS, we initiated our analysis by calculating the fraction of strong BAS, as detailed in Table 3-2. Subsequently, as outlined in Equation 3-4, we proposed that the total rate of acylation over phosphorus modified zeolites is the sum of the reaction rates of both unmodified BAS and P-induced BAS. This approach is underpinned by the fact that the rates obtained for 0P (parent zeolites) are solely attributable to BAS, with no contribution from P-induced sites. We further assume, in Equation 3-5, that the reaction rate of BAS (at a given temperature) corresponds to the total rate over the 0P catalyst, multiplied by the fraction of BAS.

- $\boldsymbol{Rate_{Total-xP} = Rate_{(BAS)} + Rate_{(xP)}} \left[\frac{mol}{hr\ g_{cat}}\right]$ ***Equation 3-4***
- $Rate_{(0P)} = 0$
- $\boldsymbol{Rate_{(BAS)} = Rate_{Total-0P} \bullet (BAS\%)} \left[\frac{mol}{hr\ g_{cat}}\right]$ ***Equation 3-5***

Leveraging the known fraction of BAS for each phosphorus-modified zeolite, as provided in Table 3-2, we can determine the rate of P-induced sites by combining both Equations 3-5 and 3-6: -

- $\boldsymbol{Rate_{(2P)} = Rate_{Total\text{-}2P} - Rate_{Total\text{-}0P} \bullet (0.73)}$
- $\boldsymbol{Rate_{(4P)} = Rate_{Total\text{-}4P} - Rate_{Total\text{-}0P} \bullet (0.5)}$

We find this to be a valid assumption and approach for several reasons. First, the TOFs for 0P, 2P, and 4P are nearly identical at lower temperatures (160-180°C), as visually depicted in Figure 3-5. The additional TOF values observed at higher temperatures (200-240°C) are attributed to the presence of P-induced BAS.

Table 3-2 retention of Brønsted acid sites (BAS) upon P incorporation

Sample	BAS (mmol/g)	BAS retention%*
0P	**0.102**	**100 %**
0.5P	**0.095**	**93%**
1P	**0.086**	**84%**
2P	**0.075**	**73%**
4P	**0.051**	**50%**

* Determined by IPA-TPRx

The deconvoluted rates, as illustrated in Figure 3-6a, reveal that as the phosphorus loading increases, there is a concurrent decline in the rate of strong BAS and a corresponding increase in P-induced rates. Moreover, the activation energies for phosphorus-induced sites in both 2P and 4P, as illustrated in Figure 3-6b, exhibit intriguingly similar barriers, with values exceeding more than twice those found in 0P (parent zeolite). This observation supports the notion that P-induced BAS possess unique activity, necessitating higher energy input to achieve the observed rates, as corroborated by our findings in Figure 3-3 and 3-5. These findings strongly suggest that the incorporation of phosphorus leads to an alteration in deprotonation energy (DPE), a key determinant of Brønsted acid strength and, consequently, catalytic activity[109-111]. We postulate that this modification occurs through the disruption of hydroxyl bridging and the formation of new Al-O-P bonds, as indicated in ^{31}P-NMR spectra presented in Figures 3-2a and b.

In addition to determining the activation barrier values for P-induced sites in 2P and 4P, we extended our investigation to assess the activation barriers for acylation over phosphorus-modified silicalite-1, as depicted in Figure 3-6c. The remarkable similarity in activation barriers

between P-silicalite-1 and the deconvoluted P-induced sites in 2P and 4P lends strong support to our successful separation of the rates of weak and strong BAS. However, it is worth noting that while P-silicalite-1 does exhibit some level of activity in the acylation process, the reaction rates are notably lower compared to those observed over phosphorus-modified and non-modified aluminosilicate zeolites, as indicated in Figure S3-6a. Furthermore, it is important to highlight that rates over P-silicalite-1 undergo rapid deactivation, rendering them impractical for acylation applications. This loss of activity could be attributed to two plausible explanations. First, it may result from the complete hydrolysis of the weak Si-O-P bonds, while the second possibility involves the cleavage of P-O-P bonds during the dehydration of acetic acid[97], or an alternative explanation could be simply that the presence of acetic acid promotes sintering of these dispersed phosphoric acid species interacting with the silicalite pores to form larger aggregates that are less accessible. Ultimately, these processes lead to the conversion of P-induced BAS into free phosphoric acid and polyphosphate species that appear to be less active for carrying out the acylation reaction.

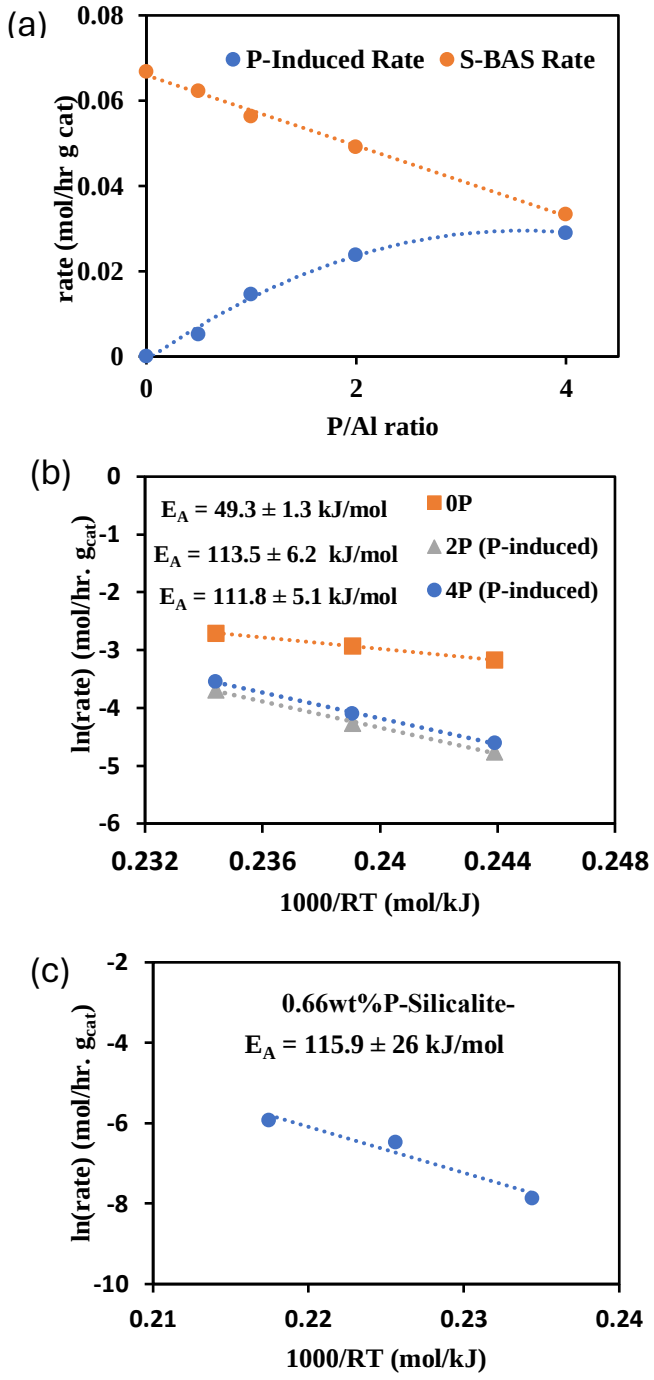


Figure 3-6 The decoupled rates for of strong BAS and P-induced sites as a function of phosphorous loading (b) Deconvoluted Activation barriers of acylation of 2-MF with AA over phosphorus induced BAS in 2P and 4P catalysts compared with parent zeolite (0P) at temperature range between 220-240°C. (c) The activation energy measured over 0.66wt% phosphorous silicalite-1 at temperature range between 240- 280°C

3.3.3 Role of phosphorous modification on catalyst stability and selectivity

One of the most well-regarded advantages of phosphorus modification to zeolites is its capacity to enhance catalyst stability both industrially to preserve crystallinity under severe hydrothermal conditions beyond the conditions utilized here,[66] as well as modifications to coke formation rates for several reactions thereby extending the catalyst's lifespan [66, 88, 112-114]. Consistent with previous research findings, we observed that the addition of phosphorus to zeolite effectively mitigates deactivation. Notably, the measured deactivation constants for acylation over 2P and 4P are approximately 25% lower than that for the 0P catalyst, as evidenced in Figure 3-7. Our proposition for the prolonged catalyst life pivots on the generation of a stronger conjugate base through phosphorus-induced sites. This, in turn, expedites the deprotonation of the Wheland intermediate[20], facilitating product desorption, as schematically depicted in Scheme 3-2. This step is crucial in preventing a sequential reaction between the adsorbed product and gaseous phase 2-MF[60]. Such sequential reactions produce heavy oligomers that pose more significant challenges when regenerating aluminosilicate zeolite catalysts in contrast to phosphorus modified zeolite (Figure S3-7). It is well-established that phosphorus zeolites exhibit lower coke formation in various reactions by preventing side or sequential oligomerization of products[112, 115, 116]. In fact, our TGA analysis of the surface species retained in spent catalysts suggests that while the amount of light oligomers is slightly higher in phosphorus zeolite, the quantity of heavy carbonaceous deposits is approximately 50% of that found in the parent zeolite, as illustrated in Figure S3-10 and Table S3-2. Additionally, the elemental analysis estimates a hydrogen-to-carbon ratio of 2 for surface oligomers in 0P and 3 in 2P, providing further evidence of reduced coke formation on phosphorus-modified zeolites.

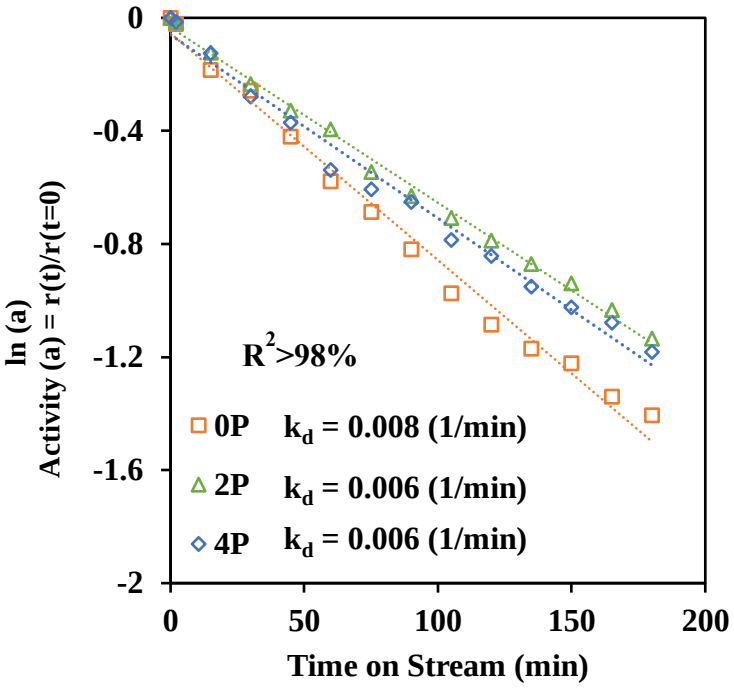
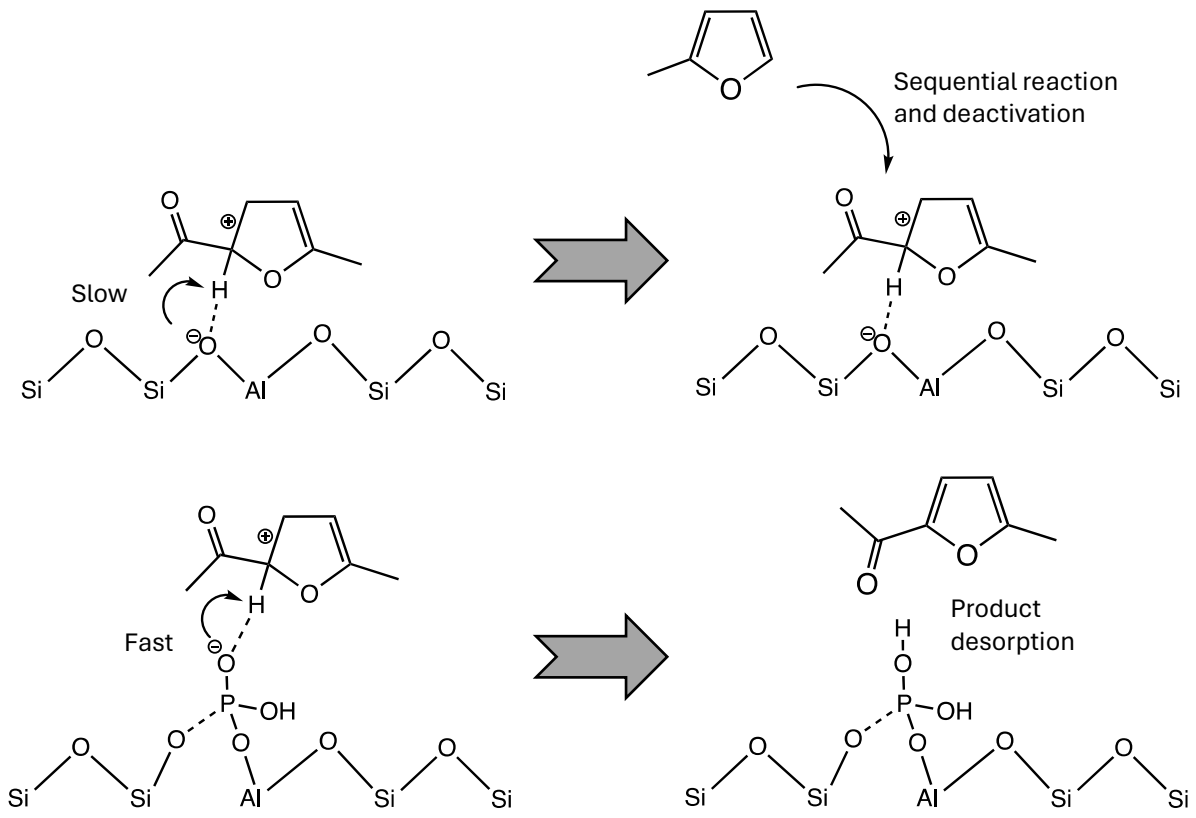


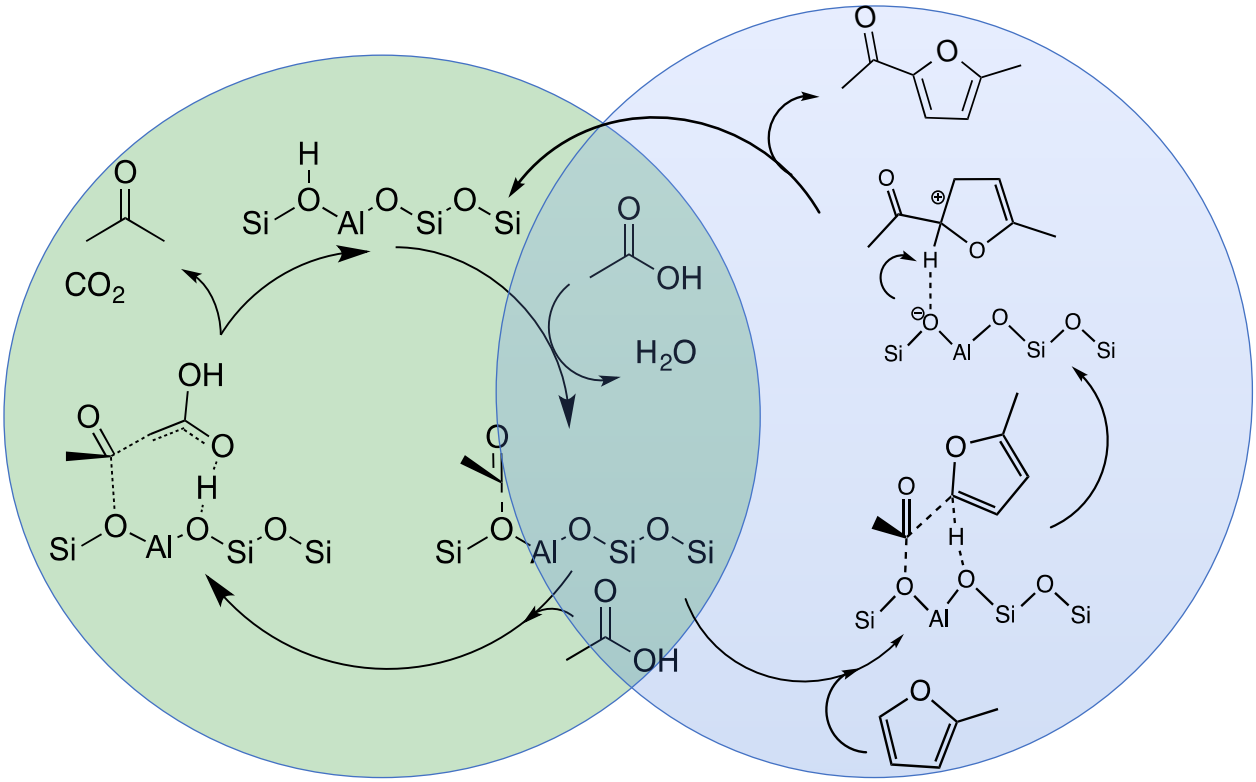
Figure 3-7 Measured deactivation constants for acylation of 2-MF with AA over parent zeolite (0P) and phosphorous modified zeolite (2P and 4P) at 240°C



Scheme 3-2 Depiction for role of intrinsic acid strength on averting a proposed deactivation mechanism of sequential reaction between adsorbed product and a gas-phase 2-MF reactant[60].

Enhancing product selectivity by limiting side reactions is another highly valuable aspect of phosphorus modified zeolites [88, 117]. In the acylation of 2-methylfuran with acetic acid over zeolites, the reaction can follow two distinct pathways depending on the conditions. One proceeds through the acylation reaction cycle, while the other diverts into the ketonization cycle, as proposed in Scheme 3-3[18, 118] where we learned that ketonization starts to occur at 250°C but ultimately favors acylation pathway's selectivity. To investigate how phosphorus impacts this side reaction, we introduced phosphorus into the high density BAS ZSM-5 zeolite (Si/Al = 40) and elevated the reaction temperature to 250°C. We selected this zeolite due to the relatively high BAS density required for noticeable acetone production through acetic acid ketonization. It's important to note that we introduced acetic acid alone to avoid complications or anomalies

arising from high acylation conversion. The results of this experiment, shown in Figure 3-8, clearly demonstrate that the addition of phosphorus mitigates the rate of ketonization, with a pronounced inhibitory effect observed at higher phosphorus loadings. This underscores another advantageous aspect of employing phosphorus modified zeolites for the acylation of furanics with carboxylic acids.



Scheme 3-3 Illustration of the two major reaction cycles during acylation of 2-MF with AA over zeolites. Left (green) is for ketonization reaction and right (blue) is for acylation.

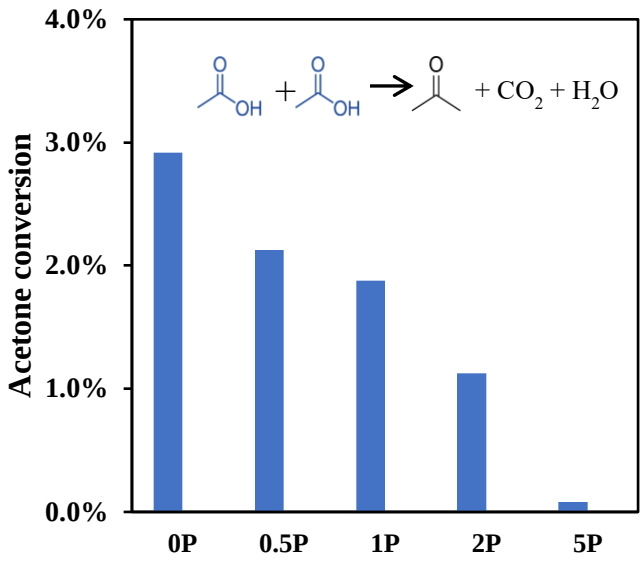


Figure 3-8 the conversion of acetic acid to acetone over parent zeolite HZSM-5(40) (0P); compared with different phosphorous modified (P/Al= 0.5, 1, 2, 5) at 250°C.

3.4 Conclusions

In summary, this study has elucidated the effects of phosphorus impregnation on the acidity of ZSM-5 zeolites, giving rise to distinct sites associated with Al-O-P and Si-O-P bonds. This alteration leads to a reduction in the density of strong Brønsted acid sites (BAS). When strong framework BAS are titrated with P species, this results in a reduction in strong BAS with weaker P modified sites that exhibit higher reaction barriers. Incorporation of additional P results in net increases in reaction rate at elevated reaction temperatures due to the nature of these active sites. Furthermore, we have decoupled reaction rates associated with traditional BAS from P modified sites, explaining the observed variation in activation barriers observed at various P loadings. The deconvoluted activation barriers for phosphorus induced sites were found to be similar for two different phosphorus loadings (2P and 4P), significantly higher than those for the parent zeolite (0P), and closely aligned with the values obtained over phosphorus-modified

silicalite-1. This suggests that the phosphorus induced sites exhibit notably larger deprotonation energies.

Additionally, lower deactivation constants are observed over P modified zeolites, which we hypothesize is due to the more facile product desorption leading to diminished sequential reactions that result in catalyst deactivation. Notably, the amount of coke formed on phosphorus zeolite was significantly lower than on the parent zeolites. Furthermore, an additional advantage of phosphorus addition is the suppression of undesired side reactions, such as the ketonization of acetic acids. These results suggest many appealing benefits to the modification of existing aluminosilicate ZSM-5 zeolites through phosphorus incorporation for the direct acylation of biomass-derived 2-methylfuran and acetic acid.

Chapter 4: Effect of Brønsted Acid Site's Local Environment on Zeolites' Catalytic Activities during Acylation of 2-Methylfuran with Acetic Acid

The work in this chapter is a collaboration between the University of Oklahoma and Dr. Jeffery White's group at Oklahoma State University. Solid state ^{27}Al-NMR characterizations were obtained from Dr. White's group at OSU, while the rest of the experimental work conducted by our research group at OU. DFT calculation was collected from Dr. Wang group at OU. This work is planned for future publication involving the authors Ismaeel Alalq, Vy Nguyen , Anya Zornes Alejandra Gomez, Bin Wang, Jeffrey White, Steven Crossley.

Abstract

Zeolites, particularly MFI, have recently emerged as highly promising catalysts for direct Friedel-Crafts acylation reactions employing renewable carboxylic acids, yielding a versatile range of high-value fuels and essential commodity chemicals. The acylation of furanic compounds using carboxylic acids presents a particularly attractive avenue for the synthesis of sustainable surfactants. While the mechanistic understanding of this process has only recently emerged, the role of extra-framework alumina (EFAL) in influencing zeolite catalyst reaction rates has not been explored for this chemistry. Although the presence of EFAL alongside framework sites is recognized to generate stronger synergistic Brønsted acid sites (BAS), the consequential impact on acylation reaction remains unknown. In this study, we undertake a comprehensive investigation into the acylation of 2-methylfuran (2-MF) using acetic acid (AA) over EFAL-incorporating MFI (Si/Al=40) and BEA (Si/Al=150) zeolites, then contrasting their behaviors after EFAL removal via ammonium hexafluorosilicate (AHFS) washing. Acid quantification of AHFS-washed zeolites through isopropylamine temperature programed reaction (IPA-TPRx) showed a marginal acid count reduction, while a qualitative verification of EFAL

removal upheld by solid-state Al^{27}-NMR analysis. Acylation under mild conditions, specifically within the 160-180°C range, remarkably uncovers higher activity over zeolites possessing EFAL, whereas reaction rates experienced a pronounced decline post-AHFS treatment. Interestingly, the removal of EFAL leads to a twofold increase in measured activation barriers, aligning them with those observed for all-framework aluminum MFI (Si/Al=140) zeolites. The aforementioned observations were settled through DFT calculations, which found activation energies effectively in line with experimental values. Understanding this complex interplay between extra-lattice alumina and Brønsted acid site is significant for comprehending the underlying factors that govern the kinetics of the reaction and holds key implications for optimizing catalytic performance. This study substantially contributes to understanding of zeolite-catalyzed acylation, offering a pivotal framework to enhance catalytic efficiency within the territory of renewable chemical synthesis.

4.1 Introduction

Acylation reactions play a critical role in organic synthesis, enabling new carbon-carbon bond formation between acylating agents (typically acyl halides and anhydrides) with aromatic acyl acceptors in the presence of catalytic materials[3, 119, 120]. This chemistry has a diverse field of applications ranging from pharmaceuticals to household essentials[4]. In conventional acylation processes, homogeneous Lewis acid catalysts, such as $AlCl_3$, have been commonly employed. However, these catalysts have been associated with the generation of environmentally hazardous by-products and waste, raising concerns about their ecological impact[5, 21]. As a result, over that past few decades, there has been a growing research emphasis on exploring alternative acylation routes utilizing non-sacrificial heterogenous aluminosilicate zeolite catalyst[4, 9, 37-40, 42]. Numerous studies have been dedicated to investigating the acylation of

biomass-derived oxygenates, driven by the aspiration to shift towards a more sustainable and environmentally friendly approach[27, 57, 59, 121].

The mild thermal transformation of complex polymers derived from biomass, such as torrefaction, selectively decomposes hemicellulose and cellulose, resulting in a blend of furanics and carboxylic acid species[15, 122]. Direct conversion of these products via acylation chemistry over zeolite catalyst has been extensively researched over the past several years[18-20, 57, 60]. During early kinetic study of acylation of 2-methylfuran (2-MF) with acetic acid (AA) over zeolites, Gumidyala et al[18]. investigated activity, selectivity, and influence of water under different reaction conditions revealing a promising new reaction pathway toward producing high-value chemicals from biomass. In other related studies, a focal point has been the meticulous examination of the reaction mechanism, which has identified the most relevant transition states during direct acylation over Brønsted zeolites. By unraveling the crucial intermediate species, the study made significant contribution in elucidating the catalytic pathways underlying acylation of 2-MF with AA over zeolite catalysts[20]. While studies have shed light on the potential of this direct acylation route using zeolites (including different topologies)[18-20], much remains unknown about the influence of the Brønsted acid site's (BAS) local environment in zeolites on the catalytic activity during acylation.

The active sites in aluminosilicate zeolite have distinct activity that is subjective to factors including local confinement, BAS proximity and presence of extra framework Aluminum (EFAL)[34, 35, 123-130]. Gounder et al. demonstrated how some reactions, such as carbonylation of dimethyl ether, have much higher turnover rates at low temperatures in smaller voids in MOR zeolites while other reactions, such as cracking of hydrocarbons, rates benefit more in spacious locations at higher temperature[124]. This observation confirms the occurrence

of enthalpy-entropy compensation, which governs the Gibbs free energies of transition states and relevant reactants, thereby influencing the activation energies that dictate turnover rates through transition state theory. Just as confinement effects exert a substantial influence on reaction rates, the close proximity of Brønsted acid sites (BAS) has demonstrated profound impacts on both reaction rates and selectivities within various chemical transformations. These effects have been particularly evident in reactions such as methanol-to-aromatics conversion, olefin oligomerization, and alkane cracking.[35, 129-131]. In alkane cracking, Kester et al. observed that rate enhancement is proportional to the fraction of paired BAS in chabazite zeolites[130]. The rate improvement was reported to reach up to 12 times higher on paired BAS in comparison to isolated BAS which was attributed to less negative apparent activation entropies found in adjacent active sites.

Direct vicinity of extra-framework aluminum (EFAL) to Brønsted acid sites (BAS) gives rise to distinct active sites exhibiting notably enhanced activity. This superior catalytic performance arises from a synergistic interplay between protons originating from the tetrahedral framework aluminum and non-framework alumina species. Numerous prior investigations have substantiated the existence and efficacy of such synergistic Brønsted acid sites (SBAS), underscoring their pivotal role in catalytic cracking of alkanes[34, 36, 126, 132-136]. In a demonstration of EFAL's crucial role in generating highly active synergistic Brønsted acid sites (SBAS) during n-pentane cracking, Schallmoser et al. employed a targeted approach, selectively eliminating EFAL through ammonium hexafluorosilicate (AHFS) treatment.[126]. Their findings revealed that the turnover frequencies (TOF) on MFI zeolites with low Si/Al ratios, characterized by a substantial EFAL fraction, underwent a reduction to levels analogous to those observed on high Si/Al zeolites featuring an all-framework aluminum composition. These observations have

been corroborated by another related study investigating the influence of water in activating EFAL within MFI zeolites, thereby generating novel highly active sites conducive to hexane cracking [34]. The impacts of EFAL within zeolites extend beyond alkane cracking. Additional studies propose the presence of Lewis acids arising from non-framework alumina, which can exert influence over diverse reactions, encompassing alkylation, dehydration, and the conversion of methanol to hydrocarbons[137-139]. While Lewis acidic non-framework Al moieties in zeolite can exist in distinctive forms with varying quadrupole moments, decoupling the intrinsic Lewis-Brønsted acid synergy of EFAL can be challenging[140]. In general, it is accepted to assume that that all synergistic Brønsted acid sites (BAS) are uniform, given their shared reaction implications, thereby rendering their application to acylation intriguing.

Within this study, we comprehensively investigate the influence of synergistic Brønsted acid sites (SBAS) on acylation chemistry, utilizing acetic acid (AA) as the acylating agent and 2-methylfuran (2-MF) as the acyl acceptor. We examine this phenomenon across diverse zeolite topologies, specifically MFI and BEA. Our approach includes the targeted extraction of EFAL from the zeolite matrix through AHFS treatment, a process confirmed via rigorous Al^{27} NMR analysis. The results of our investigation unveil remarkable shifts in reaction rates and measured activation energies post-EFAL removal, aligning closely with those observed in the all-framework aluminum MFI (Si/Al=140) zeolite. These outcomes substantiate the pivotal role of EFAL in influencing catalytic activity and provide deeper insights into the complex interplay between these acid sites and reaction kinetics. To consolidate the experimental findings, we conducted DFT calculations, revealing activation energy trajectories congruent with the experimental data. This dual approach, coupling experimental observations with theoretical insights, supports our understanding of the catalytic mechanisms at play. Our research highlights

the vital importance of exploring the nature of these acid sites and their pronounced effects on acylation reactions. By advancing this understanding, we open avenues for optimizing the acylation process employing zeolite catalysts, ultimately contributing to the broader field of sustainable and efficient chemical synthesis.

4.2 Experimental section

4.2.1 Chemicals and materials.

The zeolite catalysts sample used in this study are commercial grade obtained Zeolyst international including MFI CBV8014 (Si/Al = 40), CBV28014 (Si/A l= 140) and BEA CBV-CP811C-300 (Si/Al = 150). Ammonium hexafluorosilicate (AHFS) (99.999% trace metals basis, Sigma-Aldrich) was used to remove non-framework aluminum in zeolites. The acylating agent is acetic acid (glacial, ACS reagent, ≥99.7%, Sigma-Aldrich). The acyl acceptor is 2-Methylfuran (98+%, stab., Alfa Aesar).

4.2.2 Catalyst preparation

CBV-CP811C-300 was initially received in its proton form, designated as HBEA-150. Conversely, CBV8014 and CBV28014 were in the $NH4^+$ form and underwent a calcination process to achieve the H+ form, resulting in H-MFI(40) and H-MFI(140). The calcination process took place within a 1-inch quartz tube under a continuous air flow of 100 mL/min. The samples were gradually heated at a ramp rate of 2°C/min until reaching 600°C, at which point they were held for 5 hours. To remove excess framework aluminum from MFI(40) and BEA(150), we followed a standard procedure involving Ammonium hexafluorosilicate (AHFS) washing, as documented in literature[126]. The resulting modified samples were labeled as AHFS-MFI(40) and AHFS-BEA(150). For consistency, all catalyst samples were pelletized,

yielding particle sizes falling within the range of 90-250µm pellets. Table 4-1 provides a comprehensive summary of the physical properties of the catalyst samples utilized in this study.

Table 4-1 Properties of investigated zeolite catalyst samples

		BAS density (mmol/g)			
Catalyst	Si/Al	Theoretical	Measured [b]	Literature	EFAL % [c]
H-MFI (40)	40	0.41	0.39	0.38-0.39[34, 46, 127]	4.9
AHFS-MFI (40)	-	-	0.35	-	-
H-MFI (140)	140	0.12	0.10	0.094-0.1[34, 127, 141]	-
H-BEA (150)	150	0.11	0.096	0.1 [142]	12.7
AHFS-BEA (150)	-	-	0.085	-	-

[a] *Calculated based on Si/Al ratios.* [b] *Determined via* isopropylamine temperature programed reaction (IPA-TPRx). [c] *Determined by subtracting the theoretical BAS density by the number of BAS sites measured by IPA-TPRx.*

4.2.3 Catalyst Characterization

4.2.3.1 IPA-TPRx measurements

In order to determine the density of Brønsted acid sites (BAS) in the aforementioned catalyst samples, we employed the Isopropylamine Temperature-Programmed Reaction (IPA-TPRx) technique. The catalyst samples were carefully packed into 1/4-inch quartz tubes and subsequently pretreated under a helium flow of 30 mL/min, with a gradual temperature increase of 10°C/min until reaching 300°C, where they were held for 1 hour. Subsequently, the temperature was reduced to 100°C. The catalyst samples were subjected to a series of 2 µL IPA pulses to ensure thorough saturation of the Brønsted acid sites. Following this, helium flow was maintained for 1

hour to remove any physically or weakly adsorbed IPA species. The TPRx phase initiated with a temperature at 10°C/min ramp from 100°C to 600°C. Throughout the process, the evolution of desorbed species was continuously monitored using a Cirrus mass spectrometer (MKS), recording signals at m/z = 17 (NH_3), 44 (IPA), and 41 (propylene). The quantification of Brønsted acid site density was achieved by calibrating the mass spectrometer signals using the average of several 0.5 mL-pulses of propylene.

4.2.3.2 X-Ray diffraction

X-ray diffraction (XRD) analyses was conducted for all catalyst samples using a Rigaku diffractometer. Cu Kα radiation was generated at 44 mA and 40 kV. The diffraction angle range examined was $2\theta = 2-70°$

4.2.3.3 Solid-State NMR Spectroscopy

^{27}Al NMR experiments were acquired at 9.4 T with a Bruker Avance II console using a 4-mm double-resonance MAS probe, with samples packed in ZrO_2 rotors under ambient air. 2048 transients per spectrum were acquired with a single 30° pulse of 1.16 µs, recycle delay of 0.5s, and a spinning speed of 10 kHz. Pulse widths and chemical shifts were calibrated using a 0.1M aqueous solution of $Al(NO_3)_3$

4.2.3.4 Scanning Electron Microscopy (SEM)

Crystal morphology and particle size were assessed using the Zeiss NEON 40EsB Field-Emission SEM. To prepare the samples for SEM analysis, a small amount of the zeolite samples was placed on double-sided sticky carbon tape and then coated with sputtered iridium (Sputter coating: Emitech K575XD). SEM images were obtained at an accelerating voltage of 5 kV.

4.2.4 Kinetic Measurements

The acylation of 2-MF with AA over zeolite catalysts was conducted in the gas phase using a fixed bed tubular reactor, following established procedures. A specific quantity of catalyst, ranging from 5 to 20 mg, was mixed with glass beads, and packed between layers of quartz wools within a 1/4-inch quartz reactor tube. The catalyst was then subjected to pretreatment, involving a slow temperature ramping at a rate of 10°C/min to 300°C, where it was held for 1 hour, all under continuously flowing nitrogen to eliminate physically adsorbed moisture. Subsequently, the catalyst was cooled down to the desired reaction temperatures, within the range of 160-180°C. During the reaction, a nitrogen carrier gas was maintained at a flow rate of 125 sccm, while the reactants AA and 2-MF were introduced typically at rates of 1 mL/hr and 0.1 mL/hr, respectively. The reaction orders for both reactants can be found in Figure S4-1 and S4-2. Temperature control of the reactor was achieved via a thermocouple attached to the external surface of the reactor tube, precisely aligned with the center of the catalyst bed. After the pretreatment, the reactor temperature was set to the desired reaction temperature, and the feed rate of reactants was meticulously controlled using syringe pumps. To prevent condensation of leaving species, the reactor outlet streamline was heated to 250°C. A micro electric actuator was employed to control the six-port valve, which directed samples to an inline-connected gas chromatograph (Agilent 7890B) equipped with a flame ionization detector. Separation of reaction products was achieved using a Zebron Phase: ZB-WAX column (30m × 0.25mm × 0.25μm). To facilitate data analysis, including conversion and carbon balance, response factors for the reactants were determined. These response factors were obtained by flowing the respective reactant at the desired rate through a bed of glass beads to simulate the

catalyst bed, while standards were used for the determination of product response factors. The values for turnover frequency (TOF) were obtained using the following equation: -

$$TOF = \frac{Mole\ of\ product\ formed\ per\ second\ gram\ catalyst}{Moles\ of\ Brønsed\ acid\ sites\ per\ gram\ of\ fresh\ catalyst} \qquad \textit{Equation 4-1}$$

While the reaction conversions were estimated using equation 4-2: -

$$Conversion = \frac{Moles\ of\ acylated\ product\ formed\ per\ hour}{Moles\ of\ 2{-}methylfuran\ fed\ per\ hour} \qquad \textit{Equation 4-2}$$

The initial reaction rates were obtained by extrapolation to zero time on stream for proper evaluation for the acylation kinetics.

4.2.5 DFT Calculations.

All density functional theory (DFT) calculations were conducted using the Vienna ab initio simulation package (VASP)[143]. The projected augmented wave (PAW)[144, 145] method and the generalized gradient approximation Perdew-Burke-Ernzerhof (GGA-PBE) exchange-correlation function were employed[146]. Van der Waals interactions were incorporated using the DFT-D3 semiempirical method[147]. The MFI unit cell utilized in the calculations comprised 96 T sites and 192 O atoms, with lattice constants set to a=20.078 Å, b=19.894 Å, and c=13.372 Å, as per previous work[34, 36, 148, 149]. The structure was fully relaxed until the atomic forces converged to below 0.02 eV $Å^{-1}$. A kinetic cutoff energy of 400 eV was applied. Migration barriers of $[Al(OH)_2]^+$ were examined at the intersection, with a framework Al site positioned at T10 within a five-membered ring to balance the charge of the EFAl cation. At the intersection, $[Al(OH)_2]^+$ migrated from a position adjacent to a T7 site to one facing a T11 site, and then to a

site proximal to a T12 site. The nudged elastic band (NEB) method[150] was employed to compute the transition state.

4.3 Results and discussion

4.3.1 Characterization

While AHFS washing treatment in zeolites effectively removes excess lattice aluminum species, it is noteworthy that catalysts may experience a modest reduction in Brønsted acid count[149, 151, 152]. In line with findings from existing literature, our IPA-TPRx measurements indicate an approximate 10% decrease in BAS density for both H-MFI(40) and H-BEA(150) samples, as illustrated in Table 4-1. Furthermore, our solid-state ^{27}Al-NMR analysis in Figure 4-1 reveals a slight decrease in the 60 ppm chemical shift peak intensity, qualitatively corroborating the IPA-TPRx data. Interestingly, the ^{27}Al-NMR results suggest that AHFS treatment of H-BEA(150) selectively removes specific types of acid sites centered around 57.3 ppm, corresponding to aluminum in the T3-T9 positions, while the T1-T2 sites remain unaffected. This observation aligns with prior research findings[153]. Solid-state 27Al-NMR spectroscopy proves invaluable in elucidating the state and coordination of aluminum species, which can exist tetrahedrally, octahedrally, or in partial coordination within zeolite frameworks[152, 154].

Figure 4-1 illustrates that both H-MFI(40) and H-BEA(150) samples contain non-framework aluminum species, evident in the peak center at a chemical shift of 0 ppm. However, the application of AHFS washing to these samples results in the elimination of peaks in this region, indicating the successful removal of the EFAL (extra-framework aluminum) species from both zeolite frameworks. It is important to note that both H-MFI(40) and H-BEA(150) parent zeolites contain both EFAL and BAS, allowing us to investigate the role of synergistic active sites created by Brønsted acid sites in close proximity to non-framework coordinated aluminum. As a reference,

we included MFI(140) zeolite in this study, which is known to be free of EFAL species. This zeolite serves as a benchmark for acylation on isolated all-framework BAS. The active sites in this high Si/Al zeolite are estimated to be isolated and located at the intersection of MFI pore channels[123].

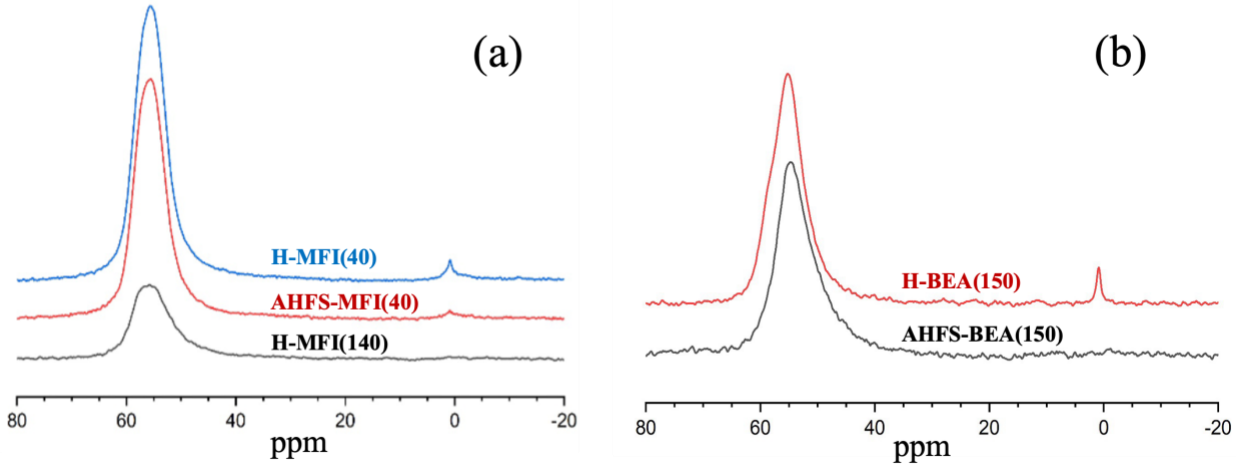


Figure 4-1 Al^{27}-NMR for (a) H-MFI(40), AHFS-MFI(40) and H-MFI(140) (b) H-BEA(150) and AHFS-BEA(150) elucidating the tetrahedral coordinated Al (framework Al) in the chemical shift at 60 ppm, while the partially coordinated Al (non-framework Al) represented in the chemical shift at 0 ppm.

Preserving the structural integrity of catalyst particles subjected to AHFS washing is crucial to ensure a fair comparison with their parent zeolites. In Figure 4-2, we present XRD patterns for all zeolite samples utilized in this study. The data demonstrates that, on the whole, the structures of the AHFS-treated zeolites remain unaltered, exhibiting no detectable damage to the crystal lattice. However, AHFS-BEA(150) exhibited a slight reduction in the relative peak intensity, coupled with a shift in the position of a narrow diffraction peak at $2\theta = 22.6°$. This shift may be attributed to changes in the Si/Al ratios within the catalyst[153, 155]. While zeolite acid

leaching can result in the formation of micropores within the zeolite structure, it is important to note that zeolites with relatively high Si/Al ratios are less susceptible to this phenomenon[156]. Additionally, the AHFS washed zeolite samples were characterized by SEM to observe their morphology and contrasted with their parent counterpart zeolite (Figure 4-3). Furthermore, we conducted SEM characterization of the AHFS-washed zeolite samples to examine their morphology, comparing them with their parent counterpart zeolites (Figure 4-3). While previous studies have noted that this type of treatment can lead to defect formation, the rate of defect formation is influenced by the aluminum content. In light of this, it is reasonable to assume that no observable changes have occurred in the morphologies of the modified samples, as illustrated in Figure 4-3.

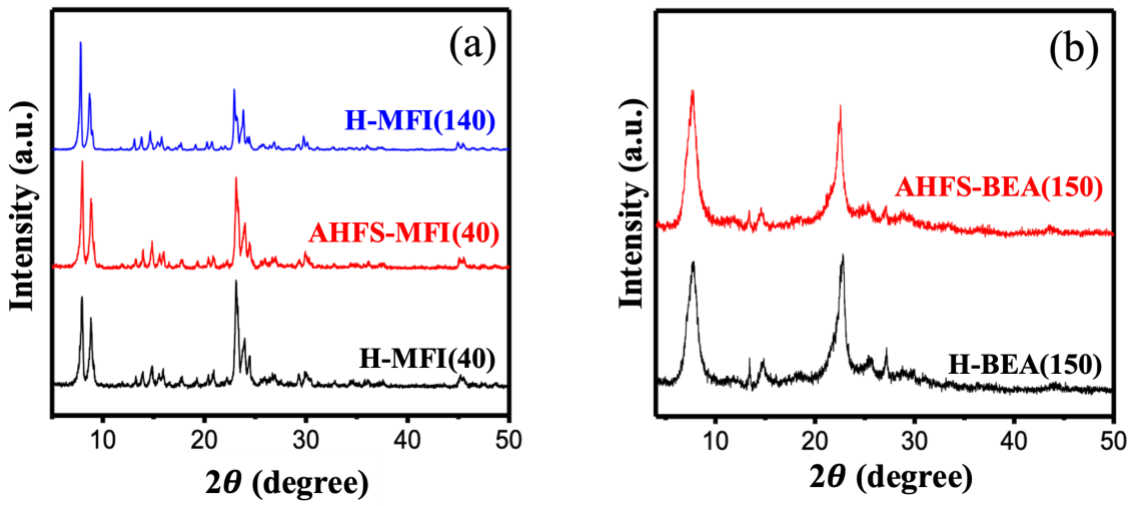


Figure 4-2 XRD result suggests removal of EFAL species via AHFS washing does not have any detectable damage to both (a) MFI and (b) BEA zeolites crystal structures

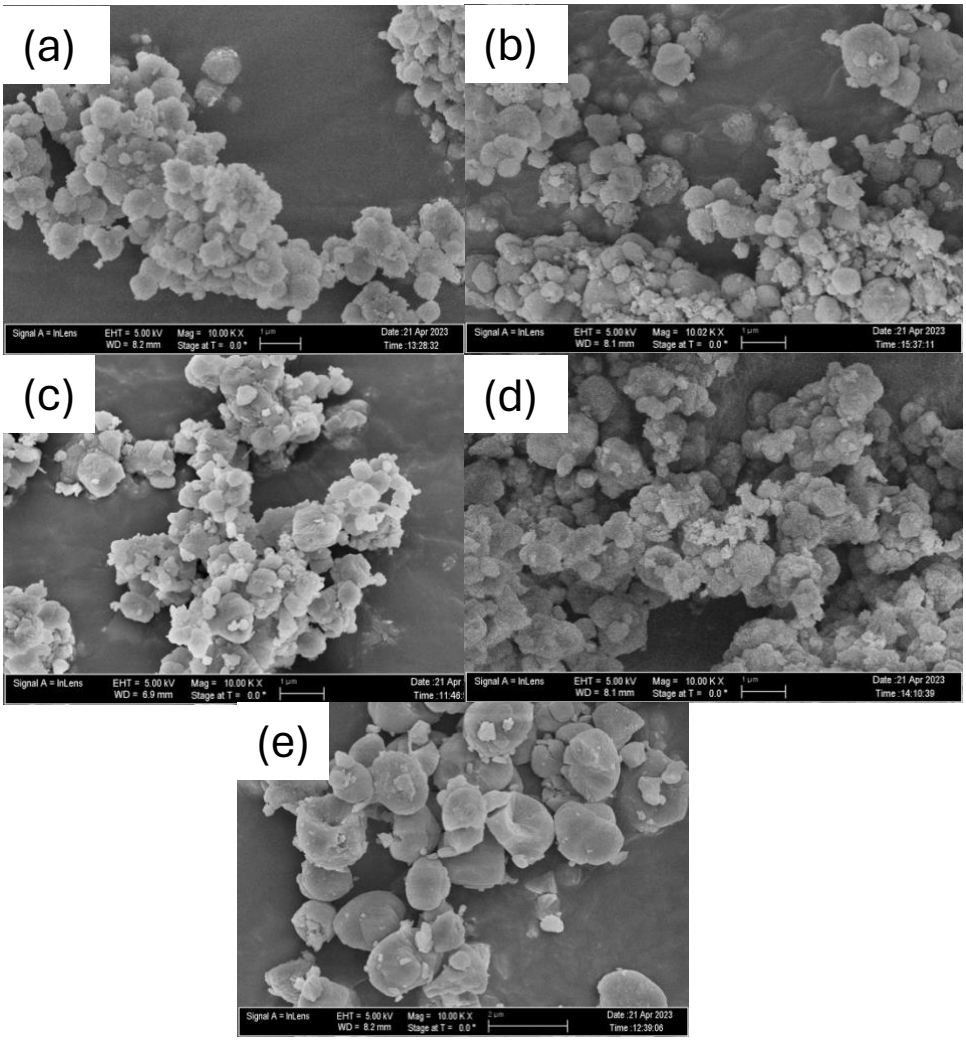


Figure 4-3 SEM images for (a) H-BEA(150) (b) AHFS-BEA(150) (c)H-MFI(40) (d) AHFS-MFI(40) (e) H-MFI(140) illustrating non-observable change in zeolite crystal morphology after AHFS treatment.

4.3.2 Role of Extra-framework Aluminum and synergistic sites on acylation reaction kinetics.

The direct acylation of 2-methylfuran with acetic acid is postulated to occur over Brønsted zeolites. This process initiates with the dehydration of the organic acid, leading to the formation of surface acyl species. Subsequently, these species then undergo coupling with the gaseous-phase furanic compounds, ultimately yielding acetyl-methylfuran product isomers[18-20, 60]. To mitigate catalyst deactivation caused by the direct adsorption of 2-MF on the active sites, it is

crucial to operate under high partial pressure of acetic acid, effectively placing the reaction in the zeroth order reaction regime[18, 19, 60]. Consequently, we adopted identical reaction conditions to prior work[60] to comprehensively assess the influence of extra-framework aluminum (EFAL) species on the kinetics of the acylation reaction.

To effectively compare the various zeolite samples, we normalized the initial rates per proton, yielding turnover frequencies (TOFs). As depicted in Figure 4-4, the acylation rate of 2-MF with AA exhibits significant variation across the different zeolite samples, with notably superior TOFs observed for H-MFI(40) and H-BEA(150). These two samples are also the only ones, as indicated by the 27Al-NMR results in Figure 4-1, to possess detectable EFAL species at the 0 ppm chemical shift. While the TOF on H-BEA(150) surpasses that of H-MFI(40) substantially, this enhancement can be attributed to a higher fraction of highly active synergistic sites, closely correlated with the presence of EFAL species. Our estimation indicates that approximately 12.7% of the aluminum in H-BEA(150) exists as non-framework aluminum, compared to 4.9% in H-MFI(40), as detailed in Table 4-1. Interestingly, the removal of EFAL from MFI(40) results in a reduction in TOF to a level approaching that of H-MFI(140), affirming that the enhancement in the reaction rate indeed stems from the synergy between Brønsted acid sites (BAS) and nearby EFAL species. The decline in TOF is more pronounced in AHFS-BEA(150), primarily due to the removal of relatively abundant EFAL in H-BEA(150). However, this decrease could also be influenced by the removal of aluminum in the T3-T9 positions, as discussed earlier. In other studies, AHFS washing has been found to reduce the rates of cracking reactions in H-MFI(11.5) and H-MFI(15), bringing them close to the rates observed in H-MFI(40) but still higher than H-MFI(140)[34, 127]. This observation was attributed mostly to Brønsted acid sites proximity (BAS pairs), while the low EFAL presence has no detectable effects on cracking rates.

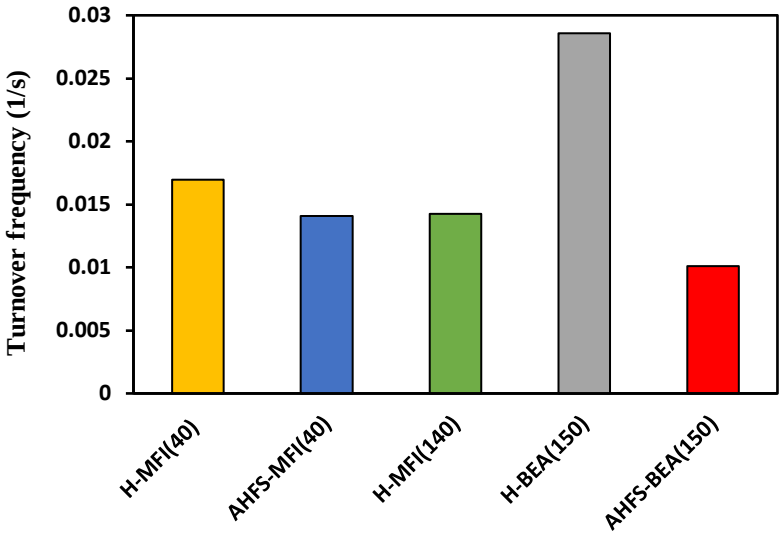


Figure 4-4 Initial turnover frequencies (TOFs) of H-MFI(40), AHFS-washed MFI(40), H-MFI(140), H-BEA(150), and AHFS-washed BEA(150) were determined under a reaction temperature of 160°C with a nitrogen flow rate of 125 ml/min. The catalyst loadings ranged from 5 to 20 mg, corresponding to a narrow range of Brønsted acid site density measured by IPA-TPRx.

Given that the presence of extra-framework aluminum (EFAL) species in zeolites has demonstrated the highest turnover rates, we conducted measurements of the activation barriers over these catalysts within the temperature range of 160-180°C. These measurements were then compared to those obtained for zeolites that potentially have all framework aluminum (Figure 4-5) vividly illustrates that the presence of EFAL in zeolites substantially reduces the activation energies to approximately half of the measured barriers observed in zeolites with an exclusively framework aluminum. This effect is further highlighted by the Arrhenius plots shown in Figure 4-5a for H-MFI(40) and H-BEA(150) zeolites, which AHFS washing closely align them with that of H-MFI(140) depicted in Figure 4-5b. To lend additional support to our observations, it is worth noting a study by Pham et al., where they deconvoluted the measured activation barrier for hexane cracking on synergistic Brønsted acid sites and contrasted it with isolated BAS[34]. Their findings indicated that hexane cracking on Brønsted acid sites located in close proximity to extra

lattice aluminum resulted in an approximately 35 kJ/mol lower activation energy compared to isolated sites. This finding further substantiates our observations regarding acylation over different zeolites with distinct active sites.

Chemical reactions are inherently reliant on the Gibbs free energies of transition states ($\Delta G^{\ddagger}$) concerning the corresponding reactants. At lower temperatures, enthalpic contributions tend to exert greater influence, where the first term in Equation 4-3 takes precedence. Conversely, as temperatures rise, entropic effects become increasingly significant. Given that the reaction temperature range in our study remains relatively low, this enables us to more effectively discern the enthalpic impact of EFAL species within zeolites on the acylation of 2-MF with AA.

$$\boldsymbol{\Delta G^{\ddagger} = \Delta H^{\ddagger} - T\,\Delta S} \qquad \textit{Equation 4-3}$$

To gain a deeper understanding of the acylation rate enhancement observed on the synergistic Brønsted acid sites (SBAS), it is essential to dissect the transition state parameters. Consequently, we applied the Eyring principle to decouple the enthalpies ($\Delta H^{\ddagger}$) and entropies ($\Delta S^{\ddagger}$) of transition state for the reactions occurring over the various zeolite samples[157, 158]. By employing Equation 4-4 to calculate these values from the Eyring-Polanyi principle depicted in Figure 4-6, we can gain valuable insights into the molecular-level mechanisms governing the reaction.

$$\boldsymbol{k = \frac{k_b T}{h}\, e^{-\left(\frac{\Delta H^{\ddagger}}{RT}\right)} e^{\left(\frac{\Delta S^{\ddagger}}{R}\right)}} \qquad \textit{Equation 4-4}$$

Where k_b is Boltzmann's constant and h is Planck's constant. Converting Equation 4-4 into a linear form, referred to as Equation 4-5, offers a more efficient approach to obtaining the transition state parameters. $\Delta H^{\ddagger}$ and $\Delta S^{\ddagger}$ can be determined from kinetic data from Figure 4-6

plot of $ln\frac{k}{T}$ against $\frac{1}{T}$. This equation results in a linear relationship, where the negative slope corresponds to $\frac{-\Delta H^{\ddagger}}{R}$, and the y-intercept is represented as $\ln\frac{k_b}{h}+\frac{\Delta S^{\ddagger}}{R}$.

$$\boldsymbol{ln\frac{k}{T}=\frac{-\Delta H^{\ddagger}}{R}\frac{1}{T}+ln\frac{k_b}{h}+\frac{\Delta S^{\ddagger}}{R}} \qquad \textbf{\textit{Equation 4-5}}$$

The determined values for enthalpies and entropies of the transition state in the acylation process over various zeolite catalyst samples are presented in Table 4-2. Notably, the presence of EFAL in H-MFI(40) and H-BEA(150) leads to enthalpic stabilization of kinetically relevant intermediates and the transition state. It's intriguing to observe that the removal of EFAL through AHFS treatment results in a twofold increase in $\Delta H^{\ddagger}$, accompanied by an entropic gain resembling values seen in H-MFI(140). While local confinement can indeed lead to substantial enthalpic stabilization in certain coupling reactions within zeolites[124, 159-161], a DFT study on the catalytic activity of faujasite zeolite suggest that the presence of the EFAL inside the sodalite substantially enhance the Brønsted acidity of the protons in the supercage [162]. With this in mind, it is reasonable to conclude that the presence of extra-lattice aluminum species within the vicinity of Brønsted acid sites results in synergistic BAS that enthalpically stabilize the relevant transition state for the acylation.

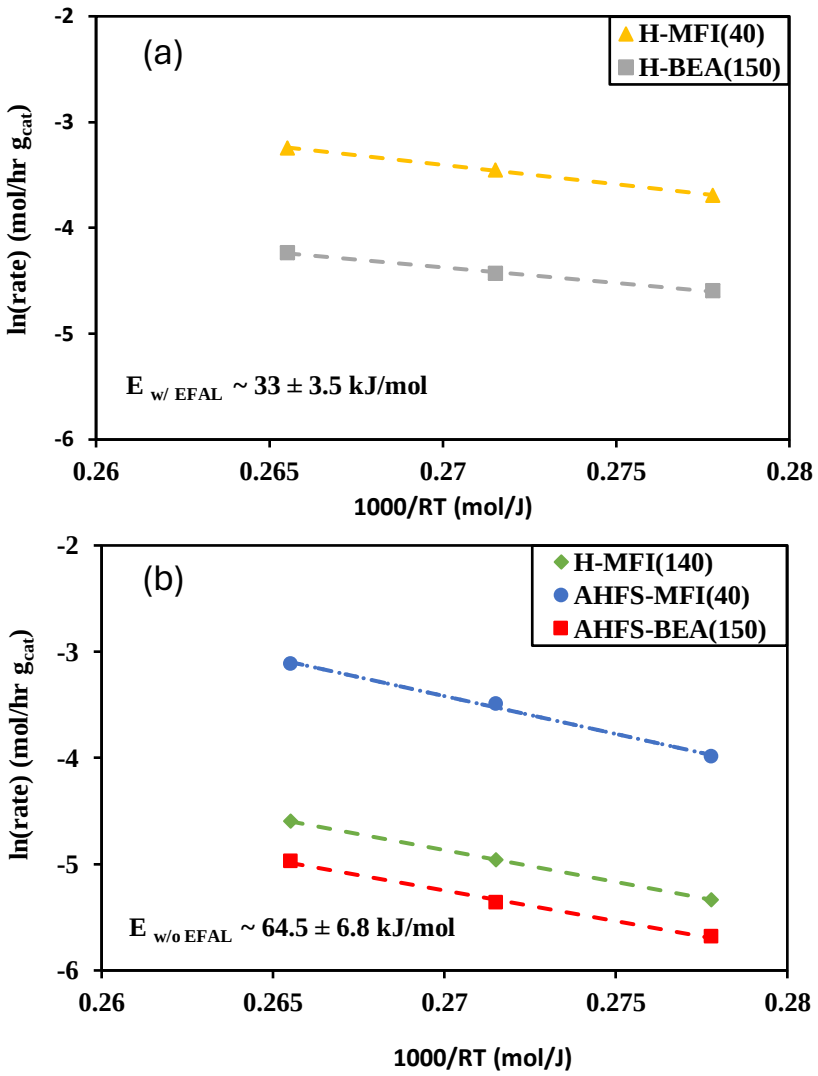


Figure 4-5 Arrhenius plot presenting the median activation energies of (a) H-MFI(40) and H-BEA(15) zeolites that contains EFAL species contrasted with (b) H-MFI(140), AHFS-washed MFI(40), and AHFS-washed BEA(150) zeolites samples which does not have EFAL. Experiments were conducted under reaction temperatures 160,170 and 180°C and flowing N_2 at 125 ml/min.

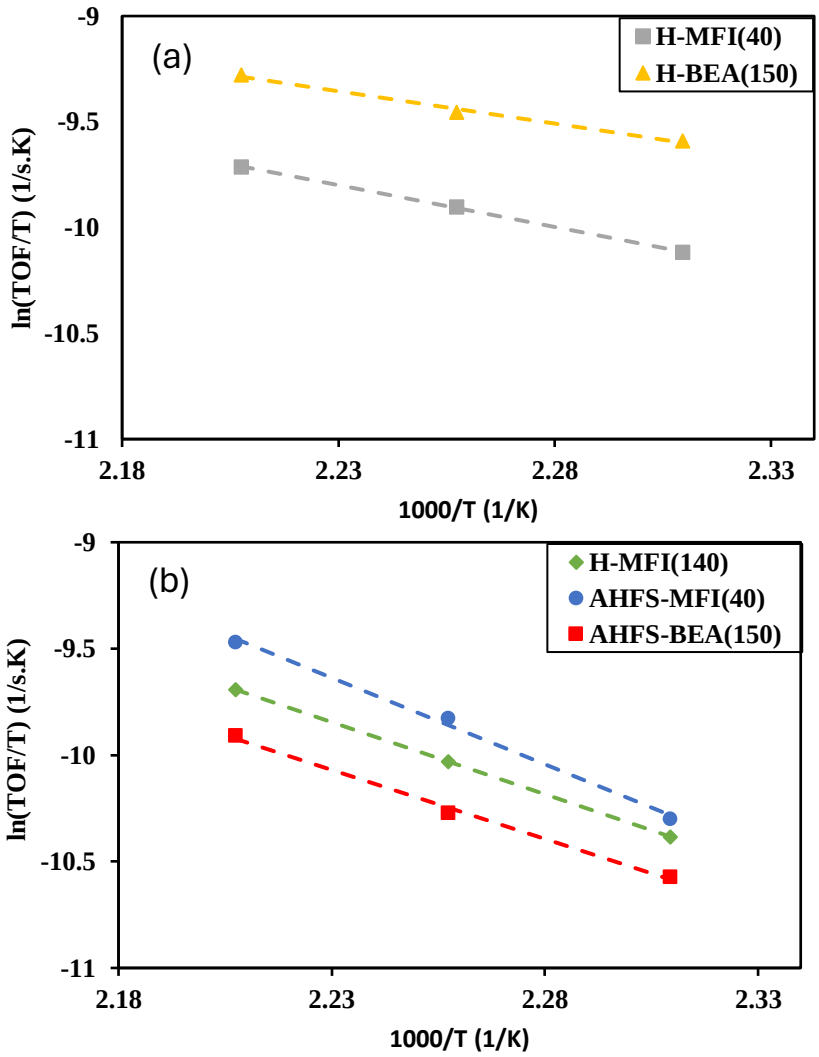


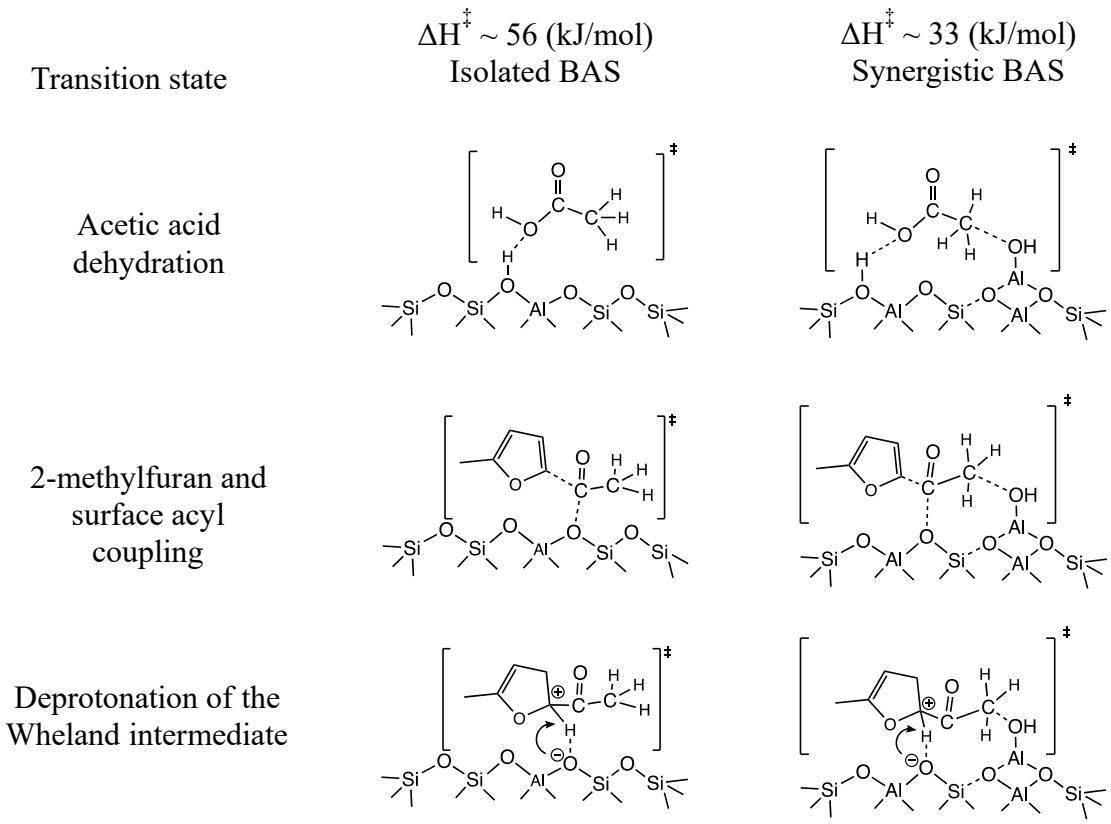
Figure 4-6 Eyring plot of acylation over (a) H-MFI(40) and H-BEA(15) zeolites that contains EFAL species contrasted with (b) H-MFI(140), AHFS-washed MFI(40), and AHFS-washed BEA(150) zeolites samples which does not have EFAL. Experiments were conducted under reaction temperatures 160,170 and 180°C and flowing N2 at 125 ml/min.

Table 4-2 Values for the activation energies, Enthalpies, and Entropies of transition state during acylation under different catalyst samples.

Catalyst	E_A (kJ/mol)[a]	$\Delta S^{\ddagger}$ (J/K)[b]	$\Delta H^{\ddagger}$ (kJ/mol)[b]
H-MFI (40)	36.6 ± 0.6	-205.7 ± 1.3	32.8 ± 0.6
AHFS-MFI (40)	71.3 ± 4.7	-127.0 ± 10.6	67.6 ± 4.7
H-MFI (140)	60.5 ± 0.01	-153.5 ± 0.1	56.3 ± 0.03
H-BEA (150)	29.5 ± 2.2	-218.7 ± 4.9	25.4 ± 2.2
AHFS-BEA (150)	57.7 ± 3.8	-161.1 ± 8.5	53.9 ± 3.8

[a] Apparent activation energies obtained using Arrhenius principle. [b] The Entropies and Enthalpies of transition are estimated using Eyring-Polanyi Equation 4-4

Throughout the acylation reaction of 2-MF with AA, there are three pivotal transition states that mark the beginning with the dehydration of acetic acid, followed by the coupling with 2-methylfuran, and concluding with the deprotonation of the Wheland intermediate[18, 20]. However, there remains a discrepancy in identifying the most kinetically relevant transition state or the rate-determining step for this reaction. To address this uncertainty, we have outlined three distinct transition state scenarios in Scheme 4-1, where the presence of EFAL could potentially exert further enthalpic stabilization effects. Computational calculations serve as a valuable tool to derive the resulting energetics for these relevant transition states and the reaction pathway, considering both isolated BAS and synergistic BAS. By meticulously examining and contrasting the sequential reaction steps over both catalysts, we aim to elucidate which step benefits significantly from the presence of EFAL species, leading to substantial enthalpic stabilization.

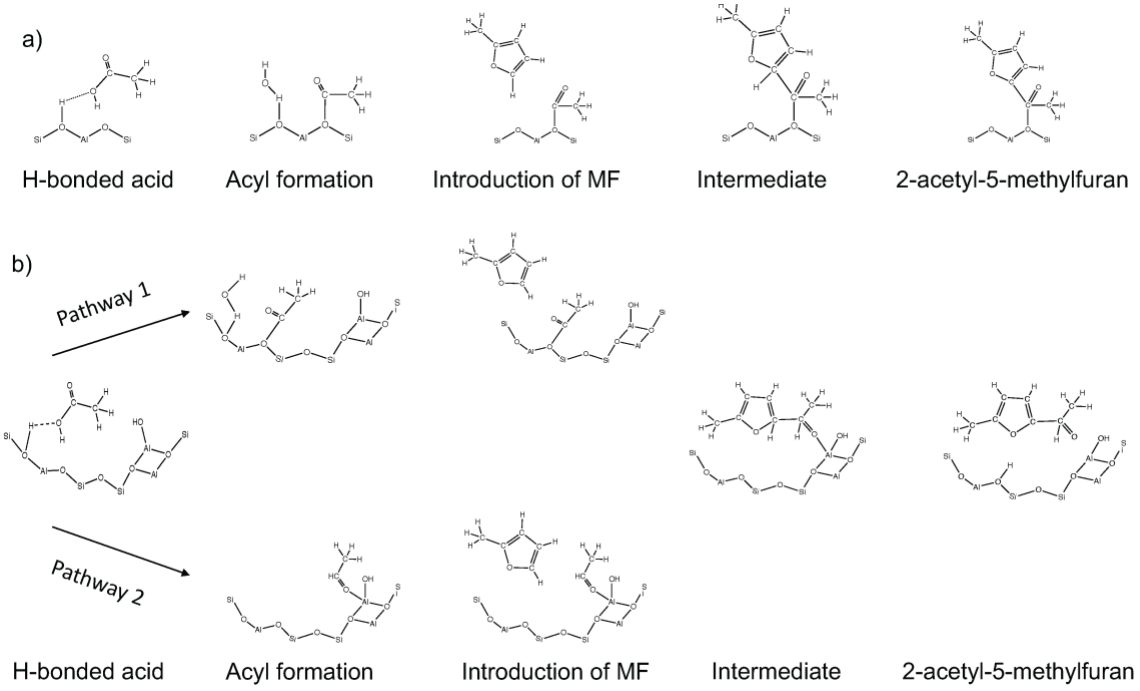


Scheme 4-1 Depiction for the three relevant transition states of acylation of 2-MF with AA over isolated BAS and synergistic BAS.

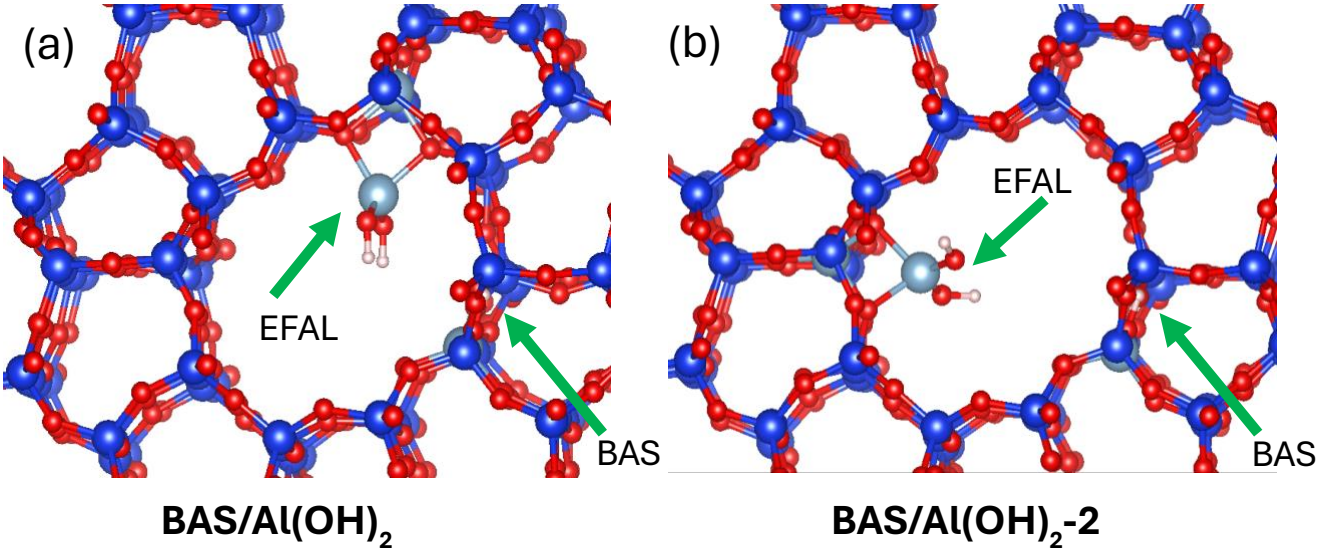
4.3.3 Evaluating acylation energies from DFT

The complete mechanism of the acylation reaction is illustrated in Scheme 4-2. In the presence of EFAL $Al(OH)_2^+$, the mechanism adheres to the pathway involving IBAS, wherein acylation takes place on two oxygen atoms connected to the same Al atom, as depicted in Scheme 4-2a. We conducted an analysis to assess the influence of EFAL $Al(OH)_2^+$ at two distinct distances from the BAS. These distances are represented by the BAS/$Al(OH)_2^+$ site, where EFAL $Al(OH)_2^+$ is two Si linking atoms away from the BAS, and the BAS/$Al(OH)_2^+$-2 site, where the EFAL is eight Si linking atoms away from the BAS, as illustrated in Scheme 4-3. The initial step involves the adsorption of acetic acid onto H-MFI, facilitated by the formation of hydrogen bonds with the BAS. Notably, this step exhibits lower energy on BAS/$Al(OH)_2^+$ and

BAS/Al(OH)$_2^+$-2, with energy values 3 and 14 kJ/mol more negative than that of IBAS, respectively (Figure 4-7). Subsequently, the formation of acyl species and water proceeds with true barriers of 96 and 105 kJ/mol on BAS/Al(OH)$_2^+$ and BAS/Al(OH)$_2^+$-2, respectively, which are comparable to the value observed for IBAS. However, the apparent activation barriers are reduced by 5 and 25 kJ/mol, respectively, when compared to IBAS. This reduction is attributed to the stronger adsorption of the acetic acid molecule. It is worth noting that the proximity of EFAL has a more pronounced impact on the adsorption of the acetic acid molecule.



Scheme 4-2 Reaction pathways of acylation reaction of 2-Methylfuran with acetic acid a) on IBAS b) on BAS/Al(OH)$_2^+$ synergistic sites



Scheme 4-3 Depiction of different arrangements of synergistic sites (a) Close EFAL proximity and (b) Relatively distanced from Brønsted acid site (BAS).

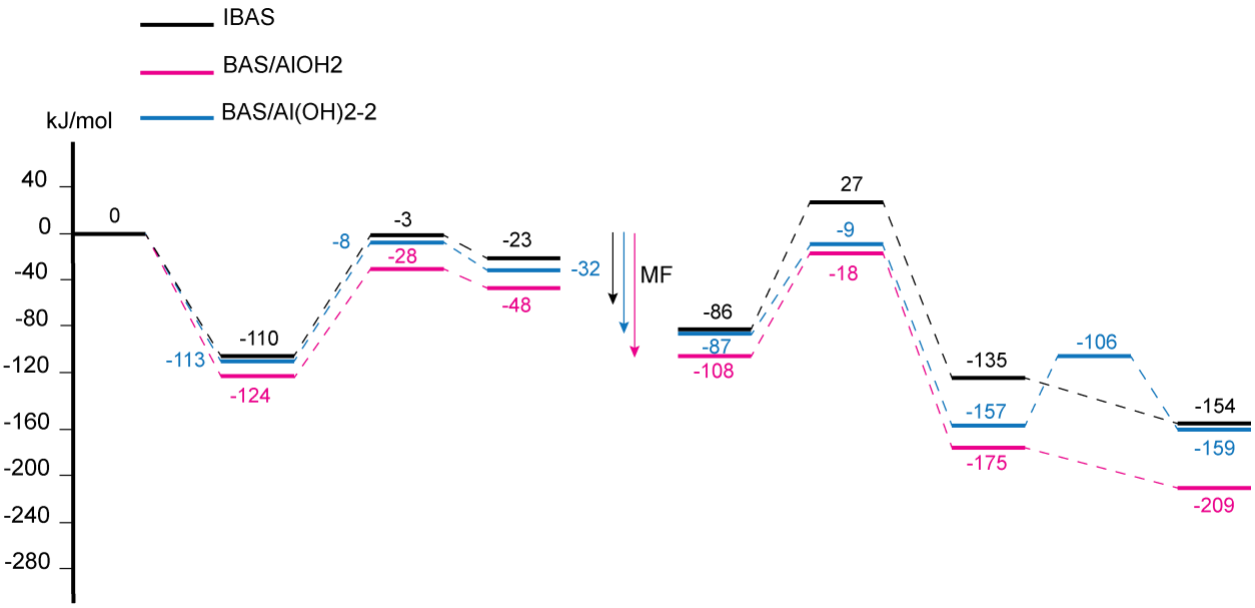


Figure 4-7 Energy profile of acylation of 2-MF with acetic acid on BAS with the presence of EFAL $Al(OH)_2^+$ in two different proximities

In contrast to the dehydration step, the subsequent C-C coupling steps exhibit remarkably lower apparent activation barriers in the presence of EFAL $Al(OH)_2^+$ at two different distances. The increased stability of acyl species on synergistic sites significantly facilitates the C-C coupling step. On the synergistic sites BAS/$Al(OH)_2^+$-2, the activation barriers for the C-C

coupling steps and dehydration are comparable, while on BAS/$Al(OH)_2^+$, the activation barrier for C-C coupling is 10 kJ/mol higher than that for the dehydration step. Even though the apparent activation barriers for both dehydration and C-C coupling steps are higher on IBAS, the difference in energies for the latter step is significantly greater, suggesting a higher level of enthalpic stabilization for the C-C coupling transition state. This suggests that the C-C coupling step is likely to be the rate-determining step. While previous studies have often focused on the deprotonation of the Wheland intermediate transition state as a potential rate-controlling step[20], our calculations suggest that there is no significant enthalpic contribution associated with the transition occurring on a synergistic site during that particular step.

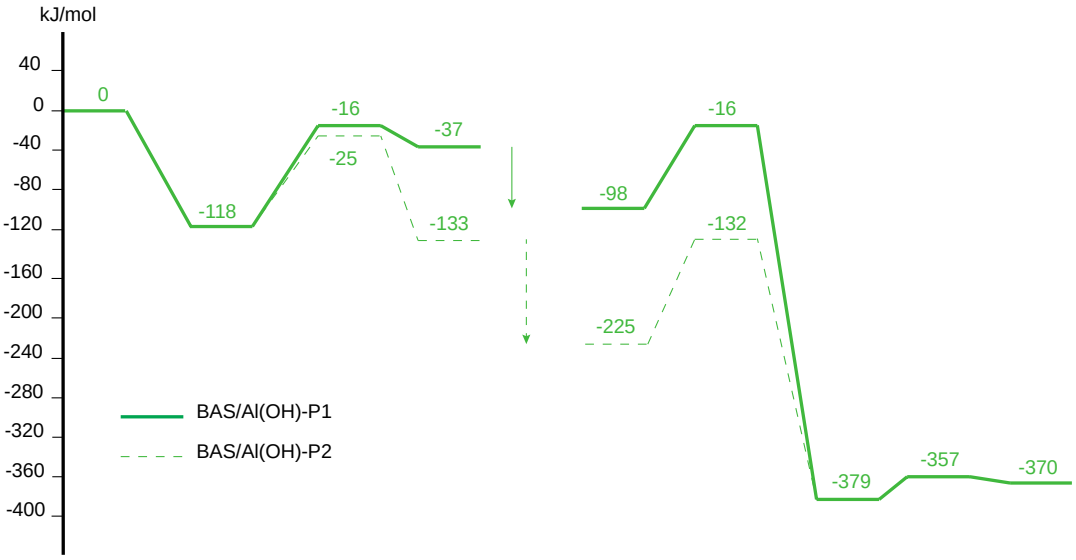


Figure 4-8 Energy profile of acylation of 2-MF with acetic acid on BAS with the presence of EFAL $Al(OH)_2^+$ in proximity. The solid line represents reaction pathway 1 and dash line represents reaction pathway 2.

Scheme 4-2b outlines potential pathways for the acylation reaction when EFAL $Al(OH)_2^+$ is located two Si linking atoms away from BAS. Pathway 1 involves a dehydration step similar to that of IBAS, while pathway 2 involves the formation of a bond between the acyl species and EFAL $Al(OH)_2^+$, resulting in significant stabilization of the acyl group. In both pathways, the

reacting intermediate, becomes bonded with EFAL $Al(OH)_2^+$, which indicates a BAS-EFAL synergy event occurred during the C-C coupling step. Compared to the highest activation barrier observed for the reaction on IBAS, the activation barriers on BAS/$Al(OH)_2^+$ are reduced by 43 and 159 kJ/mol when following pathway 1 and pathway 2, respectively (Figure 4-8). Consequently, pathway 1 presents a more plausible acylation mechanism over synergistic Brønsted acid sites.

4.4 Conclusions

Similar to many other chemical reactions, the nature of active sites within zeolites significantly influences the acylation of 2-methylfuran with acetic acid. The presence of extra-framework aluminum species (EFAL) within the zeolite creates distinct active sites that lead to a substantial enhancement in acylation rates. This enhancement arises from the proximity of EFAL to Brønsted acid sites, resulting in significant enthalpic stabilization of the kinetically relevant transition state governing the reaction rates. The removal of EFAL moieties through ammonium hexafluorosilicate (AHFS) treatment causes a two-fold increase in activation barriers, aligning them with those found in all-framework aluminum H-MFI(140) zeolites. This observation was explained through the decoupling of transition state parameters, which revealed a significant increase in enthalpy along with entropic gains. We proposed three potential transition states, including the dehydration of acetic acid, reactant coupling, and the deprotonation of the Wheland intermediate, which could be further stabilized over synergistic Brønsted acid sites. These transition states were evaluated using DFT calculations. The computational results suggest that the presence of EFAL results in lower apparent activation barriers in both the dehydration and C-C coupling steps, while the latter, involving the re-protonation of the active site, appears to be less influential. Based on the overall energy profile obtained from our DFT calculations, it is

likely that the reactant coupling step serves as the plausible rate determining step. Gaining insight into the complex interplay between extra-lattice alumina and Brønsted acid sites is crucial for a comprehensive understanding of the underlying factors that drive the kinetics of this acylation reaction. Furthermore, this understanding has significant implications for the enhancement and fine-tuning of catalytic performance in analogous systems.

Chapter 5: Role of carbon chain length in carboxylic acids on acylation of 2-methyl furan over HZSM-5 zeolite

All the work in this chapter was conducted at the University of Oklahoma This work is planned for future publication involving the authors Ismaeel Alalq, Daniel Resasco, Steven Crossley.

Abstract

The characteristics of the acylating agents during Friedel-Crafts acylation determine the behavior of the products as well as their practical applications in commodity chemicals. Recent emphasis on sustainability has led to a focus on attaining acylated products utilizing renewable oxygenated compounds and processing them over regenerable zeolite catalysts. In this study, we investigate the direct acylation of 2-methylfuran with carboxylic acids (pure and mixtures) of varying carbon chain lengths (acetic, propionic, butyric, valeric) over HZSM-5 zeolite at mild temperatures (190-210°C). Our findings demonstrate that reaction rates increase with larger acids, despite the rise in activation barriers attributed to the formation of more stable surface acyl intermediates. This stability is a result of a greater adsorption constant (K_{acid}), as predicted by the Eley-Rideal kinetic model, which considers the reaction between an adsorbed acyl species and gas-phase 2-methylfuran. Furthermore, during acylation with different carboxylic acid mixtures, the catalyst exhibited various deactivation rates, highlighting the crucial role of co-feeding acetic acid with larger carboxylic acids. Blending acetic acid not only mitigates deactivation but also maintains product selectivity towards acylation with larger carboxylic acids.

5.1 Introduction

The products of acylation reactions, typically characterized by a hydrophilic head and a hydrophobic tail with varying chain lengths, exhibit amphiphilic properties crucial for their industrial applications[163]. The balance between hydrophilicity and hydrophobicity, dictated by the structure of the acylated products, profoundly influences their solubility, stability, and

interaction with other molecules, thereby impacting their efficacy across diverse industrial processes[164]. These properties govern their behavior in various applications, including as surfactants in detergent formulations, in food processing, active ingredients in pharmaceuticals, and components in fragrance formulations[165].

Conventional acylation reactions are catalyzed by homogeneous Lewis acids such as $AlCl_3$ and predominantly rely on petroleum-derived feedstocks[21], resulting in substantial waste generation and rendering a non-sustainable process[5]. To address these challenges, extensive research efforts have been directed towards exploring reusable solid catalysts to enhance efficiency and minimize waste production[4, 42]. Among these, zeolites stand out as promising heterogeneous acid catalysts that not only offer an alternative to conventional catalysts but also enable the utilization of renewable biomass and vegetable oils[14, 25, 166].

Recent research efforts have focused on investigating the viability of direct acylation using biomass-derived feedstocks such as furanic, phenolic, and carboxylic acids, employing regenerable aluminosilicate zeolites. These investigations have yielded valuable insights into catalyst activity, selectivity, and stability during the conversion of these oxygenates[18-20, 59, 60]. However, several key challenges and opportunities remain to be addressed in this field.

One such challenge is the elucidation of alternative acyl donors beyond acetic acid and their impact on product selectivity and catalyst performance. Additionally, further investigation into the deactivation mechanisms of zeolite catalysts under operating conditions, as well as strategies to mitigate catalyst deactivation and enhance catalyst stability, are crucial for the development of sustainable acylation processes.

Few research groups have investigated the impacts of carbon chain length in carboxylic acid acylation over zeolites. For instance, Wagholikar et al. examined the role of carbon chain

length in the direct acylation of anisole across various zeolite frameworks (BEA, FAU, and MOR)[167]. Their study revealed that acylation activity varied with different zeolite frameworks and Brønsted acid site (BAS) densities. Moreover, they observed a decrease in the reactivity of carboxylic acids with increasing carbon chain length, attributing this phenomenon to diffusion limitations within zeolite pores[168]. However, it is plausible that catalyst deactivation, can be caused by the large amount of aromatics compared to carboxylic acids used, influenced their observed activities[18, 19, 60]. In another study, it was found that the acylation of p-xylene increased with an increasing carbon number, reaching a maximum with C_{16}-C_{20} acid, but decreased beyond that due to pore diffusion effects[8]. Although existing studies provide insights into the role of carbon chain length in direct acylation over zeolites, their effects on acylating biomass-derived furanics remain unexplored. Furanics are utilized in the synthesis of a novel class of renewable surfactants known as "oleo-furan sulfonates" (OFS), which exhibit superior solubility and stability in hard water[57].

In the present contribution, we study the direct acylation of 2-methylfuran (2-MF) with a range of carboxylic acids between C_2-C_6 over commercial ZSM-5 zeolite catalysts. We investigate how carboxylic acids with different carbon chain lengths influence reaction activity, catalyst stability, and product selectivity when different acid sizes are blended. Both reaction rates and activation energies are measured and compared, presenting different values corresponding to the carbon number in the carboxylic acids. Acylation with various acid blends with different ratios clarifies the importance of the stability of reaction intermediates on product selectivity. This stability is attributed to stronger adsorption of larger acids, estimated through kinetic investigation using the Eley-Rideal model. Additionally, co-feeding smaller acetic acid (AA) with larger carboxylic acids (CA) during acylation exhibits a shift in catalyst stability as a

function of the molar ratio of AA to CA, providing useful information regarding the benefit of blending carboxylic acid streams during acylation over zeolites.

5.2 Experimental section

5.2.1 Chemicals and materials

The HZSM-5 catalyst samples utilized in this study were of commercial grade obtained from Zeolyst International (CBV28014 Si/Al = 140). The samples were initially received in the ammonium-ion form and subsequently calcined to obtain the proton form. The calcination process was conducted in 1-inch quartz tubes under an airflow of 100 standard cubic centimeters per minute (SCCM), heated within an oven at a ramp rate of 2°C/min until reaching 600°C, and then maintained at this temperature for 5 hours. The acylating agents used in this study included acetic acid (AA) (glacial, ACS reagent, ≥99.7%, Sigma-Aldrich), propionic acid (PA) (≥99.5%, Sigma-Aldrich), butyric acid (BA) (≥99%, Sigma-Aldrich), valeric acid (VA) (≥99%, Sigma-Aldrich), and hexanoic acid (HA) (≥99%, Sigma-Aldrich). The acyl acceptor employed was 2-Methylfuran (98+%, stab., Alfa Aesar). Nitrogen gas (ultra-high purity GD 5.0) served as the carrier gas for the experiments. To ensure the purity of the reactants, any trace levels of the stabilizer butylated hydroxytoluene present in the purchased 2-Methylfuran were removed via distillation prior to use in the reaction.

5.2.2 Catalytic reaction

The acylation of 2-MF with AA over zeolite catalysts was conducted in the gas phase using a fixed bed tubular reactor, following established procedures. The catalyst was mixed with glass beads and packed between layers of quartz wools within a 1/4-inch quartz reactor tube. Prior to the reaction, the catalyst underwent pretreatment, involving a slow temperature ramping at a rate of 10°C/min to 300°C, where it was held for 1 hour, all under continuously flowing nitrogen to

eliminate physically adsorbed moisture. Subsequently, the catalyst was cooled down to the desired reaction temperatures, within the range of 190-210°C. During the reaction, a nitrogen carrier gas was maintained at a flow rate of 125 SCCM, while the reactants carboxylic acids and 2-MF were introduced typically at partial pressures of ~20 Torr and ~4 Torr, respectively, to maintain a fixed 5 to 1 carboxylic acids (pure or blended) to 2-MF molar ratios. Temperature control of the reactor was achieved via a thermocouple attached to the external surface of the reactor tube, precisely aligned with the center of the catalyst bed. After the pretreatment, the reactor temperature was set to the desired reaction temperature, and the feed rate of reactants was precisely controlled using syringe pumps. To prevent condensation of leaving species, the reactor outlet streamline was heated to 250°C. A micro electric actuator was employed to control the six-port valve, which directed samples to an inline-connected gas chromatograph (Agilent 7890B) equipped with a flame ionization detector. Separation of reaction products was achieved using a Zebron Phase: ZB-WAX column (30m × 0.25mm × 0.25μm). The response factors of the reactants were determined by flowing the reactants at the desired rate through a glass beads bed to mimic the catalyst bed, while the products response factor was determined by effective carbon number (ECN)[25, 169]. These response factors were used for further data analysis, such as conversion and carbon balance. Reaction rates, conversions, and selectivity were determined using the following equations: -

$$\boldsymbol{Rate} = \frac{\boldsymbol{Moles\ of\ product\ formed\ per\ hour}}{\boldsymbol{Gram\ of\ catalyst}} \left(\frac{\boldsymbol{mol}}{\boldsymbol{hr\ g_{cat}}}\right) \qquad \textit{Equation 5-1}$$

$$\boldsymbol{Conversion} = \frac{\boldsymbol{Moles\ of\ product\ formed\ per\ hour}}{\boldsymbol{Moles\ of\ 2-methylfuran\ fed\ per\ hour}} (\boldsymbol{mol}\%) \qquad \textit{Equation 5-2}$$

$$\boldsymbol{Selectivity} = \frac{\boldsymbol{Product\ formed\ from\ an\ acyl\ donor}}{\boldsymbol{Total\ acylated\ products}} (\%) \qquad \textit{Equation 5-3}$$

The initial reaction rates were determined by extrapolating the data to zero time on stream, providing a precise assessment of catalyst deactivation during acylation.

5.3 Results and Discussion

5.3.1 Carbon chain length and acylation activity

We commence our discussion by examining the impact of carbon chain length in carboxylic acids on 2-MF acylation activity over zeolites under identical conditions, contrasting a range of C2-C5 acids. The activity assessment was conducted over HZSM-5 (Si/Al =140) to minimize diffusion limitations within this reaction, at a temperature of 200°C, which is 50°C below that reported for carboxylic acids self-coupling to form ketones. Figure 5-1 illustrates how carboxylic acid acyl donors can exhibit varying acylation activities depending on the carbon content. The activity increased twofold upon switching the acylating agent from acetic acid to propionic acid, which contains only one additional carbon. However, the activity remains at a similar level when transitioning from propionic acid to butyric acid, despite the additional carbon. The enhancement in acid reactivity is likely attributed to the faster dehydration of larger carboxylic acids, leading to the formation of a more stable surface acyl reactive intermediate[170]. Interestingly, the activity starts to decline relatively with the five-carbon valeric acid, although it still exhibits higher activity than acetic acid. While diffusion limitation was initially considered responsible for this behavior, measured activation barriers suggest otherwise.

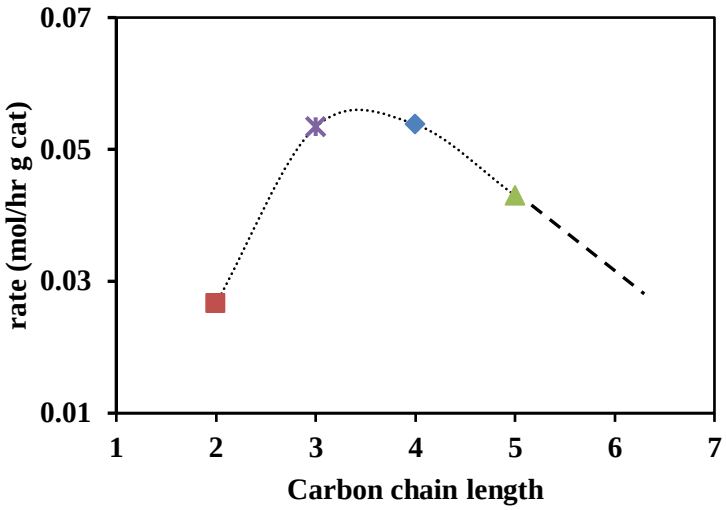


Figure 5-1 Reaction rate as a function of carbon chain length at 200°C 5-1 mol (Acid-2MF)

The measurement of apparent activation energy (E_A) was conducted within the temperature range of 190-210°C, maintaining identical conditions for all carboxylic acids. Figure 5-2 presents the results, indicating that acylation experiences an increase in apparent activation energy proportional to the chain size of the carboxylic acid. Since dehydration of acids is facilitated in larger acids, the rise in activation energy may be attributed to other transition states relevant to either the coupling of the adsorbed surface acyl and the gas phase 2-MF or the deprotonation of the Wheland intermediate species[20], likely pertaining to the C-C coupling step as suggested by findings in chapter 4. However, the decrease in reaction rate with the increase in apparent activation energy observed in valeric acid suggests a possible shift in the rate determining step from C-C coupling to active site re-protonation. Overall, C3-C5 acids exhibited higher reaction rates than acetic acid due to more stable surface acyl, highlighting the stronger adsorption of the larger carboxylic acids.

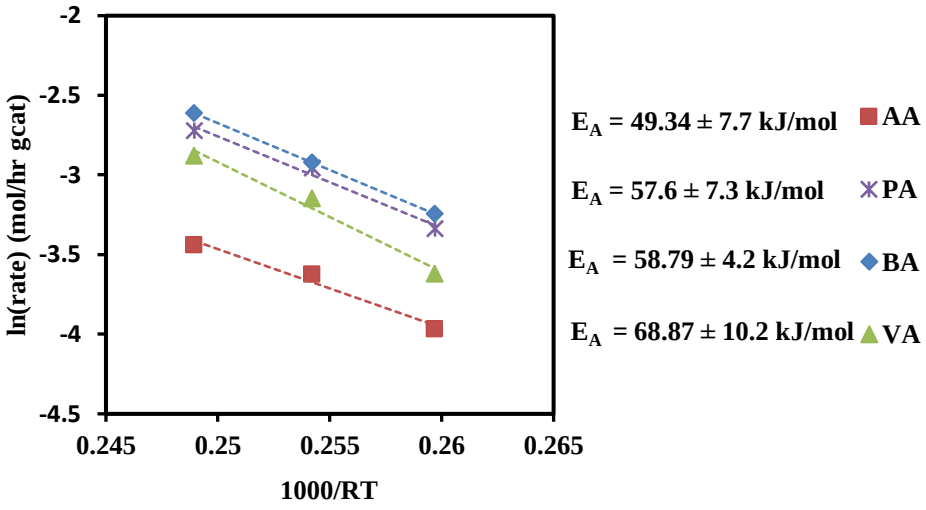


Figure 5-2 Measured Activation of 2-MF acylation with different acyl donor at T =190-210°C and 5:1 mol (Acid-2MF).

5.3.2 Product selectivity during acylation with acid mixtures

To further elucidate the pivotal role of surface acyl stability in facilitating the reaction, we blended C3, C4, and C5 carboxylic acids (CA) with acetic acid (AA) in various molar ratios ranging from 1:1 to 1:8 (CA: AA). It is important to note that the partial pressures of acids and 2-MF, maintained at ~20 Torr and ~4 Torr, respectively, remained consistent across all cases to ensure a valid comparison with the conditions in Figure 5-2. The results of blending small and larger acids are depicted in Figure 5-3a-c, illustrating varying shifts in product selectivity with increasing molar ratios of AA to the larger acids. For instance, in Figure 5-3a, equimolar mixing of AA with PA results in the dominance of (P-MF) products acylated with PA, with a decline in selectivity as the molar ratio of AA increases, until AA acylation becomes slightly more selective at a 1:8 molar ratio (PA: AA). In the case of AA-BA mixing, as shown in Figure 5-3b, obtaining AA acylation products requires doubling the amount of AA in the acid mixture, and an eight-fold increase in AA is needed to achieve relevant A-MF product selectivity. Interestingly, Figure 5-3c illustrates that cofeeding AA has minimal impact on VA surface coverage. In fact, the selectivity

toward AA acylation products remains insignificant even with the highest (8:1) AA: VA molar ratio.

To provide a clearer understanding of how the chain length of carboxylic acids impacts selectivity, we plotted the acylation selectivities as a function of carbon number for 1:8 large carboxylic acids to acetic acid, including hexanoic acid (HA), in Figure 5-4. This comparison suggests that AA appears to have negligible competitive adsorption with C_5+ carboxylic acids. While acylation with AA exhibits a lower apparent activation energy, the selectivity toward larger acyl donors is superior, indicating an increase in the equilibrium constants with the carbon number increase in the carboxylic acids.

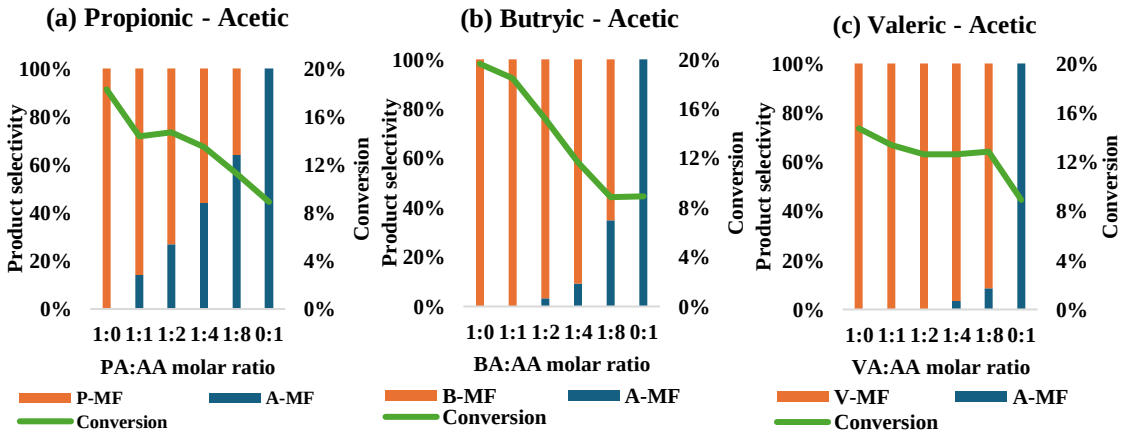


Figure 5-3 Product selectivity of reaction of (a) Propionic-Acetic, (b) Butryic-Acetic, (c) Valeric-Acetic acids mixtures with ranging molar ratios at 200°C and fixed 5:1 mol (Acids: 2-MF)

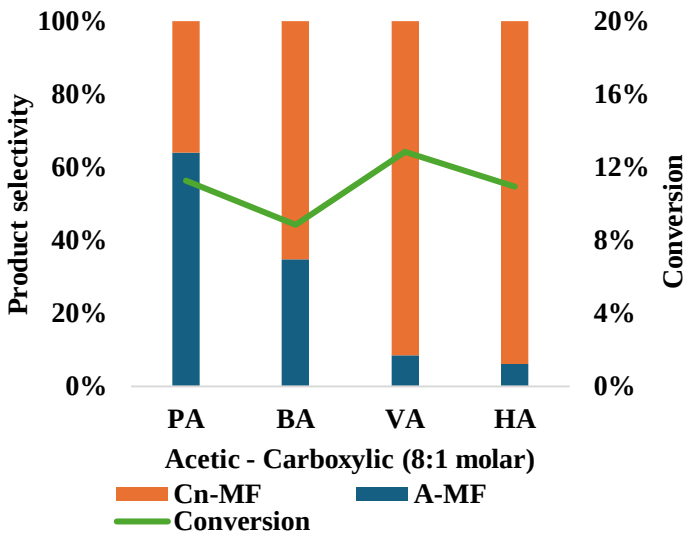


Figure 5-4 Selectivity of acyl donor in acid mixture (Acetic: C_{3-6} 8:1 mole) toward Acylation of 2-MF at fixed 5:1 mol (Acids: 2-MF) at 200°C over HZSM-5 (Si/Al=140)

5.3.3 Kinetic model and fitting parameters

Prior investigations suggest that the acylation of 2-MF with carboxylic acids initiates with the dehydration of the acylating agent, followed by subsequent reactions between an adsorbed surface acyl species and a gas-phase 2-MF[18, 20]. It is important acknowledge that 2-MF has the ability to adsorb and compete for active sites; however, this direct interaction leads to the formation of heavy carbonaceous species that irreversibly deactivate the Brønsted acid sites[18, 19, 60]. Building upon these initial findings, a series of elementary steps can be proposed and integrated into a conventional Eley-Rideal kinetic model to elucidate the reaction kinetics.

(1) Adsorption of the carboxylic acid

$$RCOOH + H^+ \xleftrightarrow{K_{acid}} RCOOH\bullet H^+$$

(2) Dehydration of carboxylic acid

$$RCOOH \bullet H^+ \xleftrightarrow{K_{acyl}} RCO^+ + H_2O$$

(3) Water site competition

$$H_2O + H^+ \xleftrightarrow{K_{H_2O}} H_2O\bullet H^+$$

(4) C-C coupling (Rate determining step)

$$RCO^+ + C_5H_6O \xrightarrow{k} R(CO)C_5H_6O\bullet H^+$$

(5) Site regeneration and product desorption

$$R(CO)C_5H_6O\bullet H^+ \xleftrightarrow{K_{R-MF}} R(CO)C_5H_6O + H^+$$

where H^+ represent the active Brønsted acid site.

While we propose that the C-C coupling, step (4), as the rate-determining step based on our findings in Chapter 4, it is important to acknowledge the significance of both steps (1) and (5)[18, 20]. Our rationale for this assumption is that the dehydration step occurs more rapidly in larger acids, yet the activation energy continues to increase with the size of the acid, as shown in Figure 5-2, indicating the presence of another transition state with higher energy requirements. Regarding site regeneration, step (5), our DFT calculations suggest that it is fast and spontaneous, indicating that it is unlikely to be kinetically relevant, at least for a small range of carboxylic acids between C2 and C5.

Given the proposed elementary steps outlined above, with C-C coupling identified as step (4) and the rate-determining step, the overall reaction rate can be expressed as follows:

$Rate = k\ P_{2MF}\ [RCO^+]$

where $[RCO^+]$ is the concentration of the surface acyl species, generated through the dehydration of carboxylic acids, can be determined using conventional expressions derived from adsorption equilibrium and quasi-equilibrated steps:

$[RCOOH] = K_{acid}P_{acid}\ [H^+]$ Step (1)

$[RCO^+] = \frac{K_{acid}P_{acid}}{P_{H2O}}[H^+]$ Step (2)

$[R(CO)C_5H_6O\bullet H^+] = K_{R-MF}\ P_{R-MF}\ [H^+]$ Step (5)

For simplicity, we assumed that acyl formation is fast and irreversible, $[RCOOH] = [RCO^+]$, and the water, $[H_2O]$, has negligible active site competition.

→ $[RCO^+] = K_{acid}P_{acid}\ [H^+]$

→ $[H_2O] = K_{H2O}P_{H2O}\ [H^+] = 0$

where $[H^+]$ is the concentration of available Brønsted sites and $[RCOOH]$, $[R(CO)C_5H_6O]$, and $[H_2O]$ are surface coverage of the acid, acylation product, and water, respectively.

By combining the above formulas and applying the assumptions, we obtain a conventional Eley-Rideal kinetic model with following rate expression:

$$\boldsymbol{Rate} = \frac{\boldsymbol{k\ P_{2MF}K_{acid}\ P_{acid}}}{\boldsymbol{(1+P_{acid}K_{acid}+P_{R-MF}K_{R-MF})}} \qquad \textbf{\textit{Equation 5-4}}$$

Co-feeding acid mixtures from previous section increase site competition between the carboxylic acids and modify the rate expression to:

$$\boldsymbol{Rate} = \frac{\boldsymbol{k_{AA}\ P_{AA}K_{AA}\ P_{2MF}+k_{CA}\ P_{CA}K_{CA}}}{\boldsymbol{(1+P_{AA}K_{AA}+P_{CA}K_{CA}+P_{A-MF}K_{A-MF}+P_{C-MF}K_{C-MF})}}\ \boldsymbol{P_{2MF}} \qquad \textbf{\textit{Equation 5-5}}$$

where subscripts AA, CA, A-MF, and C-MF for acetic acid, larger carboxylic acid, acetic acid product, and larger carboxylic acid product, respectively.

The dataset obtained from Figure 5-3a-c enables us to fit the parameters using the differential reactor method. In this approach, the feed composition varies with the acids (pure and mixtures) and products, while operating at the lowest feasible conversion. Through this method, we can qualitatively determine the adsorption constant, K_{acid}, which influences the selectivity of the acyl donor.

The parity plot depicted in Figure 5-5 compares the experimental (measured) rate of 2-MF acylation with varying carboxylic acid feed compositions to the calculated rate from Equation 5-5. This analysis allowed us to discern a relative representation of the rate constant (k)

and adsorption constant (K) for acylation with different carboxylic acids. The values for these parameters are summarized in Table 5-1, revealing that the adsorption constant (K) increases with the carbon chain length, while the reaction rate constants (k) remain similar and fall within the uncertainty range.

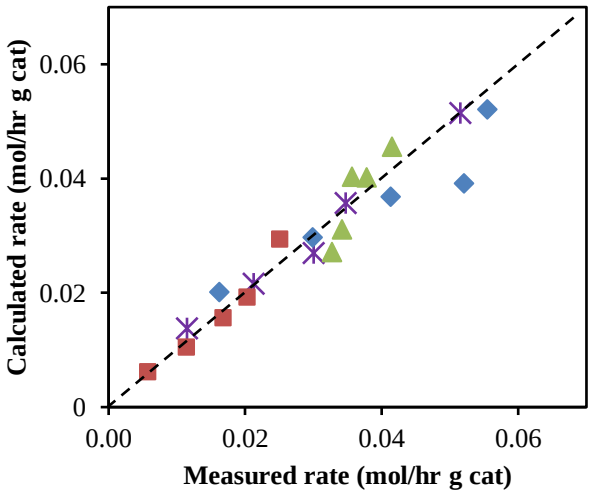


Figure 5-5 Parity plot of the calculated from Eley-Rideal model in Equation 5-5 reflected in the dashed line compared with measured rates for the different carboxylic acids acylation (acetic ■ , propionic ✳ , butyric ◆ ,valeric ▲) at 200°C and P_{acids} ~20 Torr $P_{2\text{-}MF}$ ~ 4 Torr.

It is worth noting that while another study found the heat of adsorption to be independent of the alkyl group length in carboxylic acids over Ru/TO_2 catalysts[171], it becomes evident that the adsorption strength increases over zeolites as the alkyl group size grows due to differences in proton affinity and van der Waals interaction[172-174]. Indeed, the observed decrease in active site competition of acetic acid with increasing carbon number of the blended acid, as shown in Figure 5-3a-c, and the significant increase in the adsorption constant values presented in Table 5-1, suggest that heat of adsorption values vary with different carboxylic acids. These values are crucial for determining the stability of the acyl donor, thereby leading to a more selective acylation reaction.

Table 5-1 Optimized kinetic parameter values for acylation with different carboxylic caids composition obtained in Figure 5-5 from fitting measured data and calculated data.

Parameter	Acetic	Propionic	Butyric	Valeric
k (mol/hr g cat)	0.01	0.013	0.015	0.013
K_{acid} ($Torr^{-1}$)	0.221	0.991	1.178	3.119

5.3.4 Effect of carbon chain on the transition state

To gain further insights into how the size of the acyl donors influences acylation rates, we delve into the transition state of acylation and decouple its parameters. The transition state theory postulates the existence of an activated complex that is in a quasi-equilibrium state with reactants before converting to products, offering a simple derivation of reaction rates and depiction of their progression[175]. Consequently, we can determine the enthalpies ($\Delta H^{\ddagger}$) and entropies ($\Delta S^{\ddagger}$) of the transition state (TS) for the reactions involving different acylating agents by employing data collected at various temperatures and applying the Eyring-Polanyi principle:

$$k = \frac{k_b T}{h}\, e^{-\left(\frac{\Delta H^{\ddagger}}{RT}\right)} e^{\left(\frac{\Delta S^{\ddagger}}{R}\right)} \qquad \textit{Equation 5-6}$$

During this analysis, it is essential to calculate the turnover frequency (TOF) or the activity per Brønsted acid site. By combining the Brønsted acid site density (0.106 mmol/g)[176] for the commercial HZSM-5 (Si/Al=140) with the mass of the catalyst, we can obtain the TOF value for each acyl donor at each reaction temperature.

The estimated enthalpies ($\Delta H^{\ddagger}$) and entropies ($\Delta S^{\ddagger}$) of transition state of acylation with acetic, propionic, butyric, and valeric, respectively, are summarized in Table 5-2. It clear that $\Delta H^{\ddagger}$ values increase with the increase of the chain length of the carboxylic acid, relevant to the increase measure activation barriers, Figure 5-2, for the transition state with the increase of the

carboxylic acid size. Correspondingly, entropic $\Delta S^{\ddagger}$ values become less negative with increasing the alkyl chain in acid. It is worth mentioning that this trend in transition state value agrees with previous studies of the ketonization of acetic, propionic, and valeric acid[171, 177]. This observation is a clear reflection of the compensation effect between entropy and enthalpy of transition state[178, 179]. However, it is important to note that these values obtained from relatively high surface coverage of the reactants making the derived enthalpy and entropy of transition state values close to their true values[180]. These $\Delta H^{\ddagger}$ and $\Delta S^{\ddagger}$ values represent the difference between enthalpy and entropy values of the transition state (acyl coupling with gas 2-MF) and of the surface acyl spices.

Table 5-2 Enthalpies and entropies for 2-methylfuran acylation with acetic, propionic, butyric, valeric acids over HZSM5 (Si/Al =140) at temperatures between 190-210°C

Carboxylic acid	TS enthalpies, $\Delta H^{\ddagger}$ (kJ/mol)	TS entropies, $\Delta S^{\ddagger}$ (kJ/mol)
Acetic	45.4 ± 7.7	-174.9 ± 16.3
Propionic	53.6 ± 7.3	-151.9 ± 15.5
Butyric	54.9 ± 4.2	-148.4 ± 8.9
Valeric	64.9 ± 10.2	-129.8 ± 21.6

5.3.5 Effects acetic acid cofeeding on catalyst stability.

Processing biomass-derived oxygenates over zeolite results in rapid catalyst deactivation [181, 182], and the direct acylation of 2-MF with carboxylic acid is no exception [18, 19, 60]. During reactions using various compositions of carboxylic acid mixtures, we tracked the deactivation rate for each scenario to analyze the influence of acetic acid co-feeding on catalyst stability during the selective acylation with larger carboxylic acids. Prior research suggests that coke formation is the main cause of catalyst deactivation during the acylation of 2-MF with carboxylic acid, which found to follow a first-order decay rate expression[60]:

$$\textbf{Activity } a(t) = \frac{rate\,(t)}{rate\,(t=0)} = e^{k_d t} \qquad \textit{Equation 5-7}$$

Where the activity, *a(t),* is a function of time, and specific decay constant k_d

The experimental data obtained from acylation with different acid mixture compositions resulted in varying rates as a function of time, represented as rate(t). The initial acylation rate at t=0 was extrapolated and used to derive sets of data to obtain the activity as a function of time, denoted as a(t). These different activity values were utilized to generate linear fitting plot of the natural logarithm, as depicted in Figure 5-6a-c, offering a qualitative assessment of catalyst stability with respect to acetic acid composition in the carboxylic acid mixture. The solid lines in each case represent logarithmic fittings for the activity, described by Equation 5-7, which is based on the first-order decay model. This model was employed to determine the decay constant (k_d) for each scenario.

It is noteworthy that a higher k_d value indicates a faster deactivation rate during the reaction. Table 5-3 summarizes the measured deactivation constants (k_d) during the acylation of 2-MF with various carboxylic acid compositions. The deactivation constant for acylation with AA alone was found to be higher than that for some other larger acids, likely due to not reaching full surface saturation, as illustrated in Figure S5-1. This saturation is crucial to limit direct 2-MF interaction with the active site [18, 19, 60]. Conversely, acylation with PA resulted in a significant drop in deactivation rates, possibly due to high competitive adsorption between the product and PA. We propose that this competition interferes with product stability on the surface, which may destabilize the transition state of the sequential reaction event between an adsorbed product and a gas-phase 2-MF[60]. However, mixing PA with different AA compositions does not necessarily change the deactivation rate until a 1:8 PA: AA molar ratio, suggesting that the deactivation scenario becomes more similar to when AA is fed alone. Unlike PA, increasing the

carbon chain length beyond C3 increases the deactivation constant accordingly, as seen in the cases of BA and VA. Interestingly, the catalyst experiences a substantial reduction in decay rate when mixed with AA, and the enhancement in stability increases with increasing AA composition in the carboxylic acid mixture. This observation indicates a possible change in catalyst deactivation involving interaction between larger carboxylic acids and adsorbed products. In fact, longer-chain carboxylic acids have been found to be more likely to oligomerize and form coke[177, 183]. Therefore, the reduction in catalyst deactivation with increasing AA composition for both BA and VA cases is due to the dilution of larger carboxylic acids, which reduces the probability of interaction with the adsorbed product and the formation of catalyst deactivation species.

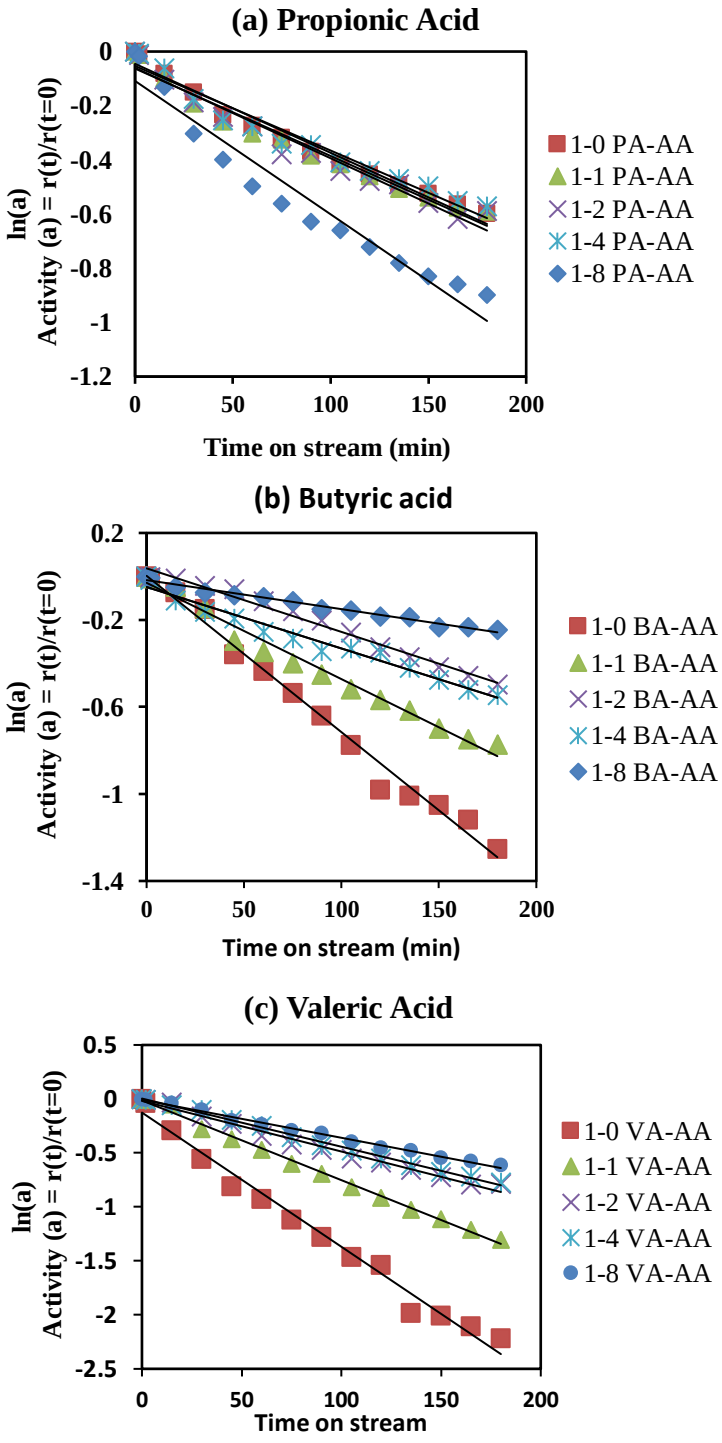


Figure 5-6 Linear fitting plots of the natural logarithm fitting of activity a(t) for acylation with various acetic acid composition in (a) propionic, (b) butyric, and (c) valeric acid mixture. Reaction carried out at 200°C and P_{acids} ~20 Torr $P_{2\text{-}MF}$ ~ 4 Torr.

Table 5-3 Estimated deactivation constant (k_d) during acylation of propionic, butyric, and valeric acids cofed with various acetic acid composition. Reaction carried out at 200°C and P_{acids} ~20 Torr, $P_{2\text{-}MF}$ ~ 4 Torr.

	Deactivation constant k_d (min^{-1})				
Carboxylic Acid to Acetic acid molar ratio	1-0	1-1	1-2	1-4	1-8
Acetic acid	0.008	-	-	-	-
Propionic acid	0.0034	0.0032	0.0033	0.0031	0.0049
Butyric acid	0.0072	0.0044	0.0029	0.0028	0.0013
Valeric acid	0.013	0.0074	0.0047	0.0045	0.0035

5.4 Conclusions

In this study, we conducted a systematic analysis of the effect of carbon chain length in carboxylic acids (acetic, propionic, butyric, valeric acids) during the direct acylation of 2-methylfuran over a zeolite catalyst, revealing a profound influence of alkyl length on kinetic parameters. While activation energies increase with the size of the carboxylic acids, the reaction rates exhibited a significant increase compared to smaller acetic acid. This improved activity is believed to result from the easier dehydration of larger acids, leading to the formation of more stable surface acyl species. This hypothesis was reinforced by stronger adsorption constants in larger acids, as obtained from fitting the Eley-Rideal kinetic model. Additionally, this trend was observed in acylation with larger acid mixtures at various acetic acid compositions, indicating significant selectivity towards larger acids even with high acetic acid content. The estimated transition state parameters suggest a compensation effect in acylation with larger acids, resulting from a substantial increase in the enthalpy of the transition state accompanied by an entropic gain. Furthermore, experiments with acid mixtures revealed an intriguing approach to extending catalyst life without compromising product selectivity. This phenomenon is attributed to the

dilution of larger carboxylic acids (valeric and butyric), which are proposed to oligomerize and contribute to catalyst deactivation while maintaining their acylation selectivity due to their stronger adsorption.

Bibliography

1. Olah, G.A., *Friedel-Crafts and related reactions*. Vol. 1. 1963: Interscience Publishers.
2. Friedel, C. and J.M. Crafts, *Sur une methode generale nouvelle de synthbse d'hydrocarbures, d'acetones, etc.* 1877.
3. Gore, P., *The Friedel-Crafts acylation reaction and its application to polycyclic aromatic hydrocarbons.* Chemical Reviews, 1955. **55**(2): p. 229-281.
4. Sartori, G. and R. Maggi, *Use of solid catalysts in Friedel− Crafts acylation reactions.* Chemical reviews, 2006. **106**(3): p. 1077-1104.
5. Dasgupta, S. and B. Torok, *Environmentally benign contemporary Friedel-Crafts chemistry by solid acids.* Current Organic Synthesis, 2008. **5**(4): p. 321-342.
6. Bhatia, S., *Zeolite catalysts: principles and applications*. 2020: CRC press.
7. Van Santen, R. and G. Kramer, *Reactivity theory of zeolitic broensted acidic sites.* Chemical Reviews, 1995. **95**(3): p. 637-660.
8. Chiche, B., et al., *Friedel-Crafts acylation of toluene and p-xylene with carboxylic acids catalyzed by zeolites.* The Journal of Organic Chemistry, 1986. **51**(11): p. 2128-2130.
9. Corma, A., et al., *Design of synthetic zeolites as catalysts in organic reactions: acylation of anisole by acyl chlorides or carboxylic acids over acid zeolites.* Applied catalysis, 1989. **49**(1): p. 109-123.
10. Chiche, B., et al., *Acylation over cation-exchanged montmorillonite.* Journal of molecular catalysis, 1987. **42**(2): p. 229-235.
11. Corma, A., S. Iborra, and A. Velty, *Chemical routes for the transformation of biomass into chemicals.* Chemical reviews, 2007. **107**(6): p. 2411-2502.
12. Wettstein, S.G., et al., *A roadmap for conversion of lignocellulosic biomass to chemicals and fuels.* Current Opinion in Chemical Engineering, 2012. **1**(3): p. 218-224.
13. Gallezot, P., *Conversion of biomass to selected chemical products.* Chemical Society Reviews, 2012. **41**(4): p. 1538-1558.
14. Resasco, D.E., B. Wang, and S. Crossley, *Zeolite-catalysed C–C bond forming reactions for biomass conversion to fuels and chemicals.* Catalysis Science & Technology, 2016. **6**(8): p. 2543-2559.
15. Meng, J., et al., *The effect of torrefaction on the chemistry of fast-pyrolysis bio-oil.* Bioresource technology, 2012. **111**: p. 439-446.
16. Czernik, S. and A.V. Bridgwater, *Overview of applications of biomass fast pyrolysis oil.* Energy & fuels, 2004. **18**(2): p. 590-598.
17. Bui, T.V., S. Crossley, and D.E. Resasco, *C–C coupling for biomass-derived furanics upgrading to chemicals and fuels*. 2016, Wiley-VCH Verlag and Co. KGaA. p. 431-494.
18. Gumidyala, A., B. Wang, and S. Crossley, *Direct carbon-carbon coupling of furanics with acetic acid over Brønsted zeolites.* Science advances, 2016. **2**(9): p. e1601072.

19. Ji, Y., et al., *Probing direct carbon-carbon acylation of furans and long-chain acids over H-ZSM-5*. Applied Catalysis A: General, 2019. **577**: p. 107-112.
20. Chen, T.-H., D.G. Vlachos, and S. Caratzoulas, *Brønsted Acid Catalysis of the Direct Acylation of 2-Methylfuran by Acetic Acid. Theoretical Insights into the Role of Brønsted Acidity and Confinement.* ACS Catalysis, 2021. **11**(15): p. 9916-9925.
21. Olah, G.A., *Friedel-crafts chemistry*, in *Across Conventional Lines: Selected Papers of George A Olah Volume 1*. 2003, World Scientific. p. 119-121.
22. Park, D.S., et al., *Tunable Oleo-Furan Surfactants by Acylation of Renewable Furans*. ACS Central Science, 2016. **2**(11): p. 820-824.
23. Zaimes, G.G., et al., *Multistage torrefaction and in situ catalytic upgrading to hydrocarbon biofuels: analysis of life cycle energy use and greenhouse gas emissions.* Energy & Environmental Science, 2017. **10**(5): p. 1034-1050.
24. Beck, A.W., et al., *Systems-Level Analysis of Energy and Greenhouse Gas Emissions for Coproducing Biobased Fuels and Chemicals: Implications for Sustainability*. ACS Sustainable Chemistry & Engineering, 2018. **6**(5): p. 5826-5834.
25. Herron, J.A., et al., *A systems-level roadmap for biomass thermal fractionation and catalytic upgrading strategies.* Energy Technology, 2017. **5**(1): p. 130-150.
26. Duong, N.N., et al., *Enhancing the Acylation Activity of Acetic Acid by Formation of an Intermediate Aromatic Ester.* ChemSusChem, 2017. **10**(13): p. 2823-2832.
27. Gutiérrez-Rubio, S., et al., *Vapor phase acylation of guaiacol with acetic acid over micro, nano and hierarchical MFI and BEA zeolites.* Applied Catalysis B: Environmental, 2021. **285**: p. 119826.
28. Koehle, M., et al., *Production of p-Methylstyrene and p-Divinylbenzene from Furanic Compounds.* ChemSusChem, 2017. **10**(1): p. 91-98.
29. Koehle, M., et al., *Acylation of methylfuran with Brønsted and Lewis acid zeolites*. Applied Catalysis A: General, 2018. **564**: p. 90-101.
30. Green, S.K., et al., *Diels–Alder cycloaddition of 2-methylfuran and ethylene for renewable toluene.* Applied Catalysis B: Environmental, 2016. **180**: p. 487-496.
31. Schüth, F., M.D. Ward, and J.M. Buriak, *Common pitfalls of catalysis manuscripts submitted to chemistry of materials*. 2018, ACS Publications.
32. Koros, R. and E. Nowak, *A diagnostic test of the kinetic regime in a packed bed reactor.* Chemical Engineering Science, 1967. **22**(3): p. 470.
33. Madon, R.J. and M. Boudart, *Experimental criterion for the absence of artifacts in the measurement of rates of heterogeneous catalytic reactions.* Industrial & Engineering Chemistry Fundamentals, 1982. **21**(4): p. 438-447.
34. Pham, T.N., et al., *Quantifying the influence of water on the mobility of aluminum species and their effects on alkane cracking in zeolites.* ACS Catalysis, 2021. **11**(12): p. 6982-6994.
35. Pham, T.N., et al., *Influence of Brønsted Acid Site Proximity on Alkane Cracking in MFI Zeolites.* ACS Catalysis, 2023. **13**(2): p. 1359-1370.
36. Chen, K., et al., *Brønsted–Brønsted synergies between framework and noncrystalline protons in zeolite H-ZSM-5.* ACS Catalysis, 2019. **9**(7): p. 6124-6136.

37. Botella, P., et al., *Acylation of toluene with acetic anhydride over beta zeolites: Influence of reaction conditions and physicochemical properties of the catalyst*. Journal of Catalysis, 2000. **195**(1): p. 161-168.
38. Padro, C. and C.R. Apesteguía, *Acylation of phenol on solid acids: Study of the deactivation mechanism*. Catalysis today, 2005. **107**: p. 258-265.
39. Neves, I., et al., *Acylation of phenol with acetic acid over a HZSM5 zeolite, reaction scheme*. Journal of molecular catalysis, 1994. **93**(2): p. 169-179.
40. Jayat, F., et al., *Acylation of phenol with acetic acid. Effect of density and strength of acid sites on the properties of MFI metallosilicates*, in *Studies in Surface Science and Catalysis*. 1997, Elsevier. p. 1149-1156.
41. Chowdhury, A.D. and J. Gascon, *The curious case of ketene in zeolite chemistry and catalysis*. Angewandte Chemie International Edition, 2018. **57**(46): p. 14982-14985.
42. Bejblova, M., D. Prochazkova, and J. Čejka, *Acylation reactions over zeolites and mesoporous catalysts*. ChemSusChem: Chemistry & Sustainability Energy & Materials, 2009. **2**(6): p. 486-499.
43. Wang, C., et al., *HD Exchange of Simple Aromatics as a Measure of Brønsted-Acid Site Strengths in Solids*. Catalysis Letters, 2018. **148**: p. 3548-3556.
44. Gorte, R.J. and S.P. Crossley, *A perspective on catalysis in solid acids*. Journal of Catalysis, 2019. **375**: p. 524-530.
45. Vinter, K.P. and P.J. Dauenhauer, *Inert competitive adsorption for the inhibition of oligomerization of alkenes during alcohol dehydration*. Catalysis Science & Technology, 2018. **8**(15): p. 3901-3909.
46. Wan, S., et al., *Decoupling HZSM-5 catalyst activity from deactivation during upgrading of pyrolysis oil vapors*. ChemSusChem, 2015. **8**(3): p. 552-559.
47. Corma, A., C. Martínez, and E. Doskocil, *Designing MFI-based catalysts with improved catalyst life for C3= andC5= oligomerization to high-quality liquid fuels*. Journal of Catalysis, 2013. **300**: p. 183-196.
48. Williams, P.T. and P.A. Horne, *The influence of catalyst regeneration on the composition of zeolite-upgraded biomass pyrolysis oils*. Fuel, 1995. **74**(12): p. 1839-1851.
49. Aguayo, A.T., et al., *Coke aging and its incidence on catalyst regeneration*. Industrial & engineering chemistry research, 2003. **42**(17): p. 3914-3921.
50. Díaz, M., et al., *Coke deactivation and regeneration of HZSM-5 zeolite catalysts in the oligomerization of 1-butene*. Applied Catalysis B: Environmental, 2021. **291**: p. 120076.
51. Epelde, E., et al., *Differences among the deactivation pathway of HZSM-5 zeolite and SAPO-34 in the transformation of ethylene or 1-butene to propylene*. Microporous and mesoporous materials, 2014. **195**: p. 284-293.
52. Valle, B., et al., *Deactivating species in the transformation of crude bio-oil with methanol into hydrocarbons on a HZSM-5 catalyst*. Journal of Catalysis, 2012. **285**(1): p. 304-314.
53. Bachiller-Baeza, B. and J. Anderson, *FTIR and reaction studies of the acylation of anisole with acetic anhydride over supported HPA catalysts*. Journal of Catalysis, 2004. **228**(1): p. 225-233.

54. Jaya, G.T., et al., *One-pot conversion of lignocellulosic biomass to ketones and aromatics over a multifunctional Cu–Ru/ZSM-5 catalyst*. Applied Catalysis B: Environmental, 2022. **312**: p. 121368.
55. Cai, R., et al., *Biomass catalytic pyrolysis over zeolite catalysts with an emphasis on porosity and acidity: a state-of-the-art review*. Energy & Fuels, 2020. **34**(10): p. 11771-11790.
56. Mardiana, S., et al., *Hierarchical zeolite for biomass conversion to biofuel: A review*. Fuel, 2022. **309**: p. 122119.
57. Park, D.S., et al., *Tunable oleo-furan surfactants by acylation of renewable furans*. ACS central science, 2016. **2**(11): p. 820-824.
58. Gomez, L.A., et al., *Selective Reduction of Carboxylic Acids to Aldehydes with Promoted MoO3 Catalysts*. ACS Catalysis, 2022. **12**(11): p. 6313-6324.
59. Chau, H.K., et al., *Acylation of m-cresol with acetic acid supported by in-situ ester formation on H-ZSM-5 zeolites*. Journal of Catalysis, 2022. **406**: p. 48-55.
60. Alalq, I., H. Nguyen-Phu, and S. Crossley, *Shifts in catalyst deactivation mechanisms as a function of surface coverage during Friedel-Crafts acylation in zeolites*. Journal of Catalysis, 2023. **426**: p. 222-233.
61. Walker, T.W., et al., *Fundamental catalytic challenges to design improved biomass conversion technologies*. Journal of Catalysis, 2019. **369**: p. 518-525.
62. Serrano, D.P., et al., *Progress in the design of zeolite catalysts for biomass conversion into biofuels and bio-based chemicals*. Catalysis Reviews, 2018. **60**(1): p. 1-70.
63. Butter , S.A.W.W., Kaeding, *Methylation of toluene*, M. Corporation, Editor. 1976: United States.
64. Stephen, B.W., Kaeding, *Phosphorus-containing zeolite catalyst*, in *Mobil Corporation*. 1976: United states.
65. Kaeding, W.W. and S.A. Butter, *Production of chemicals from methanol--1. Low molecular weight olefins*. J. Catal.; (United States), 1980. **61:1**: p. Medium: X; Size: Pages: 155-164 2016-05-13.
66. van der Bij, H.E. and B.M. Weckhuysen, *Phosphorus promotion and poisoning in zeolite-based materials: synthesis, characterisation and catalysis*. Chemical Society Reviews, 2015. **44**(20): p. 7406-7428.
67. Losch, P., et al., *Phosphorous modified ZSM-5 zeolites: impact on methanol conversion into olefins*. Topics in Catalysis, 2015. **58**: p. 826-832.
68. Song, Z., et al., *Phosphorus-modified ZSM-5 for conversion of ethanol to propylene*. Applied Catalysis A: General, 2010. **384**(1-2): p. 201-205.
69. Yao, W., et al., *Thermally stable phosphorus and nickel modified ZSM-5 zeolites for catalytic co-pyrolysis of biomass and plastics*. Rsc Advances, 2015. **5**(39): p. 30485-30494.
70. Mante, O.D., et al., *The effect of hydrothermal treatment of FCC catalysts and ZSM-5 additives in catalytic conversion of biomass*. Applied Catalysis A: General, 2012. **445**: p. 312-320.
71. Cho, H.J., et al., *Renewable p-Xylene from 2, 5-Dimethylfuran and Ethylene Using Phosphorus-Containing Zeolite Catalysts*. ChemCatChem, 2017. **9**(3): p. 398-402.

72. Zhao, R., et al., *Renewable p-xylene synthesis via biomass-derived 2, 5-dimethylfuran and ethanol by phosphorous modified H-Beta zeolite.* Microporous and Mesoporous Materials, 2022. **334**: p. 111787.
73. Abdelrahman, O.A., et al., *Biomass-derived butadiene by dehydra-decyclization of tetrahydrofuran.* ACS Sustainable Chemistry & Engineering, 2017. **5**(5): p. 3732-3736.
74. Gulbinski, J., et al., *Role of silica support in phosphoric acid catalyzed production of p-xylene from 2, 5-dimethylfuran and ethylene.* Industrial & Engineering Chemistry Research, 2020. **59**(51): p. 22049-22056.
75. Kresnawahjuesa, O., R.J. Gorte, and D. White, *The acylation of propene by acetic acid over H-[Fe] ZSM-5 and H-[Al] ZSM-5.* Journal of Molecular Catalysis A: Chemical, 2004. **212**(1-2): p. 309-314.
76. Yokoi, T., et al., *Control of the Al distribution in the framework of ZSM-5 zeolite and its evaluation by solid-state NMR technique and catalytic properties.* The Journal of Physical Chemistry C, 2015. **119**(27): p. 15303-15315.
77. Kim, D.J. and H.S. Chung, *Synthesis and characterization of ZSM-5 zeolite from serpentine.* Applied Clay Science, 2003. **24**(1-2): p. 69-77.
78. Zhuang, J., et al., *Solid-state MAS NMR studies on the hydrothermal stability of the zeolite catalysts for residual oil selective catalytic cracking.* Journal of catalysis, 2004. **228**(1): p. 234-242.
79. Zhang, D., R. Wang, and X. Yang, *Effect of P content on the catalytic performance of P-modified HZSM-5 catalysts in dehydration of ethanol to ethylene.* Catalysis Letters, 2008. **124**: p. 384-391.
80. Ramesh, K., et al., *Structure and reactivity of phosphorous modified H-ZSM-5 catalysts for ethanol dehydration.* Catalysis Communications, 2009. **10**(5): p. 567-571.
81. van der Bij, H.E., et al., *Phosphatation of Zeolite H-ZSM-5: A Combined Microscopy and Spectroscopy Study.* ChemPhysChem, 2014. **15**(2): p. 283-292.
82. Caeiro, G., et al., *Stabilization effect of phosphorus on steamed H-MFI zeolites.* Applied Catalysis A: General, 2006. **314**(2): p. 160-171.
83. Göhlich, M., W. Reschetilowski, and S. Paasch, *Spectroscopic study of phosphorus modified H-ZSM-5.* Microporous and Mesoporous Materials, 2011. **142**(1): p. 178-183.
84. Tanwar, M., D. Bhatia, and M.P. Harold, *Analysis of inter-particle dilution effects in a catalytic packed bed reactor.* Chemical Engineering Journal, 2018. **337**: p. 750-754.
85. Koros, R.M. and E.J. Nowak, *A diagnostic test of the kinetic regime in a packed bed reactor.* Chemical Engineering Science, 1967. **22**(3): p. 470.
86. Chen, N.Y., W.W. Kaeding, and F.G. Dwyer, *Para-directed aromatic reactions over shape-selective molecular sieve zeolite catalysts.* Journal of the American Chemical Society, 1979. **101**(22): p. 6783-6784.
87. Janardhan, H.L., G.V. Shanbhag, and A.B. Halgeri, *Shape-selective catalysis by phosphate modified ZSM-5: Generation of new acid sites with pore narrowing.* Applied Catalysis A: General, 2014. **471**: p. 12-18.

88. Takahashi, A., et al., *Effects of added phosphorus on conversion of ethanol to propylene over ZSM-5 catalysts.* Applied Catalysis A: General, 2012. **423**: p. 162-167.
89. Rumplmayr, G. and J.A. Lercher, *Modification of HZSM-5 with trimethylphosphine.* Zeolites, 1990. **10**(4): p. 283-287.
90. Jiang, G., et al., *Highly effective P-modified HZSM-5 catalyst for the cracking of C4 alkanes to produce light olefins.* Applied Catalysis A: General, 2008. **340**(2): p. 176-182.
91. Kresnawahjuesa, O., et al., *A simple, inexpensive, and reliable method for measuring Brønsted-acid site densities in solid acids.* Catalysis letters, 2002. **82**: p. 155-160.
92. Caro, J., et al., *NMR and IR studies of zeolite H-ZSM-5 modified with orthophosphoric acid.* Journal of Catalysis, 1990. **124**(2): p. 367-375.
93. Zhao, Y., et al., *A comparison on the hydrothermal stability of nano-sized H-ZSM-5 zeolite modified by ammonium dihydrogen phosphate and trimethylphosphate.* Catalysis Letters, 2019. **149**: p. 2169-2179.
94. Jentys, A., G. Rumplmayr, and J.A. Lercher, *Hydroxyl groups in phosphorus-modified HZSM-5.* Applied catalysis, 1989. **53**(2-3): p. 299-312.
95. Blasco, T., A. Corma, and J. Martínez-Triguero, *Hydrothermal stabilization of ZSM-5 catalytic-cracking additives by phosphorus addition.* Journal of catalysis, 2006. **237**(2): p. 267-277.
96. Aramendıa, M.A., et al., *Synthesis and characterization of magnesium phosphates and their catalytic properties in the conversion of 2-hexanol.* Journal of colloid and interface science, 1999. **217**(2): p. 288-298.
97. Jain, S.K., et al., *P-site structural diversity and evolution in a zeosil catalyst.* Journal of the American Chemical Society, 2021. **143**(4): p. 1968-1983.
98. Seo, G. and R. Ryoo, *31P, 27Al, and 129Xe NMR study of phosphorus-impregnated HZSM-5 zeolite catalysts.* Journal of Catalysis, 1990. **124**(1): p. 224-230.
99. Costa, A.F., et al., *BEA and MOR as additives for light olefins production.* Applied Catalysis A: General, 2007. **319**: p. 137-143.
100. de Oliveira Lima, E.C., et al., *Aluminum polyphosphate thermoreversible gels: A study by31P and27Al NMR spectroscopy.* Journal of colloid and interface science, 1995. **176**(2): p. 388-396.
101. Damodaran, K., et al., *Modification of H-ZSM-5 zeolites with phosphorus. 2. Interaction between phosphorus and aluminum studied by solid-state NMR spectroscopy.* Microporous and mesoporous materials, 2006. **95**(1-3): p. 296-305.
102. Derewinski, M., et al., *Reversibility of the Modification of HZSM-5 with Phosphate Anions.* The Journal of Physical Chemistry C, 2014. **118**(12): p. 6122-6131.
103. van der Bij, H.E. and B.M. Weckhuysen, *Local silico-aluminophosphate interfaces within phosphated H-ZSM-5 zeolites.* Physical Chemistry Chemical Physics, 2014. **16**(21): p. 9892-9903.
104. Chen, K., et al., *First-Formed Framework Species and Phosphate Structure Distributions in Phosphorus-Modified MFI Zeolites.* The Journal of Physical Chemistry C, 2022. **126**(1): p. 227-238.

105. Xue, N., et al., *Understanding the enhancement of catalytic performance for olefin cracking: Hydrothermally stable acids in P/HZSM-5*. Journal of Catalysis, 2007. **248**(1): p. 20-28.
106. Jang, H.-G., et al., *Tetramethylbenzenium radical cations as major active intermediates of methanol-to-olefin conversions over phosphorous-modified HZSM-5 zeolites*. Journal of catalysis, 2013. **299**: p. 240-248.
107. Yi, D., et al., *Catalytic performance of modified ZSM-5 designed with selectively passivated external surface acidity by phosphorus*. Industrial & Engineering Chemistry Research, 2019. **58**(24): p. 10154-10163.
108. Vinek, H., G. Rumplmayr, and J.A. Lercher, *Catalytic properties of postsynthesis phosphorus-modified H-ZSM5 zeolites*. Journal of Catalysis, 1989. **115**(2): p. 291-300.
109. Deshlahra, P. and E. Iglesia, *Reactivity descriptors in acid catalysis: acid strength, proton affinity and host–guest interactions*. Chemical Communications, 2020. **56**(54): p. 7371-7398.
110. Noh, G., S.I. Zones, and E. Iglesia, *Consequences of acid strength and diffusional constraints for alkane isomerization and β-scission turnover rates and selectivities on bifunctional metal-acid catalysts*. The Journal of Physical Chemistry C, 2018. **122**(44): p. 25475-25497.
111. Jones, A.J. and E. Iglesia, *The strength of Brønsted acid sites in microporous aluminosilicates*. Acs Catalysis, 2015. **5**(10): p. 5741-5755.
112. Dong, H., et al., *Catalytic performance of phosphorus modified HZSM-5 zeolite catalysts in the co-cracking reaction of n-hexane and methanol*. Catalysis Letters, 2022: p. 1-11.
113. Zhou, Z., et al., *One-pot Synthesis of Phosphorus-modified ZSM-5 Zeolite by Solid-state Method and its MTO Catalytic Performance*. Chemistry–A European Journal, 2023. **29**(14): p. e202203095.
114. Ding, J., et al., *Combined desilication and phosphorus modification for high-silica ZSM-5 zeolite with related study of hydrocarbon cracking performance*. Applied Catalysis A: General, 2015. **503**: p. 147-155.
115. Soh, J.C., et al., *Catalytic ethylene production from ethanol dehydration over non-modified and phosphoric acid modified Zeolite HY (80) catalysts*. Fuel Processing Technology, 2017. **158**: p. 85-95.
116. Shan, J., et al., *Enhancement in catalytic performance of HZSM-5 zeolite for glycerol dehydration after acidity regulation*. Chemical Engineering Journal, 2023. **460**: p. 141741.
117. Abubakar, S.M., et al., *Structural and Mechanistic Investigation of a Phosphate-Modified HZSM-5 Catalyst for Methanol Conversion*. Langmuir, 2006. **22**(10): p. 4846-4852.
118. Gumidyala, A., T. Sooknoi, and S. Crossley, *Selective ketonization of acetic acid over HZSM-5: The importance of acyl species and the influence of water*. Journal of Catalysis, 2016. **340**: p. 76-84.
119. Baddeley, G. and D. Voss, *The mechanism of Friedel–Crafts acylation*. Journal of the Chemical Society (Resumed), 1954: p. 418-422.

120. Welch, J., *Organic Chemistry, Synthesis*, in *Encyclopedia of Physical Science and Technology (Third Edition)*, R.A. Meyers, Editor. 2003, Academic Press: New York. p. 497-515.
121. Aleixo, R., et al., *Zooming in with QSPR on Friedel-Crafts acylation reactions over modified BEA zeolites.* Molecular Catalysis, 2019. **476**: p. 110495.
122. Prins, M.J., K.J. Ptasinski, and F.J. Janssen, *Torrefaction of wood: Part 2. Analysis of products.* Journal of analytical and applied pyrolysis, 2006. **77**(1): p. 35-40.
123. Janda, A. and A.T. Bell, *Effects of Si/Al ratio on the distribution of framework Al and on the rates of alkane monomolecular cracking and dehydrogenation in H-MFI.* Journal of the American Chemical Society, 2013. **135**(51): p. 19193-19207.
124. Gounder, R. and E. Iglesia, *The roles of entropy and enthalpy in stabilizing ion-pairs at transition states in zeolite acid catalysis.* Accounts of chemical research, 2012. **45**(2): p. 229-238.
125. Gounder, R. and E. Iglesia, *The catalytic diversity of zeolites: confinement and solvation effects within voids of molecular dimensions.* Chemical Communications, 2013. **49**(34): p. 3491-3509.
126. Schallmoser, S., et al., *Impact of the local environment of Brønsted acid sites in ZSM-5 on the catalytic activity in n-pentane cracking.* Journal of Catalysis, 2014. **316**: p. 93-102.
127. Chau, H.K., et al., *Effect of Water on Cumene Dealkylation over H-ZSM-5 Zeolites.* ACS Catalysis, 2021. **13**: p. 9158-9170.
128. Li, T., et al., *Influence of active-site proximity in zeolites on Brønsted acid-catalyzed reactions at the microscopic and mesoscopic levels.* Chem Catalysis, 2023.
129. Mlinar, A.N., et al., *Effects of Brønsted-acid site proximity on the oligomerization of propene in H-MFI.* Journal of catalysis, 2012. **288**: p. 65-73.
130. Kester, P.M., et al., *Effects of Brønsted acid site proximity in chabazite zeolites on OH infrared spectra and protolytic propane cracking kinetics.* Journal of Catalysis, 2021. **395**: p. 210-226.
131. Song, C., et al., *Cooperativity of adjacent Brønsted acid sites in MFI zeolite channel leads to enhanced polarization and cracking of alkanes.* Journal of Catalysis, 2017. **349**: p. 163-174.
132. Masuda, T., et al., *Changes in catalytic activity of MFI-type zeolites caused by dealumination in a steam atmosphere.* Applied Catalysis A: General, 1998. **172**(1): p. 73-83.
133. van Bokhoven, J.A., et al., *An explanation for the enhanced activity for light alkane conversion in mildly steam dealuminated mordenite: The dominant role of adsorption.* Journal of catalysis, 2001. **202**(1): p. 129-140.
134. Yu, Z., et al., *Brønsted/lewis acid synergy in H–ZSM-5 and H–MOR zeolites studied by 1H and 27Al DQ-MAS solid-state NMR spectroscopy.* The Journal of Physical Chemistry C, 2011. **115**(45): p. 22320-22327.
135. Zhang, Y., et al., *Promotion of protolytic pentane conversion on H-MFI zeolite by proximity of extra-framework aluminum oxide and Brønsted acid sites.* Journal of Catalysis, 2019. **370**: p. 424-433.

136. Maier, S.M., A. Jentys, and J.A. Lercher, *Steaming of zeolite BEA and its effect on acidity: A comparative NMR and IR spectroscopic study*. The Journal of Physical Chemistry C, 2011. **115**(16): p. 8005-8013.
137. Bailleul, S., et al., *A supramolecular view on the cooperative role of Brønsted and Lewis acid sites in zeolites for methanol conversion*. Journal of the American Chemical Society, 2019. **141**(37): p. 14823-14842.
138. Zhi, Y., et al., *Dehydration Pathways of 1-Propanol on HZSM-5 in the Presence and Absence of Water*. Journal of the American Chemical Society, 2015. **137**(50): p. 15781-15794.
139. Al-Khattaf, S., et al., *The effect of coke deposition on the activity and selectivity of the HZSM-5 zeolite during ethylbenzene alkylation reaction in the presence of ethanol*. Catalysis Science & Technology, 2014. **4**(4): p. 1017-1027.
140. Ravi, M., V.L. Sushkevich, and J.A. van Bokhoven, *Towards a better understanding of Lewis acidic aluminium in zeolites*. Nature materials, 2020. **19**(10): p. 1047-1056.
141. Abdelrahman, O.A., et al., *Simple quantification of zeolite acid site density by reactive gas chromatography*. Catalysis Science & Technology, 2017. **7**(17): p. 3831-3841.
142. Luo, J., et al., *The effect of oxide acidity on HMF etherification*. Catalysis Science & Technology, 2014. **4**(9): p. 3074-3081.
143. Kresse, G. and J. Furthmüller, *Efficient iterative schemes for ab initio total-energy calculations using a plane-wave basis set*. Physical review B, 1996. **54**(16): p. 11169.
144. Kresse, G. and D. Joubert, *From ultrasoft pseudopotentials to the projector augmented-wave method*. Physical review b, 1999. **59**(3): p. 1758.
145. Blöchl, P.E., *Projector augmented-wave method*. Physical review B, 1994. **50**(24): p. 17953.
146. Perdew, J.P., K. Burke, and M. Ernzerhof, *Generalized gradient approximation made simple*. Physical review letters, 1996. **77**(18): p. 3865.
147. Grimme, S., et al., *A consistent and accurate ab initio parametrization of density functional dispersion correction (DFT-D) for the 94 elements H-Pu*. The Journal of chemical physics, 2010. **132**(15).
148. Zeets, M., D.E. Resasco, and B. Wang, *Enhanced chemical activity and wettability at adjacent Brønsted acid sites in HZSM-5*. Catalysis Today, 2018. **312**: p. 44-50.
149. Chen, K., et al., *Structure and catalytic characterization of a second framework Al (IV) site in zeolite catalysts revealed by NMR at 35.2 T*. Journal of the American Chemical Society, 2020. **142**(16): p. 7514-7523.
150. Henkelman, G., B.P. Uberuaga, and H. Jónsson, *A climbing image nudged elastic band method for finding saddle points and minimum energy paths*. The Journal of chemical physics, 2000. **113**(22): p. 9901-9904.
151. Abdolrahmani, M., K. Chen, and J.L. White, *Assessment, control, and impact of Brønsted acid site heterogeneity in zeolite HZSM-5*. The Journal of Physical Chemistry C, 2018. **122**(27): p. 15520-15528.

152. Chen, K., et al., *Distribution of aluminum species in zeolite catalysts: 27Al NMR of framework, partially-coordinated framework, and non-framework moieties*. Journal of the American Chemical Society, 2021. **143**(17): p. 6669-6680.
153. Li, J., et al., *Carboxylic acids to butyl esters over dealuminated–realuminated beta zeolites for removing organic acids from bio-oils*. RSC advances, 2017. **7**(54): p. 33714-33725.
154. Bourgeat-Lami, E., et al., *Study of the state of aluminium in zeolite-β*. Applied catalysis, 1991. **72**(1): p. 139-152.
155. Baran, R., et al., *Influence of the nitric acid treatment on Al removal, framework composition and acidity of BEA zeolite investigated by XRD, FTIR and NMR*. Microporous and Mesoporous Materials, 2012. **163**: p. 122-130.
156. Dutartre, R., et al., *Mesopore formation during steam dealumination of zeolites: influence of initial aluminum content and crystal size*. Microporous materials, 1996. **6**(5-6): p. 311-320.
157. Eyring, H., *The Activated Complex and the Absolute Rate of Chemical Reactions*. Chemical Reviews, 1935. **17**(1): p. 65-77.
158. Laidler, K.J. and M.C. King, *The development of transition-state theory*. J. phys. Chem, 1983. **87**(15): p. 2657-2664.
159. Jones, A.J. and E. Iglesia, *Kinetic, spectroscopic, and theoretical assessment of associative and dissociative methanol dehydration routes in zeolites*. Angewandte Chemie, 2014. **126**(45): p. 12373-12377.
160. Jones, A.J., et al., *Acid strength and solvation in catalysis by MFI zeolites and effects of the identity, concentration and location of framework heteroatoms*. Journal of Catalysis, 2014. **312**: p. 58-68.
161. Jones, A.J., S.I. Zones, and E. Iglesia, *Implications of transition state confinement within small voids for acid catalysis*. The Journal of Physical Chemistry C, 2014. **118**(31): p. 17787-17800.
162. Liu, C., et al., *Relationship between acidity and catalytic reactivity of faujasite zeolite: A periodic DFT study*. Journal of Catalysis, 2016. **344**: p. 570-577.
163. Rosen, M.J., *The relationship of structure to properties in surfactants*. 1972, Wiley Online Library.
164. Raffa, P., et al., *Polymeric surfactants: synthesis, properties, and links to applications*. Chemical reviews, 2015. **115**(16): p. 8504-8563.
165. Falbe, J., *Surfactants in consumer products: Theory, Technology and Application*. 2012: Springer Science & Business Media.
166. Bui, T.V., S. Crossley, and D.E. Resasco, *C□C Coupling for Biomass-Derived Furanics Upgrading to Chemicals and Fuels*. Chemicals and Fuels from Bio-Based Building Blocks, 2016: p. 431-494.
167. Wagholikar, S., et al., *Acylation of anisole with long-chain carboxylic acids over wide pore zeolites*. Applied Catalysis A: General, 2007. **317**(2): p. 250-257.
168. Ma, Y., et al., *Friedalĥ Crafts acylation of anisole over zeolite catalysts*. Applied Catalysis A: General, 1997. **165**(1-2): p. 199-206.

169. Sternberg, J., W. Gallaway, and D. Jones. *The mechanism of response of flame ionization detectors*. in *Gas Chromatography, Third International Symposium, Academic Press, New York*. 1962.
170. Godavarthy, M., *Carboxylic Acid Ketonization on Zeolites*. 2016.
171. Pham, T.N., D. Shi, and D.E. Resasco, *Reaction kinetics and mechanism of ketonization of aliphatic carboxylic acids with different carbon chain lengths over Ru/TiO2 catalyst*. Journal of catalysis, 2014. **314**: p. 149-158.
172. Eder, F., M. Stockenhuber, and J. Lercher, *Brønsted acid site and pore controlled siting of alkane sorption in acidic molecular sieves*. The Journal of Physical Chemistry B, 1997. **101**(27): p. 5414-5419.
173. Denayer, J.F., et al., *High-temperature low-pressure adsorption of branched c5− c8 alkanes on zeolite beta, zsm-5, zsm-22, zeolite y, and mordenite*. The Journal of physical chemistry B, 1998. **102**(23): p. 4588-4597.
174. Yeh, Y.-H., et al., *Adsorption of small alkanes on ZSM-5 zeolites: influence of Brønsted sites*. The Journal of Physical Chemistry C, 2016. **120**(22): p. 12132-12138.
175. Pechukas, P., *Transition state theory*. Annual Review of Physical Chemistry, 1981. **32**(1): p. 159-177.
176. Chau, H.K., et al., *Effect of water on cumene dealkylation over H-ZSM-5 zeolites*. ACS Catalysis, 2023. **13**(13): p. 9158-9170.
177. Cao, J., et al., *Conversion of C2–4 carboxylic acids to hydrocarbons on HZSM-5: effect of carbon chain length*. Industrial & Engineering Chemistry Research, 2019. **58**(24): p. 10307-10316.
178. Galwey, A., *Compensation effect in heterogeneous catalysis*, in *Advances in Catalysis*. 1977, Elsevier. p. 247-322.
179. Bond, G.C., et al., *Compensation phenomena in heterogeneous catalysis: general principles and a possible explanation*. Catalysis Reviews, 2000. **42**(3): p. 323-383.
180. Bhan, A., et al., *Entropy considerations in monomolecular cracking of alkanes on acidic zeolites*. Journal of Catalysis, 2008. **253**(1): p. 221-224.
181. Gayubo, A.G., et al., *Transformation of oxygenate components of biomass pyrolysis oil on a HZSM-5 zeolite. I. Alcohols and phenols*. Industrial & Engineering Chemistry Research, 2004. **43**(11): p. 2610-2618.
182. Gayubo, A.G., et al., *Transformation of oxygenate components of biomass pyrolysis oil on a HZSM-5 zeolite. II. Aldehydes, ketones, and acids*. Industrial & engineering chemistry research, 2004. **43**(11): p. 2619-2626.
183. Lee, K., M.Y. Kim, and M. Choi, *Effects of fatty acid structures on ketonization selectivity and catalyst deactivation*. ACS sustainable chemistry & engineering, 2018. **6**(10): p. 13035-13044.

Appendices

Appendix-A: supporting information for Chapter 2**.....***Error! Bookmark not defined.*

Shifts in catalyst deactivation mechanisms as a function of surface coverage during Friedel-Crafts acylation in zeolites

Appendix-B: supporting information for Chapter 3**.....***Error! Bookmark not defined.*

Consequence of altering acid strength in MFI zeolites via Phosphorus modification and their effects on acylation reaction

Appendix-C: supporting information for Chapter 4**.....***Error! Bookmark not defined.*

Effect of Brønsted Acid Site's Local Environment on Zeolites' Catalytic Activities during Acylation of 2-Methylfuran with Acetic Acid

Appendix-D: supporting information for Chapter 5**.....***Error! Bookmark not defined.*

Role of carbon chain length in carboxylic acids on acylation of 2-methyl furan over HZSM-5 zeolite

Appendix-A: supporting information for Chapter 2

Shifts in catalyst deactivation mechanisms as a function of surface coverage during Friedel-Crafts acylation in zeolites

1) Equilibrium limitation

To confirm that results are not influenced by thermodynamic equilibrium limitations, conversion is reported with increasing catalyst mass, revealing that kinetic results in Figure S2-1 are obtained far from thermodynamic equilibrium limits. The partial pressure of the limiting reactant, 2-methylfuran, is 2.6 torr. Under these conditions, both reactants (P_{AA}= 40 Torr, $P_{2\text{-MF}}$ = 2.6 Torr) at 160°C are in the 0^{th} order kinetic regime.

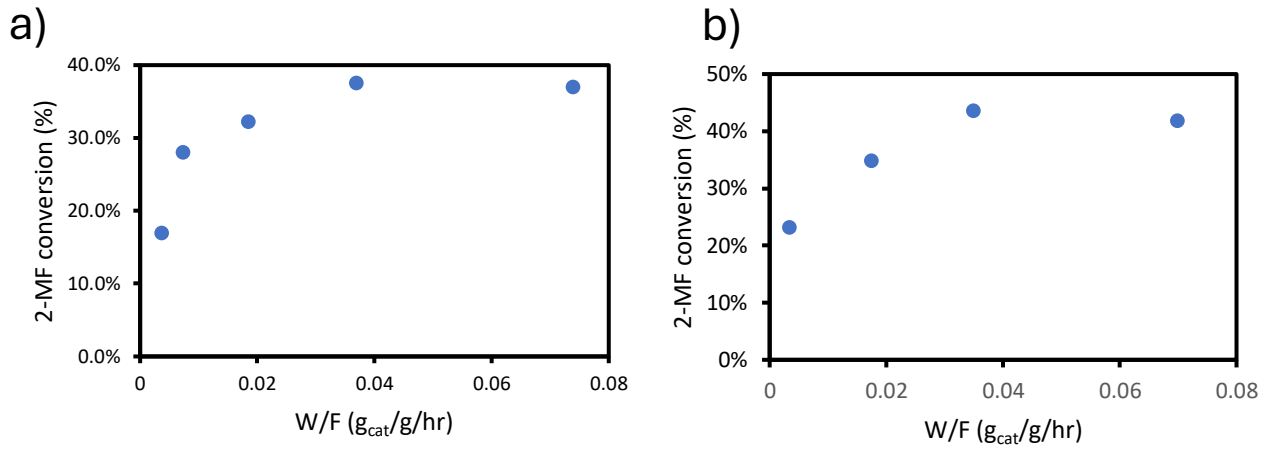


Figure S 2-1. a) Testing thermodynamic influence. Catalyst masses used 5, 10, 25, 50, 100 mg HZSM-5 Si/Al= 40 at temperature 180°C Molar AA:2-MF molar ratio = 15:1 b) Identical experiment carried out with 4, 20, 40, and 80 mg of HZSM-5 Si/Al=140 at 240°C.

2) Experiment reproducibility

Figure S2-2 reveals the low level of experimental uncertainty between runs conducted in triplicate.

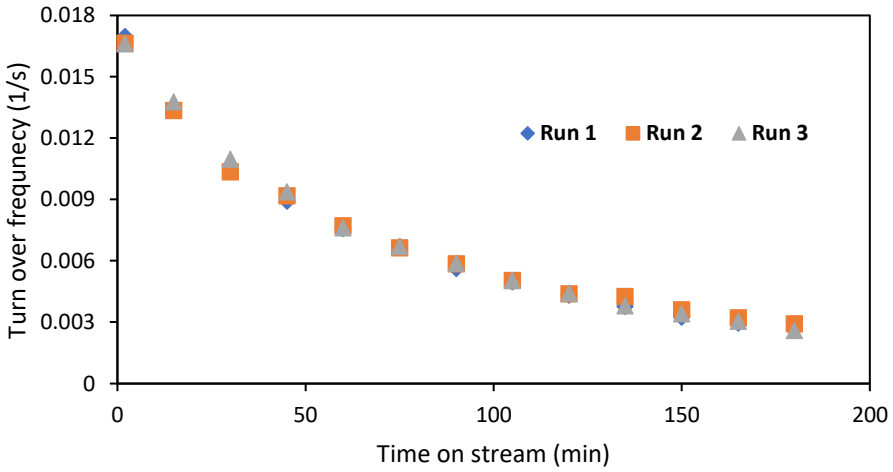


Figure S 2-2 Reproducibility test for the gas phase acylation reaction on 5 mg H-ZSM-5 (Si/Al = 40) catalyst at 160°C AA:2-MF molar ratio = 15:1.

3) Deactivation constant.

To obtain the relative rate of deactivation for each species, a series of species were introduced, independently, to a fresh catalyst before feeding both reactants. For example, in Figure S2-3, 2-MF was introduced to the catalyst alone for varying amounts of time prior to concurrent injection of AA. The reduction in rate observed at 0TOS reflects the catalyst deactivation that was incurred over this time. Similar experiments are performed via co-feeding of 2-MF, the product (Ac-MF), and AA.

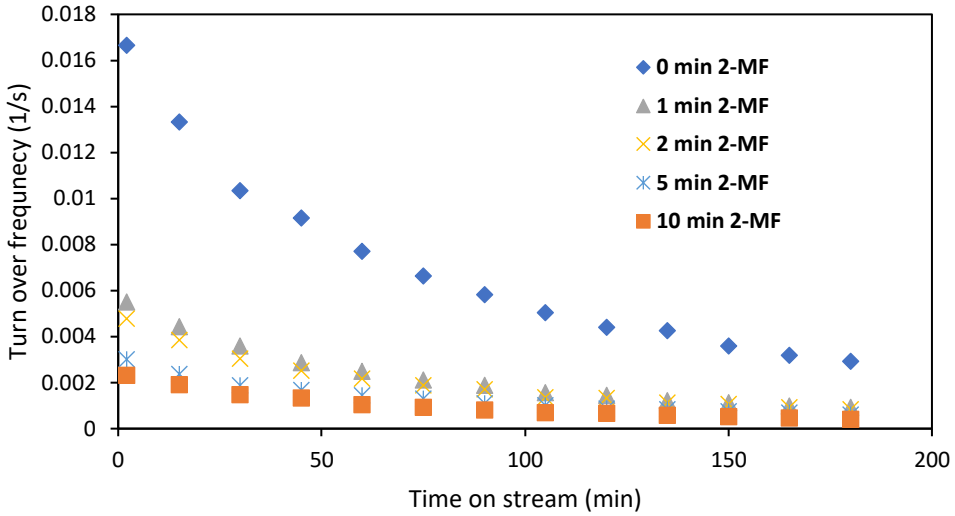


Figure S 2-3: Comparing initial active site loss resulted from introduction of 2-MF for 1,2,5, and 10 minutes prior to adding the other reactant (AA) to the feed to start the reaction. 5mg HZSM-5 (Si/Al=40) at 160°C after catalyst pretreatment at 300°C for 1 hour to remove the physiosorbed water. PP_{AA}=40 Torr, $PP_{2\text{-}MF}$= 2.6 Torr

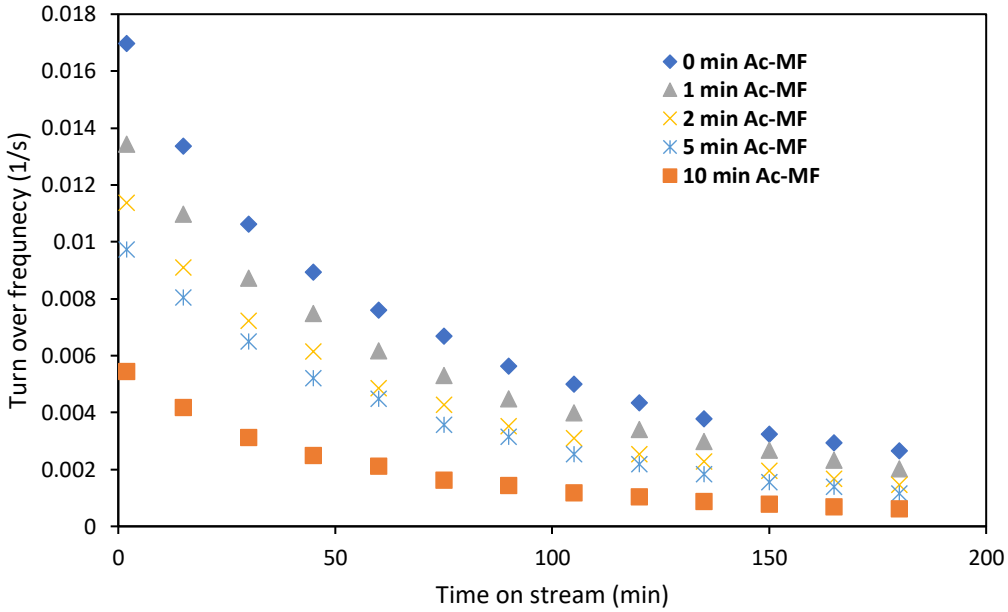


Figure S 2-4: Comparing initial active site loss resulted from introduction of the product (Ac-MF) for 1,2,5, and 10 minutes prior to adding the reactants to the feed to start the reaction. 5mg HZSM-5 (Si/Al=40) at 160°C after catalyst pretreatment at 300°C for 1 hour to remove the physiosorbed water. PP_{AA}=40 Torr, $PP_{2\text{-}MF}$= 2.6 Torr. Molar flow rates during prefeed for both 2-MF and Ac-MF are equal.

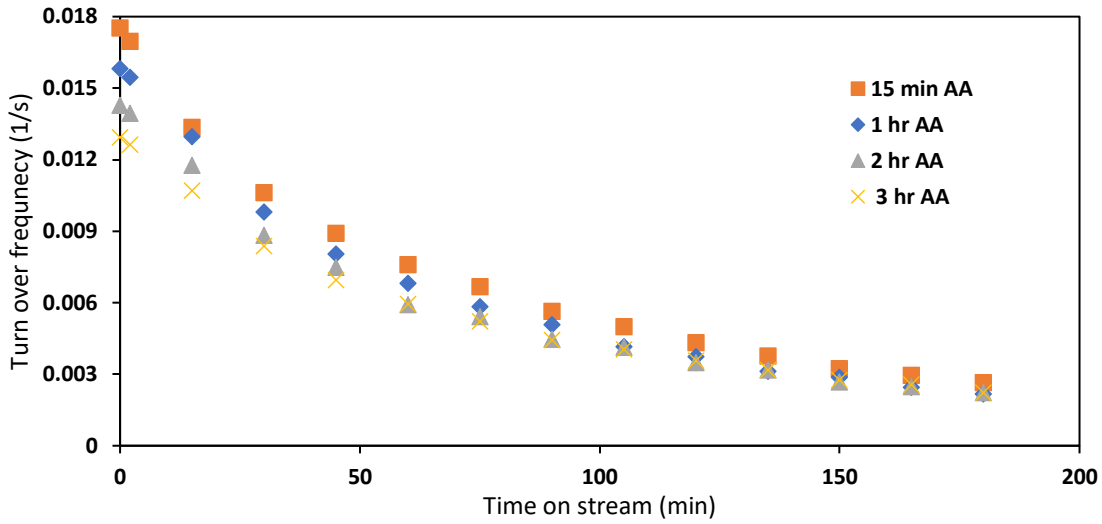


Figure S 2-5: Comparing initial active site loss resulted from introduction of AA for 15, 60 ,120, and 180 minutes prior to adding the other reactant (2-MF) to the feed to start the reaction. 5mg HZSM-5 (Si/Al=40) at 160°C after catalyst pretreatment at 300°C for 1 hour to remove the physiosorbed water. PP_{AA}=40 Torr, $PP_{2\text{-}MF}$= 2.6 Torr.

4) Inert co-feeding.

The addition of an inert species modifies the surface coverage of various gas phase species. Here, toluene was added as inert since reaction rates with toluene are negligible under the conditions reported here. Figure S2-6 represent series of experiments where AA and 2-MF are held at constant partial pressure while varying the partial pressure of toluene. Another series of experiments shown in Figure S2-7 have Toluene and 2-MF constant partial pressure while varying AA partial pressure. This experimental work was repeated at higher temperature to ensure data was not corrupted by capillary condensation of reactants or products as illustrated in Figures S2-8 - S2-10.

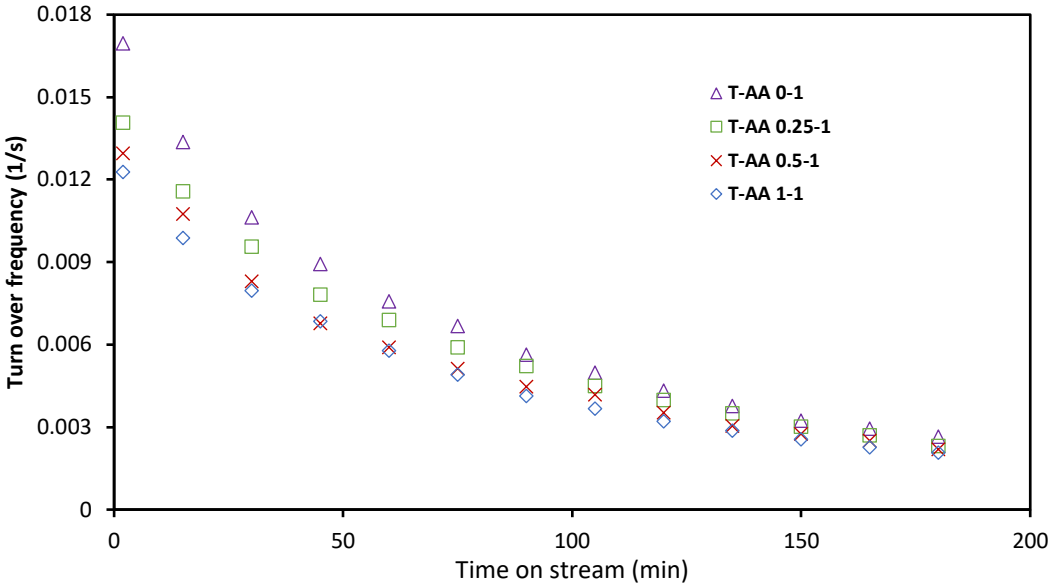


Figure S 2-6Constant feeding of AA and 2-MF while varying feeding of the inert (toluene). 5mg HZSM-5 (Si/Al=40) at 160°C after catalyst pretreatment at 300°C for 1 hour to remove the physiosorbed water. PP_{AA}=40 Torr, $PP_{2\text{-}MF}$= 2.6 Torr PP_T=0-40 Torr

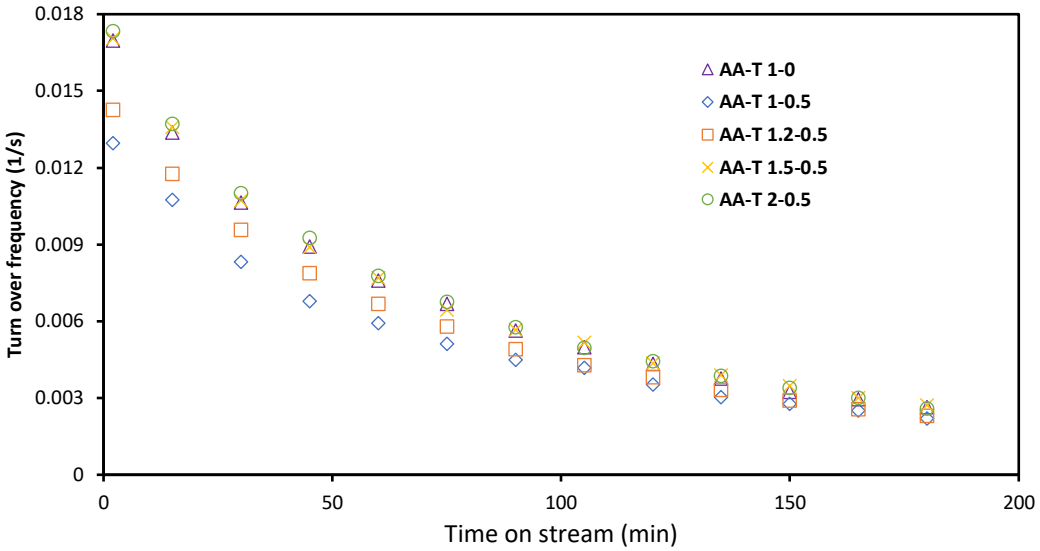


Figure S 2-7: Constant feeding of inert (toluene) and 2-MF while varying feeding of the AA 5mg HZSM-5 (Si/Al=40) at 160°C after catalyst pretreatment at 300°C for 1 hour to remove the physiosorbed water. PP_{AA}=40-80 Torr, $PP_{2\text{-}MF}$= 2.6 Torr, PP_T= 20 Torr

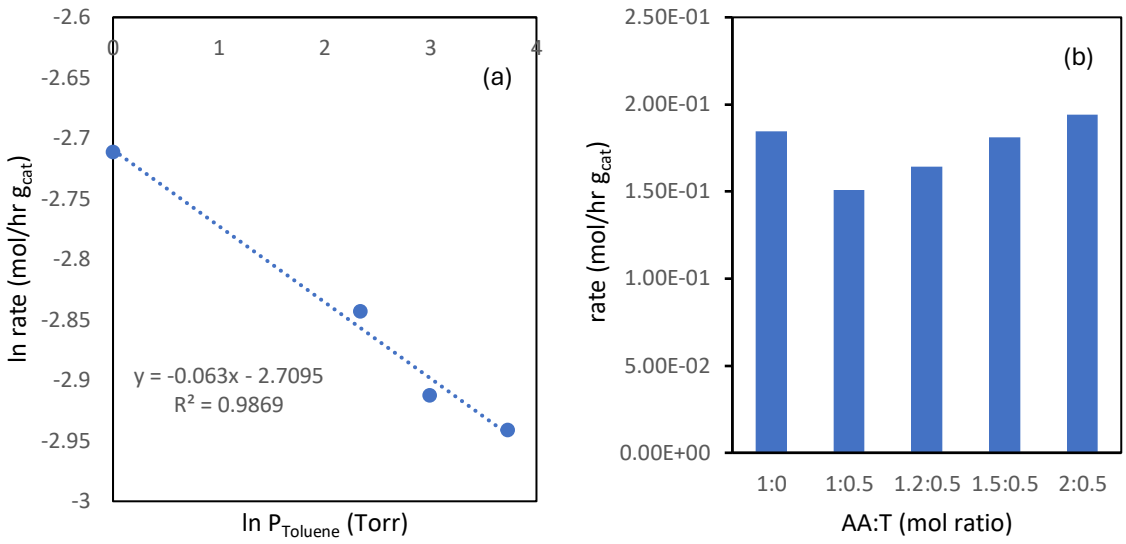


Figure S 2-8: Effect of co-feeding toluene at 240°C on HZSM-5 (Si/Al= 140) a) Rate of AA-MF formation at constant partial pressure of AA and 2-MF while varying inert (toluene) partial pressure. b) Rate of product formation at constant 2-MF partial pressure as a function AA and toluene partial pressure.

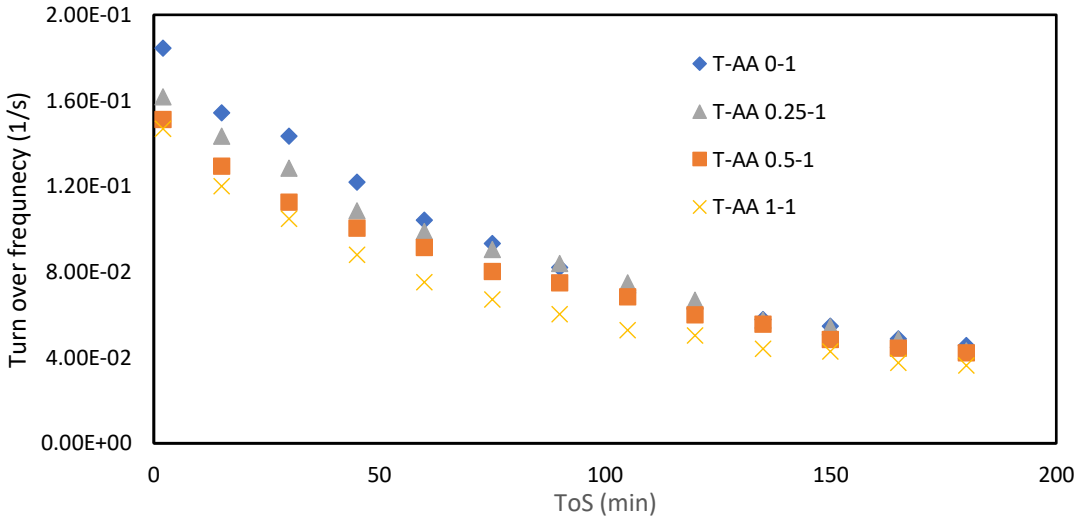


Figure S 2-9:Constant feeding of AA and 2-MF while varying feeding of the inert (toluene). 5mg HZSM-5 (Si/Al=140) at 240°C after catalyst pretreatment at 300°C for 1 hour to remove the physiosorbed water. PP_{AA}=40 Torr, $PP_{2\text{-}MF}$= 2.6 Torr PP_T=0-40 Torr

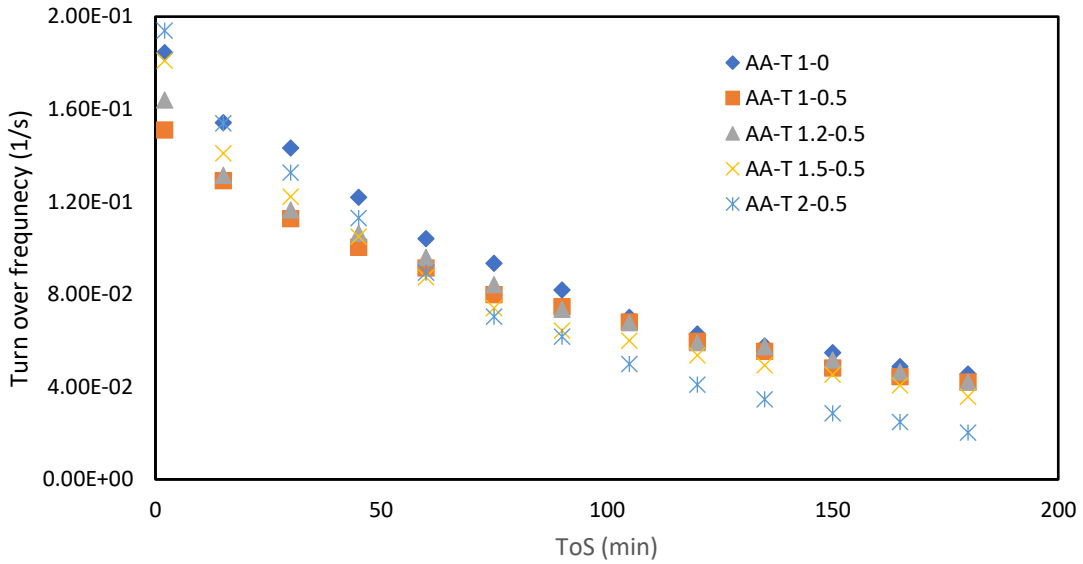


Figure S 2-10: Constant feeding of inert (toluene) and 2-MF while varying feeding of the AA 5mg HZSM-5 (Si/Al=140) at 240°C after catalyst pretreatment at 300°C for 1 hour to remove the physiosorbed water. PP_{AA}=40-80 Torr, $PP_{2\text{-}MF}$= 2.6 Torr, PP_T= 20 Torr

5) Varying partial pressure of 2-MF

Figure S2-11 presents signs of sequential reactions between 2-MF and the product where the surface coverage of 2-MF is varied via the addition of toluene. Here, lowing 2-MF feed resulted a decrease in decay rate even at equivalent overall reaction rates, illustrating that the product is indeed reacting directly with 2-MF.

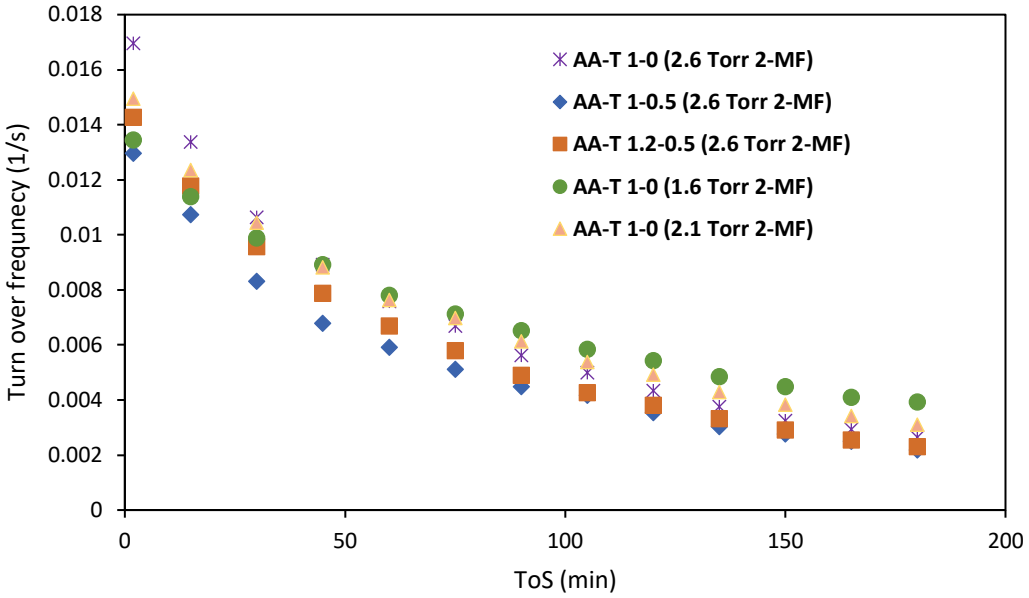


Figure S 2-11: Comparing deactivation of inert cofed reactions with reduced 2-MF flow at similar initial yields illustrating how decay decreases with lowering 2-MF feed demonstrating that it further reacts with the product.

6) BAS density measurements

The amount of active site in HZSM-5 (Si/Al =140) and Na-ZSM-5 (Si/Al =140) were quantified via IPA-TPR$_x$ technique. Figure S2-12 show the propylene signals resulted from the conversion of isopropyl amine over 50 mg catalyst samples. The area under the curve of propylene peaks was calculated then BAS densities obtained by correlation of propylene calibration peaks.

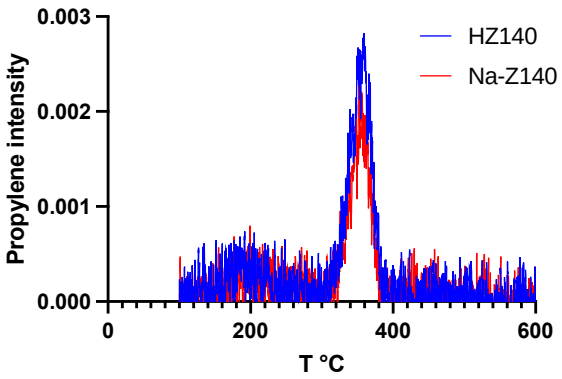


Figure S 2-12: Propylene peaks resulted from IPA-TPRx of HZSM-5 (HZ140) and Na-ZSM-5 (Na-Z140) catalyst samples used for BAS density quantification.

7) Coke analysis

Identifying the retained species in spent catalyst was obtained via several avenues. One approach we consider is to ramp the temperature (after the end of acylation reaction at 160°C) at a rate of 10°C/min to 500°C and held for an hour under flowing N_2 at 125 mL/min. The outlet line is connected to a cold trap contains n-decane to dissolve the desorbing species from the spent catalyst. The collected solution was injected and analyzed in GC-MS and the desorbed species (light coke) are assigned in figure S2-13.

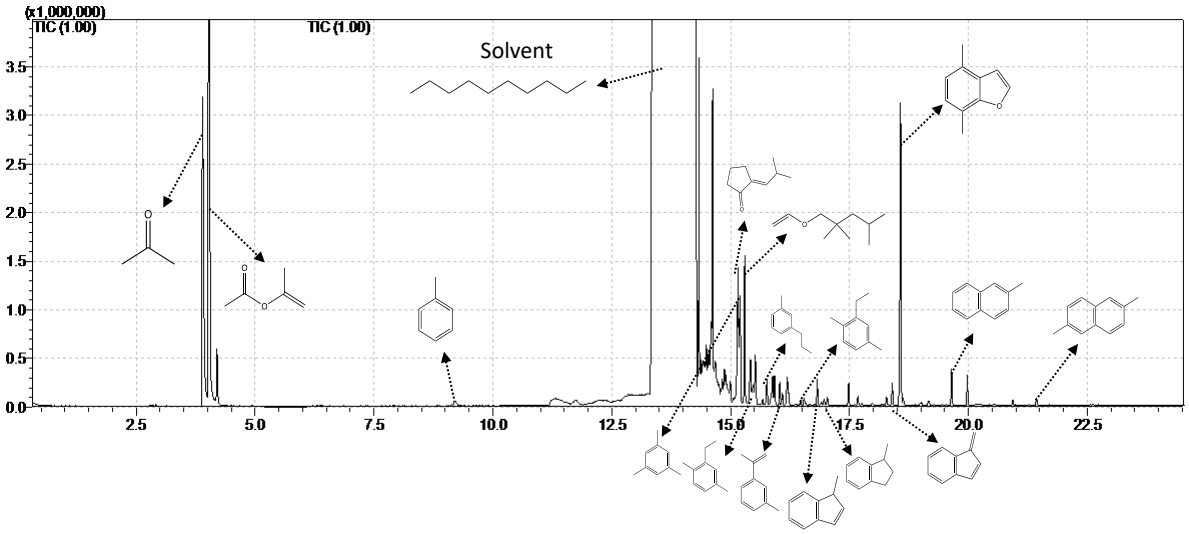


Figure S 2-13: GC-MS analysis of desorbed product collected from spent HZSM-5 (Si/Al=40) via temperature program sweeping with nitrogen (TPS-N_2).

The second method is to analyze spent catalyst samples using pyroprobe system connected to GC-MS at 3 different temperatures 300, 400, 500°C. The signals and the identity of retained species are illustrated in figure S2-14a-c.

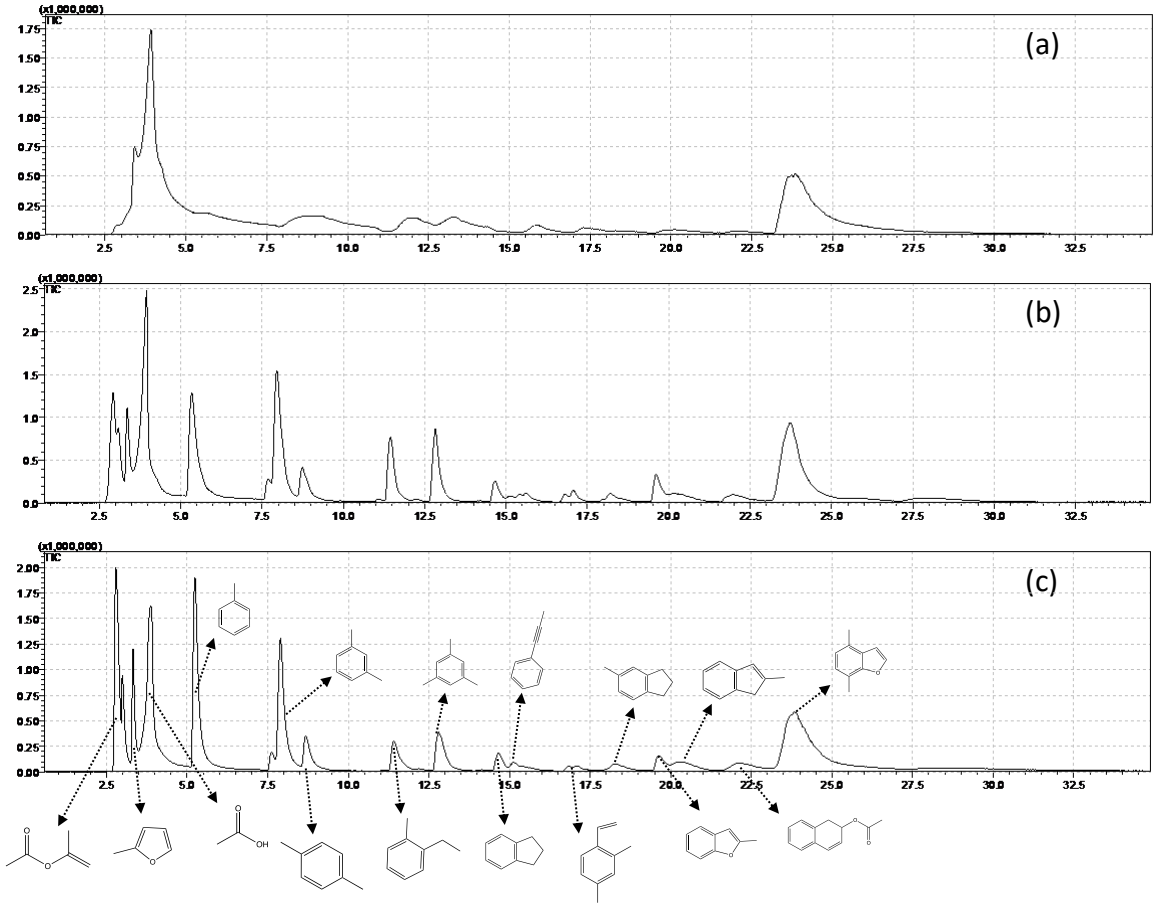


Figure S 2-14: Projected species from spent catalyst analyzed using the pyroprobe system at different temperatures (a) 300°C, (b) 400°C and (c) 500°C

The surface species in spent catalyst after acylation reaction were characterized using FTIR. Scans were taking before high temperature treatment to observe the evolution of spectra. Figure S2-15 shows the deconvolution of the spectra present major peaks between 2800-3000 cm^{-1} and 3100-3200 cm^{-1} were assigned for olefinic cyclic species.

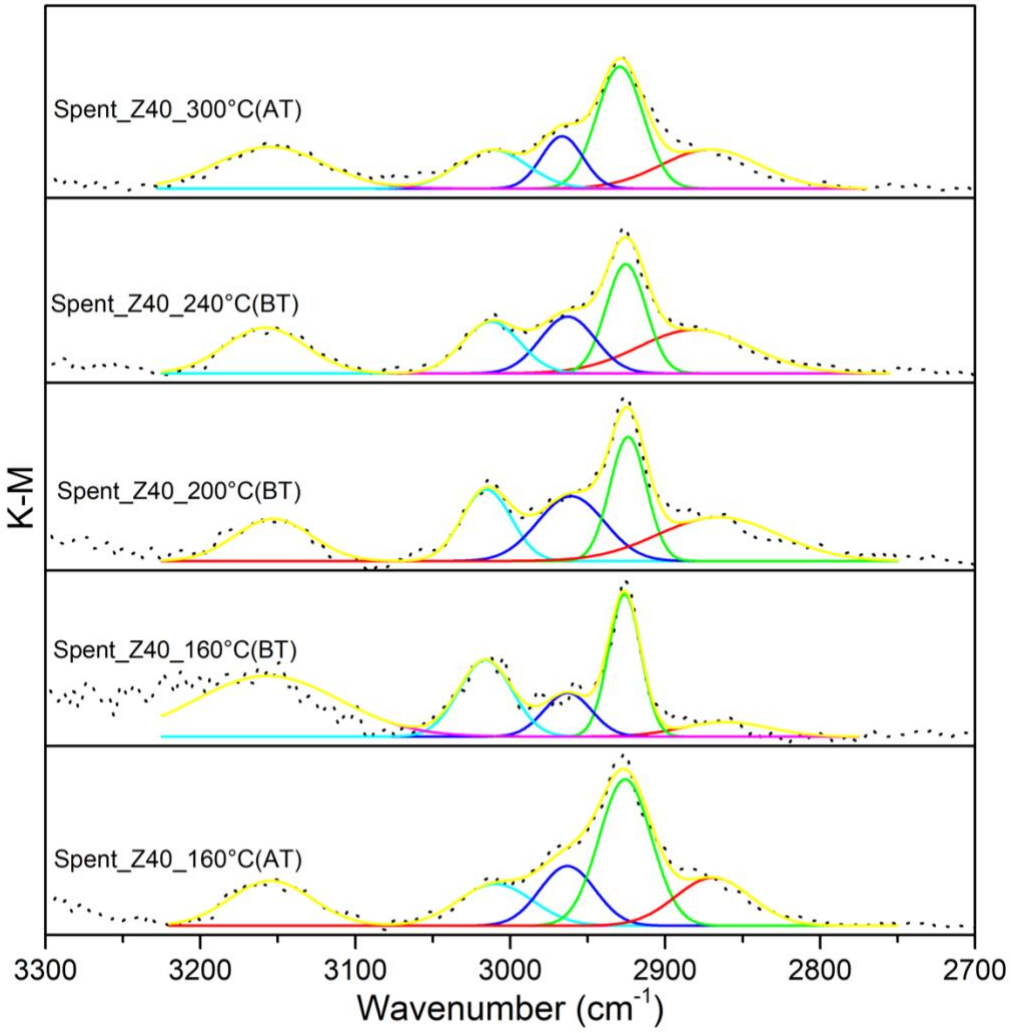


Figure S 2-15: Deconvoluted IR spectra of Spent HZSM-5 (Si/Al=40) (Z40) as function of temperature (BT= before treatment at 300°C, AT= after treatment at 300°C)

Coke accumulation in catalyst pore is expected to result a reduction in pore volume. Therefore, BET measurement was conducted of fresh catalyst and a spent catalyst after removing light coke (temperature program sweeping with N_2 for 1 hour). The Isotherm plots of fresh and spent catalyst are presented in Figure S2-16 which elucidate the significant loss of N_2 quantity adsorbed in spent catalyst compared the fresh.

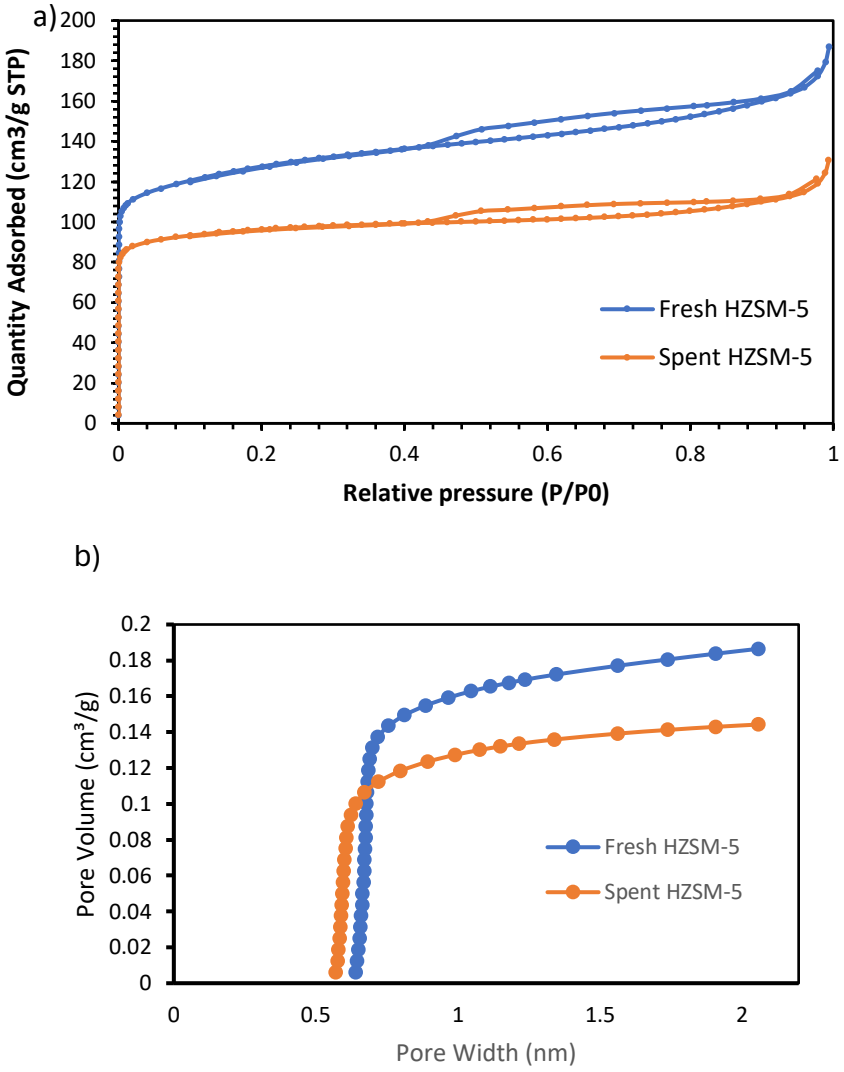


Figure S 2-16 a)Isotherm linear plot of fresh and HZSM-5 (Si/Al=40) and spent HZSM-5 (Si/Al =40) after removing soft coke via TPS-N_2, b) Micropore volume as estimated from the Horvath-Kawazoe method.

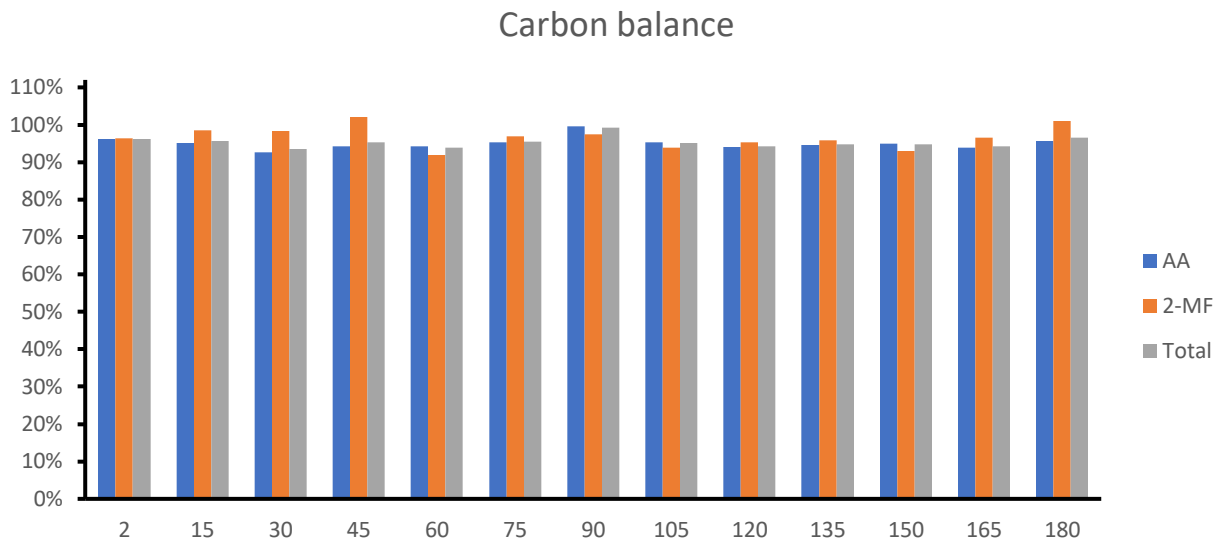


Figure S 2-17Carbon Balance Example, AA= 40 Torr, 2-MF=2.6 Torr at 160°C

The overall carbon balance for all experiments reported in this manuscript ranges from 95-101%.

Appendix-B: supporting information for Chapter 3

Consequence of altering acid strength in MFI zeolites via Phosphorus modification and their effects on acylation reaction

1) XRD for synthesized material

Silicalite-1 was synthesized to impregnate with phosphorous to explore the activity of the phosphorus-induced sites resulting from phosphorus binding with silanol group. The synthesis method followed a recipe found in literature [1], which indeed resulted a material that possess MFI structure, as seen in Figure S3-1, that is identical to the aluminosilicate MFI zeolite material used in this study.

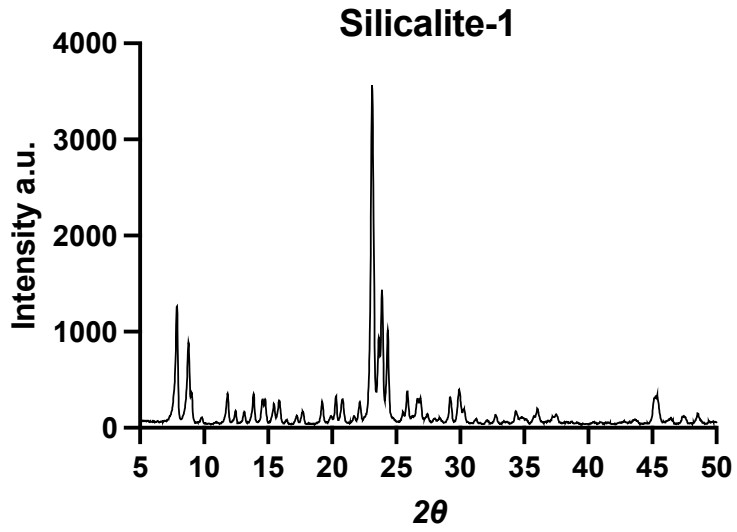


Figure S 3-1 XRD analysis of synthesized silicalite-1 confirming its MFI structure

2) Isopropylamine temperature program reaction (IPA-TPRx)

The IPA-TPRx technique was used to quantify Brønsted acid site (BAS) density by saturating a temperature pretreated catalyst with several (2 μL) pulses of IPA at 100°C under flowing Helium

gas. After 1 hour to allow the physically adsorbed excess IPA to leave, the temperature starts to ramp at 10°C/min to 600°C. During this time, we track three mass signals of m/z = 41,17, and 44, corresponding to propylene, NH_3 and IPA, respectively as seen in figure S3-2. Propylene is main useful signal for BAS quantification as illustrated in Figure 3-1b and Table 3-1.

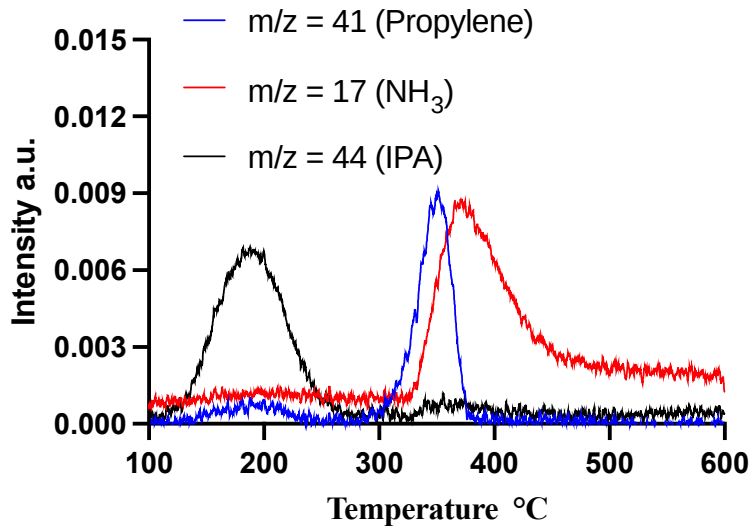


Figure S 3-2 Spectra of IPA-TPRx experiment showing the three signals for propylene, NH_3 and IPA

3) Catalyst crystallinity calculation

The crystallinity of the phosphorus modified catalyst samples was calculated using Equation S3-1 based on approach found in literature [2]. It is proposed that the relative crystallinity of MFI zeolite equals the sum of their characteristic peaks area at 2θ ~ 8.2, 9.1, 23.3, 24.1, and 24,6 for modified materials divided by the sum area of the same peaks for a standard material, which in our case is the parent zeolite (0P)

$$R_C = \frac{\sum(MFI\ characteristic\ peaks\ area)_{xP}}{\sum(MFI\ characteristic\ peaks\ area)_{0P}} \qquad Equation\ S3-1$$

4) N_2 adsorption measurement

This characterization technique was used to measure the BET surface area, micropore volume and total pore volume for the catalyst sample used in our study. The Isotherm and H-K Plots in Figure S3-3a,b of parent zeolite (0P) which elucidate the significant loss of N_2 quantity adsorbed in phosphorous modified (0P, 0.5, 1P, 2P, and 4P) zeolites. The Surface area (SA) values are presented in Table S3-1

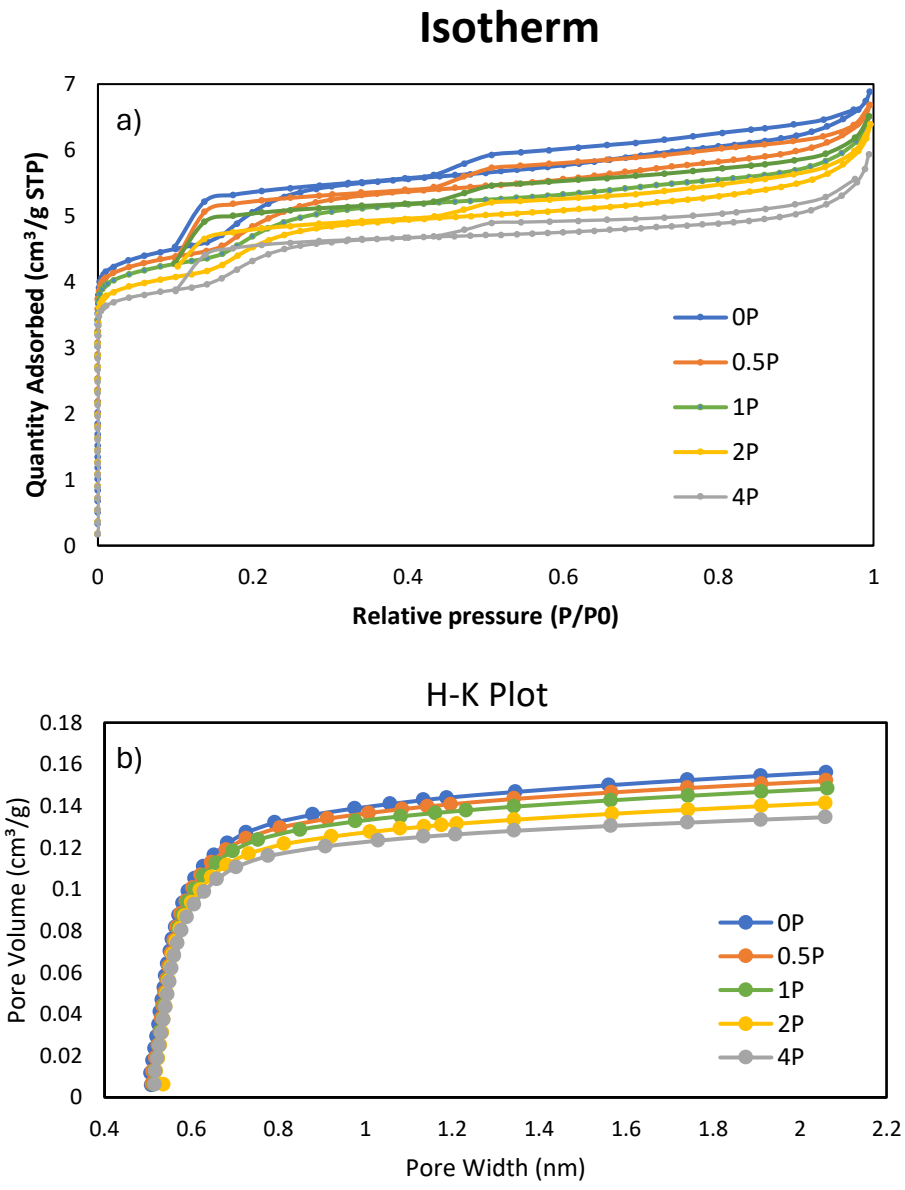


Figure S 3-3 a) Isotherm linear plot of parent zeolite (0P) and phosphorous modified (0.5P, 1P, 2P, 4P) zeolites b) Micropore volume as estimated from the Horvath-Kawazoe method (H-K Plot) .

Table S 3-1 Surface area (SA) values of parent zeolite (0P) and phosphorous modified (0.5P, 1P, 2P, 4P) zeolites

Catalyst Sample	(P/Al) mo[a]	wt%P	SA (m^2/g)
0P	0	0	400.1
0.5P	0.5	0.17	376.4
1P	1	0.33	362.5
2P	2	0.66	350.7
4P	4	1.3	335.9

5) FTIR of synthesized materials

We employed FTIR spectroscopy on Silicalite-1 and different phosphorous loadings (0.66,1.3 wt% phosphorus) to confirm the P-OH stretching region after introducing phosphorus to zeolites. We observed that adding phosphorus to silicalite-1 result decrease in Si-OH peak intensity in the regions between (3745 - 3725 cm^{-1}). Simultaneously, A new peak appeared in the region 3672 cm^{-1} similar to zeolites as seen in Figure S3-4.

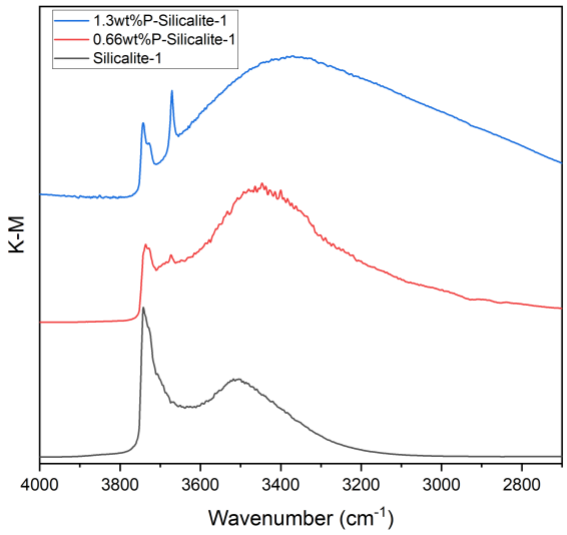


Figure S 3-4 FTIR spectra for P-Silicalite-1 with different wt% loadings compared with fresh non-modified Silicalite-1

6) Internal diffusion limitation assessment

To ensure a valid kinetic assessment for the phosphorus modified samples, it is important to ensure that the acylation reaction is not within diffusion limited regime. Therefore, we carried the reaction over sodium-exchange zeolite (Na-ZSM-5 – 25% exchanged BAS) and compared the turnover frequencies (TOF) of both parent zeolite (0P) and Na-ZSM-5. Figure S3-5 illustrate that acylation over both catalyst samples exhibited identical TOF values during the entire experiment time, which suggest that reaction is far from pore diffusion limitations.

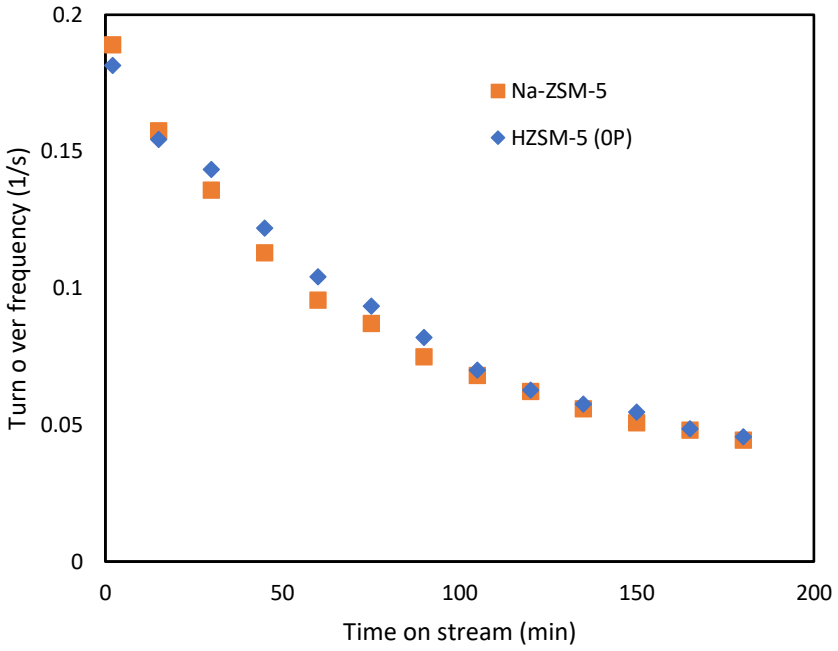


Figure S 3-5 Testing diffusion and reaction within parent zeolite samples HZSM-5 (0P) at 240°C after catalyst pretreatment at 300oC for 1 hour to remove the physiosorbed water. P_{AA}= 40 torr, $P_{2\text{-}MF}$= 2.6 torr.

7) Activity assessment of phosphorous-induce sites

Silica supported phosphate species are known for their activity as weak Brønsted acid sites. We carried out acylation reaction over Silicalite-1 supported phosphorus to assess their intrinsic acylation activity of phosphate species. Figure S3-6a, b presents the rate extremely low

acylation rate over Silicalite-1 supported phosphorus compared to aluminosilicate zeolite material (0P). It required more than 6 times more mass of P-Silicalite-1 compared to 0P catalyst to achieve initial conversions close to the one found over parent zeolite (0P). Additionally, P-Silicalite-1appears to be ultra-unstable since it was found to undergoes instant catalyst deactivation compared to the zeolites. This instability is possibly due to phosphates hydration during the dehydration of the acetic acid or/and to their mobility within the microporous materials.

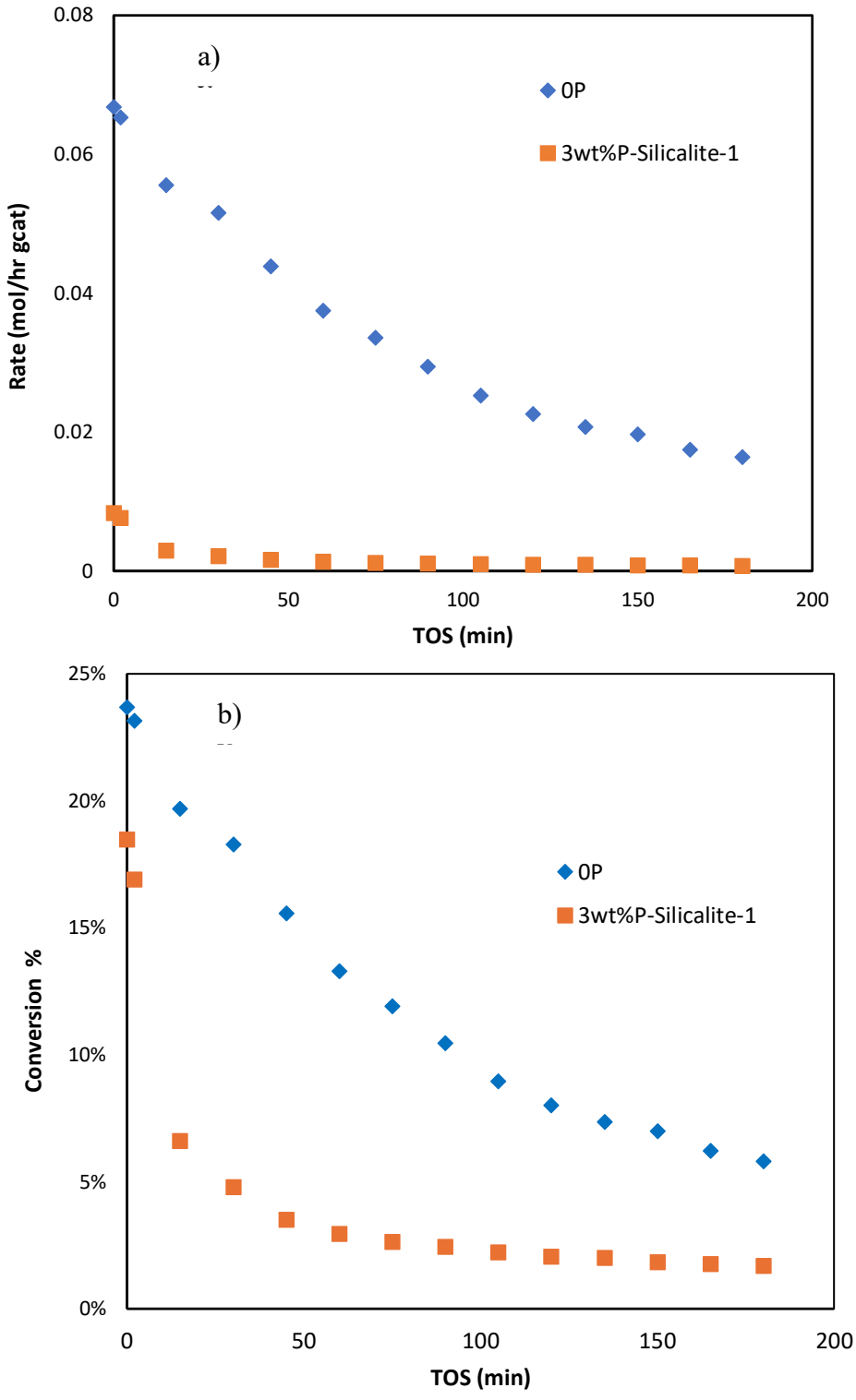


Figure S 3-6 a) Reaction rates (mol/hr g_{cat}) and b) conversions for acylation over parent HZSM-5 zeolite (0P) and 3wt%P-Silicalite-1 at 240°C, P_{AA}= 40 torr, $P_{2\text{-}MF}$= 2.6 torr.

8) Catalyst regeneration

The ability to regenerate catalyst materials is a desired feature that allow a process to minimize waste and improve efficiency. While phosphorus incorporated zeolites (2P) exhibited significant activity and stability relative to the parent zeolite (0P), it is important to examine the ability to recover the activity post reaction. To cover this part, we implemented a post treatment for both catalyst samples via temperature programed sweeping under flowing N_2 gas (TPS-N_2) while ramping the reaction temperature from 240°C to 300°C at 10°C/min. The treatment temperature was held for 1 hour to remove as much carbonaceous deposits as possible. The results for this mild treatment, as presented in Figure S3-7, show higher recovery rates with P-zeolite (74%) compared to parent (49%) of their initial fresh catalyst rates. This remarks an additional benefit for phosphorus addition in zeolite for acylation chemistry.

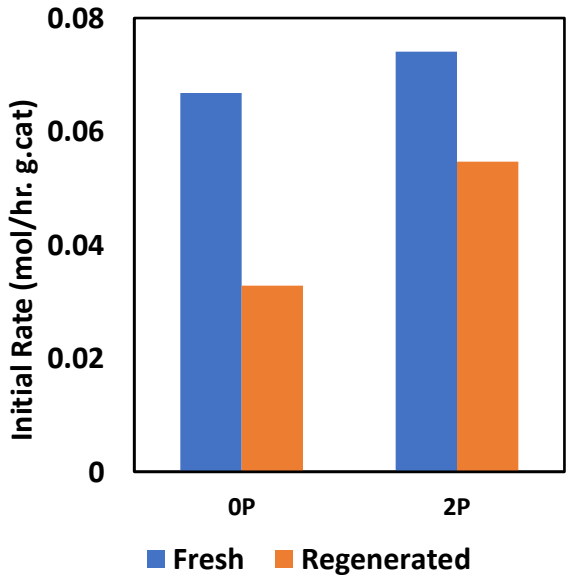


Figure S 3-7 Initial conversions for fresh and TPS-N_2 regenerated parent zeolite (0P) and phosphorous incorporated zeolite (2P) catalyst at 240°C, P_{AA}= 40 torr, $P_{2\text{-}MF}$= 2.6 Torr.

We discussed previously that phosphorus addition to zeolite results in new phosphorus associated active sites overserved in FTIR analysis, Figure S3-4, from P-OH stretching in the 3672 cm^{-1} regions. It worth mentioning that some regular BAS at the 3610 cm^{-1} region in fresh parent zeolite convert to weak P-induced sites found in 3672 cm^{-1} regions. FTIR spectroscopy of spent 0P and 2P catalyst in Figure S3-8 indicate that mild treating spent 2P catalyst recover notable amount of the P-induced sites. On the other hand, recovering the -OH stretching at the 3610 cm^{-1} region for active sites in parent zeolite appears to be negligible. Furthermore, parent zeolite 0P retained more carbonaceous deposit region (3200-2850 cm^{-1}) compared to 2P catalyst.

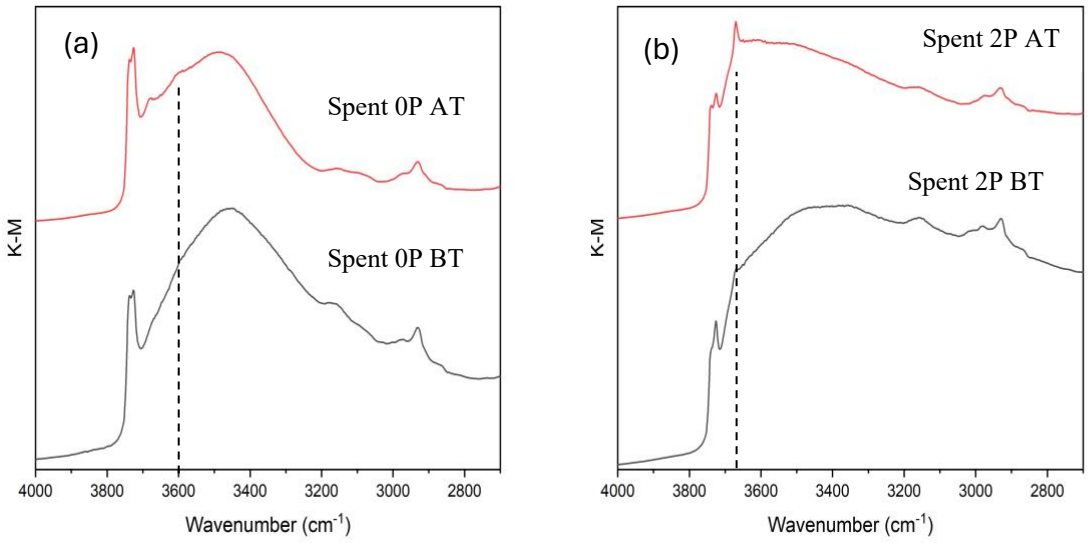


Figure S 3-8 FTIR of a) spent parent zeolite (0P) and b) phosphorus incorporated zeolite (2P) before (BT) and after treatment (AT) at 300°C for 1 hour under flowing helium.

9) Analysis of the retain species in spent catalyst samples.

Dissecting the retained surface species in deactivated catalyst offers an applicable understanding deactivation routes and scenarios that the active sites experienced before losing their catalytic activity. In this case, we implemented a systematic TGA analysis separate surface species in spent parent zeolite (0P) and phosphorus modified zeolite (2P) to quantify the amount

water, soft coke, and hard coke. This was carried out in two stages where first the catalyst is heated to 300°C at a ramp rate of 10°C/min under flowing argon gas which, allowed us to obtain the amount of water and soft coke as seen in Figure S3-9a. Then, the temperature was cooled down to 100°C to prepare for the second stage to carry out the temperature program oxidation to quantify the hard coke retained in the spent catalyst samples. This was carried out by ramping at of 10°C/min to 600°C under flowing air, Figure S3-9b. It worth noting that the water mass spectra signals were calibrated using calcium oxalate monohydrate and water-soaked zeolite A.

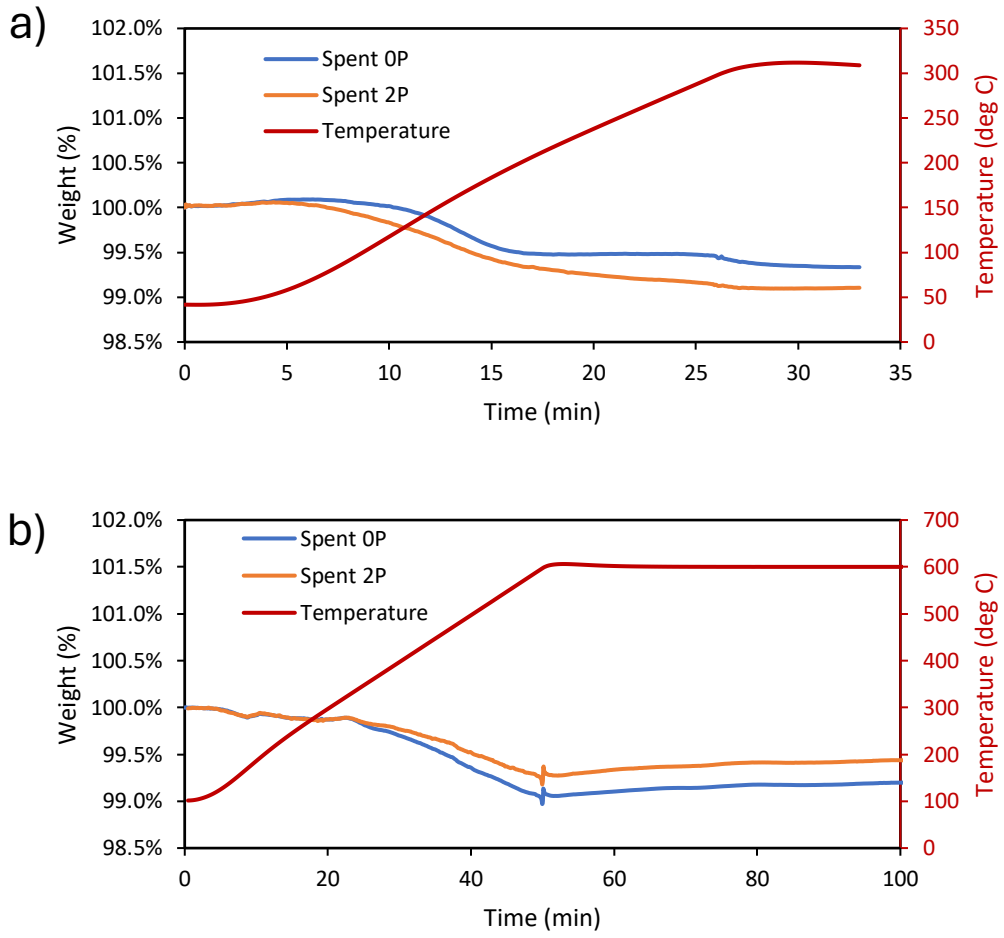


Figure S 3-9 TGA analysis of spent catalyst (0P) and (2P) for a) water and soft coke quantification in stage 1by heating in argon to 300°C and b) hard coke quantification in stage 2 by calcining in air to 600°C.

Table 1 provide the resulted quantitative TGA analysis for the retained surface species in spent 0P and 2P catalyst, which was obtained from the two stage temperature programed treatment. The relative increase in retained water in the catalyst is likely due to the hydrophilic nature of phosphate species. While we observed a slight increase in the fraction soft coke on phosphorus modified zeolite (2P), the amount of hard coke that can only be removed by combustion dropped to 50% of that resulted from parent zeolite (0P), Figure S3-10. We propose that more soft coke can be expected to form on 2P attributed to lower product surface retention due to their weak acidity. Consequently, that mitigates further transformation of soft coke that can be removed by mild treatment to hard coke that needs combustion to dispose.

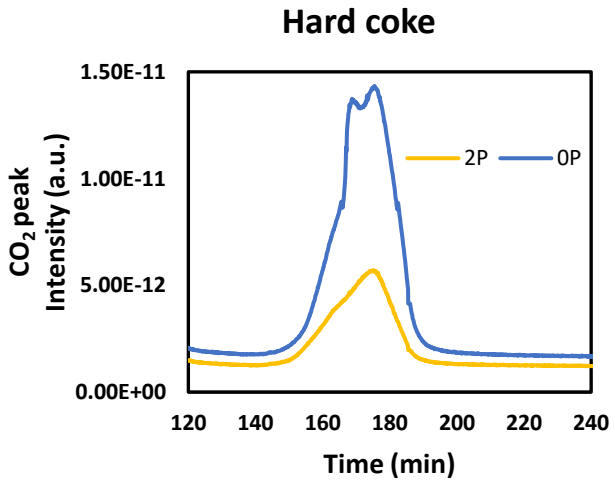


Figure S 3-10 Comparison of the CO_2 signal generated from combusting spent 0P and 2P catalyst samples

Table S 3-2 weight fractions for retained species in spent 0P and 2P catalyst samples

	Spent catalyst wt%	
	0P	2P
Water	0.66%	0.79%
Soft coke	0.42%	0.47%
Hard coke	0.39%	0.19%

Reference:

[1] J. Phys. Chem. C 2015, 119, 15303−15315

[2] Applied Clay Science, 2003. 24(1-2): p. 69-77.

Appendix-C: supporting information for Chapter 4

Effect of Brønsted Acid Site's Local Environment on Zeolites' Catalytic Activities during Acylation of 2-Methylfuran with Acetic Acid

1) Reaction order of the reactants

Operating at high surface coverage of reactants is essential for measuring near true values for enthalpy and entropy of transition state ($\Delta H^{\ddagger}$ and $\Delta S^{\ddagger}$). Therefore, we operated at high partial pressure of acetic acid (P_{AA} ~ 40 Torr) which was proven from previous work [1] that is in 0^{th} order reaction regime with respect to AA over MFI(40) and MFI(140) under reaction temperatures at 160°C and 240°C, respectively as seen if Figure S4-1a, b. Reaction over all other catalyst samples are expected to reach 0^{th} order with respect to AA due to extremely high P_{AA}.

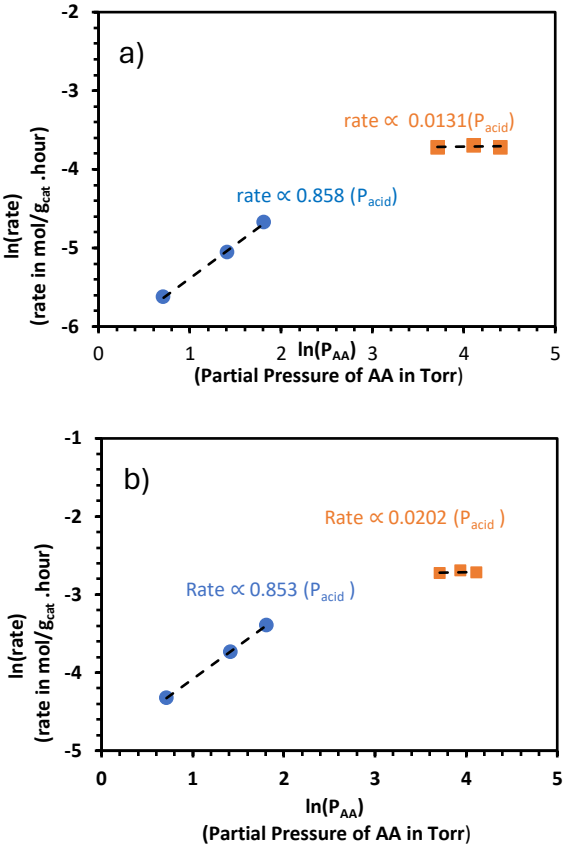


Figure S 4-1 Reaction order wrt AA at low (P_{AA} = 2-6 Torr) and high (P_{AA} = 40-80 Torr) coverages of AA obtained from reaction on a) MFI(40) at 160°C while b) collected from reaction on MFI(140) at 240°C with partial pressure of 2-MF of $P_{2\text{-}MF}$ = 2.6 Torr [1]

While the reaction order with respect to 2-MF varies between 0^{th}-0.5^{th} depending on the catalyst sample used, it is important to note that the partial pressures are relatively low ($P_{2\text{-}MF}$ = 2-3 Torr). This selected range was necessary to avoid 2-MF contributions to catalyst deactivation. However, the reaction order with respect to 2-MF appears to approach 0^{th} reaction order regime at $P_{2\text{-}MF}$ = 2.6 Torr, Figure S4-2, which is the partial pressure used in all kinetic assessment for this study.

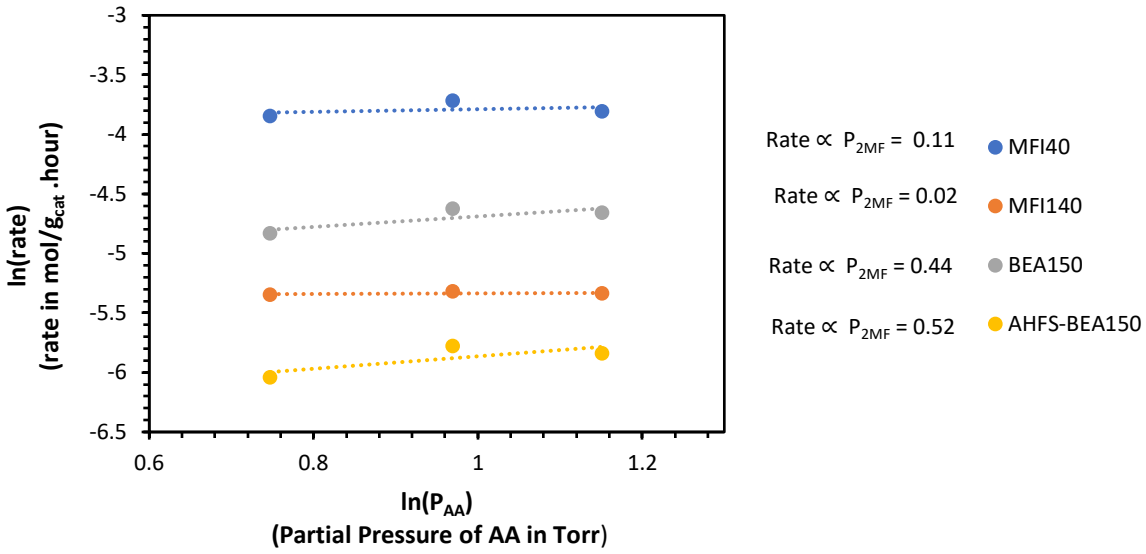


Figure S 4-2 Reaction order wrt 2-MF measured at $P_{2\text{-}MF}$ = 2.1-3.2 Torr obtained from reaction at 160°C and P_{AA} = 40 Torr

2) Experimental reproducibility

We conducted multiple run for various catalyst samples including BEA (150), MFI(140) MFI(40) and AHFS-BEA(150) to ensure a high reproducibility and confidence level in the collected data. BEA(180) was included to compare and to confirm the accuracy of the observations found in acylation over BEA(150). BEA(180) was received in proton form from Alfa Aesar (SiO_2:Al_2O_3 mole ratio 360:1). Figure S4-3 show the experimental data points for several catalyst samples at different time on stream with low error bars reflecting the high confidence in our results. It is important to note that the faster catalyst deactivation observed in BEA zeolite is likely due to larger pore volumes that facilitate product oligomerization [1].

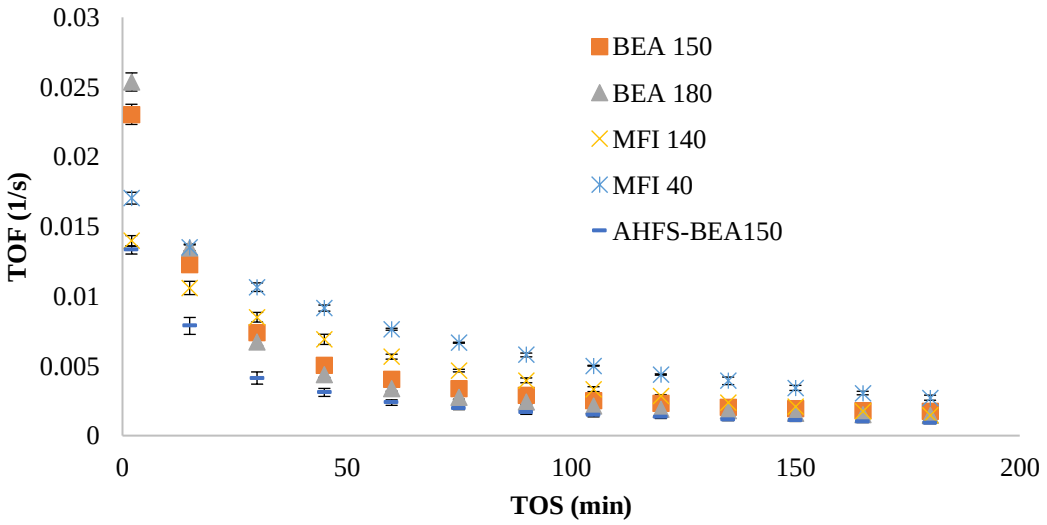


Figure S 4-3 Reproducibility assessment for acylation of various catalyst samples (5-20 mg) at 160°C $P_{2\text{-}MF}$ = 2.6 and P_{AA} = 40 Torr

3) Isopropylamine temperature program reaction (IPA-TPRx)

This characterization technique is used quantify the Brønsted acid site (BAS) density from reacting IPA and convert to propylene. Figure S4-4 illustrate the propylene signals collected from characterizing various zeolite samples used in this study to obtain BAS densities for measuring turnover frequency (TOF) during acylation.

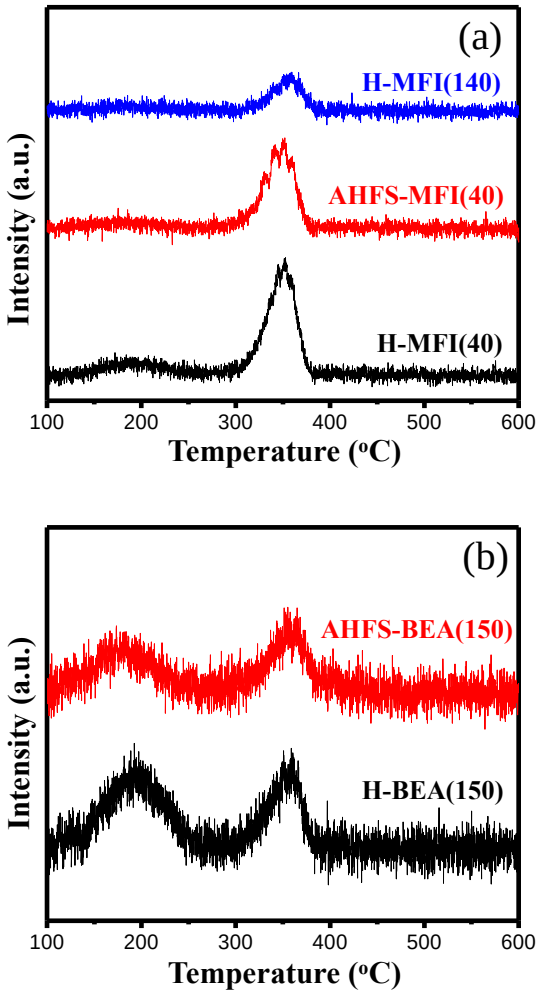


Figure S 4-4 Propylene signals of IPA-TPRx experiment for a) MFI and b) BEA zeolites

Reference:

[1] Journal of Catalysis 426, 222-233

Appendix-D: supporting information for Chapter 5

Role of carbon chain length in carboxylic acids on acylation of 2-methyl furan over HZSM-5 zeolite

1) Reaction order with respect to carboxylic acids.

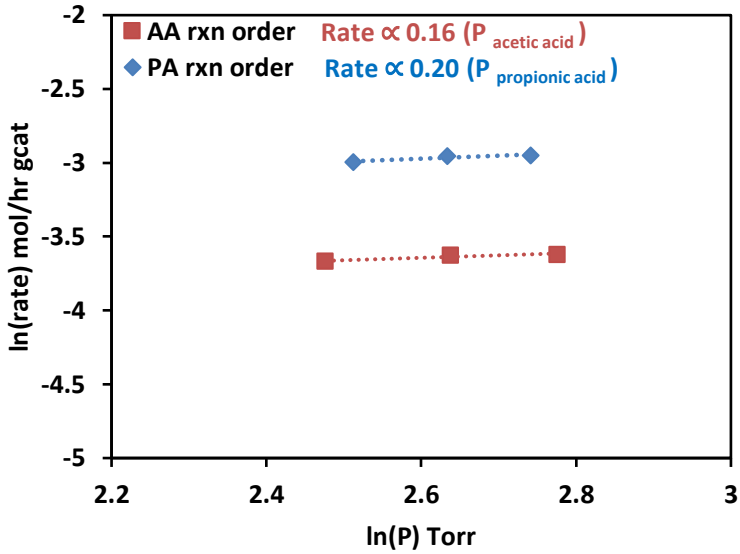


Figure S 5-1 Reaction rates as a function partial pressure (12-16 Torr) of carboxylic acids at 200°C with ~5-1 mol (Acid-2MF) over HZSM-5 (Si/Al=140)

2) Presence of alpha H2

2-MF can easily accept acylating carboxylic acid as long there is one alpha H_2. In the case of lack of alpha H_2 , acylation becomes challenging and less selective

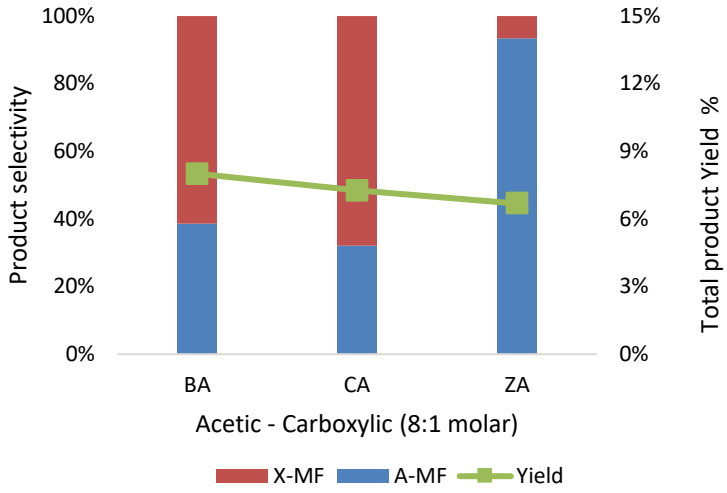


Figure S 5-2 Conversion and product selectivity for acylation with carboxylic acid blends with molar ratios of 8:1 acetic acid (AA) to butyric (BA), crotonic (CA) or benzoic (ZA) acids at 200°C with ~5-1 mol (Acid-2MF) over HZSM-5 (Si/Al=140)